



## A Study of Nano Diesel Particulate Matter (nDPM) Behaviour and Physico-chemical Changes in Underground Hard Rock Mines of Western Australia

MRIWA PROJECT M495

SILVIA BLACK and BEN MULLINS

FINAL REPORT

13 June 2019

PREPARED FOR

MRIWA

100, Plain Street

East Perth WA 6004

## CORRESPONDENCE DETAILS

Dr. Silvia Black

Manager Project Development

Scientific Services Division,

ChemCentre, Resources and Chemistry Precinct, South Wing, Building 500, Manning Road, BENTLEY WA 6102.

Phone: 08 9422 9964

Fax: 08 9422 9801

E-mail: [sblack@chemcentre.wa.gov.au](mailto:sblack@chemcentre.wa.gov.au)

A/Prof Ben Mullins

School of Public Health,

Curtin University, Manning Road, BENTLEY WA 6102.

Phone: 08 9266 7029

E-mail: [b.mullins@curtin.edu.au](mailto:b.mullins@curtin.edu.au)

## EXECUTIVE SUMMARY

Underground mining in Western Australia is heavily reliant upon diesel-powered equipment. This is likely to remain so for some time to come, especially when expanding the mining envelope to deeper mines. This is largely because cost and production efficiencies offered by diesel-powered equipment are unrivalled by any competing systems (e.g. battery-electric or plug-in electric equipment). Mining in the Eastern Goldfields is progressively getting deeper as shallow orebodies are depleted. The economics of underground mining will progressively become more reliant on the cost and production efficiencies offered by using diesel equipment. Future green fields discoveries are likely to be under deep mineralogical cover in the east of the state and are likely to have dependence upon the cost and production efficiencies offered by using diesel equipment.

The use of diesel-powered equipment has been continuously increasing in underground metal/non-metal mines. This extensive utilization of diesel-powered equipment generates the potential for exposure of underground miners to diesel particulate matter (DPM), including nano diesel particulate matter (nDPM). Nanoparticles are generally defined as <100 nm in size. The majority (by numbers) of the diesel particles are in the nano size range, hence the term nDPM. In 2012, the International Agency for Research on Cancer (IARC) classified diesel engine exhaust (DE – which includes DPM) as carcinogenic to humans (Group 1)<sup>1</sup>.

The health implications of nDPM are known to extend beyond the lungs and the particles are small enough to diffuse throughout the body<sup>2,3</sup> and even penetrate the blood-brain barrier<sup>4</sup>.

The management of diesel emissions in underground mines is a significant challenge. Although emissions from plant are increasingly lowered (through OEM or after-market exhaust after-treatment), deeper mines and more stringent guidelines/limits increase management difficulty. In addition, current guidelines for diesel particulate matter (DPM) are based on the measurement of elemental carbon (EC), which (a) is most strongly correlated with mass of DPM rather than number or surface area, and (b) may not be representative of the most harmful components of the exhaust. There is increasing interest in understanding the importance of nDPM in underground mines, and managing such particles effectively. Nanoparticles are generally defined as particles <100 nm, which typically represent the majority of diesel exhaust, in terms of both mass and number.

There are critical gaps of knowledge on the character of nDPM, its behaviour and also size-, number- and mass-based concentrations in underground hard rock mine environments. Furthermore, no studies have examined the effects of elevated pressures and temperatures (as found in deeper mines) on nDPM formation and evolution.

To ensure the continued availability of using diesel equipment into the future as an option for operations in underground mines as the mining envelop expands with deeper mines, the characterisation of nDPM is critical as it will need good management and controls going forward.

This project therefore aimed to study nDPM in a Western Australian mine with the intent to trial and develop the methodology at one mine, in order to ensure it captures all necessary data. The finalised methodology would then be implemented at other hard-rock mines in Western Australia, in order to better determine effective management strategies for nDPM into the future.

This was a collaborative project between ChemCentre, Curtin University's WA School of Mines (WASM) and School of Public Health (SPH), BBE Consulting Australasia and Queensland University of Technology. The project represented one of the largest and most comprehensive studies of the underground mine environment conducted in Australia, if not the world, to-date.

The objectives of the project were to:

- Generate datasets on size, number concentration, mass concentration and EC concentration of nDPM at representative locations in one mine (including personal monitoring of representative tasks);
- Measure Real-Time measurement of gaseous components (CO, CO<sub>2</sub>, NO<sub>x</sub>, SO<sub>x</sub>, VOCs);
- Study the diesel exhaust flow behaviour and source contribution relative to proximate equipment operators using tracer gas technology;
- Study the dispersal of gaseous and ultrafine particulate emissions from diesel exhaust, particularly nDPM, and the dilution efficiency of the mine ventilation with particular focus on the auxiliary ventilation at the face of development headings;
- Study physico-chemical composition of nDPM and changes post emission in an underground mine;
- To determine the impact of ventilation practises on the exposure levels and physico-chemical composition of particles;
- Perform chamber studies of simulated mine environments to investigate the physico-chemical composition of nDPM and changes post emission in existing mines depths and depths up to 4 km (1.4 atm. pressure);
- Improve the understanding of the impact of nano-diesel particulate matter (nDPM) on air quality from diesel exhaust emissions; and
- These studies will inform nDPM exposure assessments in existing and future deeper mines.

### **Part A: ChemCentre/BBE Study**

There are critical gaps of knowledge on the character of nDPM and its behaviour in underground hard rock mine environments.

The mine ventilation system plays an important role in mitigating human exposure to diesel particulate matter (DPM) emissions, exhaust gases and heat in underground mines. The mine's secondary ventilation systems are critical for diluting contaminants when working at the face of a heading.

It is important to understand the localized flow profiles on a "micro scale" to identify areas of improvement and ensure that the ventilation system is optimized to maximise dilution of exhaust gases. The application of tracer gas technology enables reliable measurements of flow behaviour and differentiation between the contribution of various contaminant sources including nano DPM (nDPM).

Previous studies performed by ChemCentre and in collaboration with USA researchers (confidential work not published) showed that the smaller the particle size (< 80 nm) the more likely the particle would behave like a gas. Hence, tracer gas technology is an appropriate tool for studying nanoparticles, such as nDPM.

In this project, tracer gas technology was applied successfully at an underground gold mine to better understand and inform the following;

- SF<sub>6</sub> flow behaviour as a surrogate for diesel exhaust and relative source contribution to exposure of nearby equipment operators;
- The dispersal of gaseous and ultrafine particulate emissions from diesel exhaust, i.e. particularly nDPM, and the dilution efficiency of the mine ventilation with particular focus on the auxiliary ventilation at the face of a development heading;
- The impact of ventilation practises on the exposure levels; and
- The potential impact of nano-diesel particulate matter (nDPM) on air quality.

Key findings from this study were;

- The tracer gas study of a number of underground mining activities, such as charging, bogging, hydro-scaling, shotcreting and truck driving, demonstrated that during those activities there were relatively higher SF<sub>6</sub> concentrations measured during the hydro-scaling and shotcreting activities.
- During shotcreting, the Agi truck operator experienced approximately the same exposure of SF<sub>6</sub> from the Agi truck and spraymec exhaust (Section 3.4). In contrast, the spraymec operator received almost twice the exposure from the spraymec exhaust than from the Agi truck exhaust. The Agi operator in this instance was at greater risk.
- During a short duration activity in a development heading, an unventilated cuddy (as represented by the stockpile in this study) could be a natural 'place of safety' or shelter area for personnel that are in the general area but not involved with the actual activity at a development heading.

In Summary;

- The tracer gas study effectively identified anomalies and concentration differences for different activities;
- The information can be utilised to better inform the planning of administrative controls to manage activities around other major diesel activities; and
- Controlled experimental set-ups with different secondary ventilation configurations should be considered to allow comparative studies that will enable ventilation optimisation. e.g. 1: different distances of end ducting to the face of heading; e.g. 2: comparison study between three secondary ventilation systems (force system, exhaust system and force-exhaust system).

## Part B: Curtin University/QUT Study

The findings from the personal and stationary monitoring, ventilation modelling and deeper mines study were as followed;

- Underground workers in the study were found to be exposed to significant levels of DPM, both in terms of EC levels (16% were above guideline levels - before any correction for shift length or work pattern is applied) and particulate number (nanoparticle) concentration. A statistically significant correlation (Pearson correlation = 0.82) was however found between mean EC and mean (nano)particle exposure for each worker. However, deviations from the agreement were most notable on the nanoparticle side (high number concentration exposure with comparatively low EC mass concentration exposure). These results must be interpreted in conjunction with appropriate biological/health data (separate report) to determine which measure most strongly correlated with health effects. EC exposure would however appear to be a reasonable indicator of nanoparticle exposure, and vice versa, implying that; (a) standard EC monitoring methods remain appropriate and (b) nanoparticle monitors are suitable for real-time/operational monitoring of DPM exposure in mines, as the method produces more timely management information.
- Stationary monitoring revealed significant levels of all particle sizes in the mine, as well as gases (NO<sub>2</sub> and CO) at significant levels. Particulate and gas levels were generally found to increase with depth in the mine, as well as activity level. Significant transient variation in particulate number, size and mass was found due to local activity level. Most notably, modal sizes of DPM/nanoparticles in the mine were found to be significantly lower than in previous studies (further into the nano range). Diesel engines consistently produce a peak particle size at or near 80 nm, however this study generally found significantly smaller particles. Given the nature of the mine, some interference from salt nuclei can be expected, however it is most likely that the decreased size was due to the widespread treatment of diesel particulate filters (DPFs) to most of the heavy plant.
- Correlations between DPM (EC) mass and particle count are provided for both the personal monitoring and stationary monitoring. While these are both significant, it should be noted there is a shift in particle count between the two correlations. This is expected due to the measurement limits of the different instruments used, the more sophisticated SMPS systems used for stationary monitoring having higher and lower size cut-off, and hence higher counts. While mathematical expressions for both correlations are given, these should be used with caution as they are clearly device (and possibly mine / equipment) specific. The correlations may however be suitable for mine managers or ventilation officers to verify quantitative exposure to nDPM in real-time.
- CFD analyses of key activities in the mine and re-circulation of exhaust air from the mine portal highlighted key areas where ventilation could be improved. Correlations between DPM and tracer gas were also developed, demonstrating the accuracy of the CFD method at determining mean SF<sub>6</sub> levels and determination of correlations between DPM and SF<sub>6</sub>.
- The deeper mine study found no significant changes in DPM due to pressures up to 1.4 atmospheres and ammonia concentrations up to 100 ppm. However significant changes

were found if ozone or UV light were introduced. Therefore care should be taken to ensure sources of UV and/or ozone are not present in the mine, particularly if diesel engines with selective catalytic reduction are in use. The findings from the deeper mine study can be found in Appendix-2.

This work has found that the widespread use of diesel particulate filters in the mine tended to result in a slightly reduced modal particle diameters in the mine, hence reducing particle sizes to which miners are exposed. Nevertheless, it was found that nanoparticle exposures and EC exposures possessed a reasonable (and more importantly statistically significant) correlation. Further analysis of the data in conjunction with appropriate biological/health data (separate report) should be (and will be) conducted to determine the most appropriate monitoring strategy for the future. i.e. whether traditional EC monitoring methods are sufficient or whether real time nanoparticle spectrometry is required. At minimum, real-time nanoparticle monitoring is a useful management tool, which correlated well with EC. Although real-time EC monitoring methods exist, trends in vehicle emissions are leading to lower EC/particle ratios, thereby a dual approach of EC and number concentration monitoring (ultrafine particle counting) seems most beneficial.

## Recommendations for Future Work

1. Tracer gas technology can be utilised effectively to identify the transport of nDPM between source and proximate diesel equipment operators and to better inform the efficiency of secondary ventilation systems. The key benefit of tracer gas studies is that they enable differentiation between nDPM sources and allow accurate characterisation of air flow behaviour. The information can be utilised to better inform the planning of administrative controls to manage activities around other major diesel activities.
2. It would be possible to correlate SF<sub>6</sub> tracer gas measurements with dispersal of nanoparticles if particle characterisation data is available from the sites studied using tracer gas. This would require particle analysers to be co-located with the tracer gas detectors. The unavailability of suitable power supplies precluded this activity being undertaken in the current study.

The tracer gas study performed at the underground mine focused on a development heading that was not serviced by an electricity supply and hence the Curtin Uni. team could not perform particle characterisation measurements at or in the vicinity of this heading.

Previous studies performed by ChemCentre in collaboration with USA researchers (confidential work not published) showed that the smaller the particle size (< 80 nm) the more likely the particle would behave like a gas.

It is recommended that future research on nDPM in underground mines includes both tracer gas study and particle characterisation at the same location.

3. It would be advisable that standards or guidelines be developed for (nano) DPM (personal) number concentration monitoring in underground mines, similar to the measurement standards for nanoparticle testing from vehicle exhausts which exist under the EURO emissions standards. i.e. requiring both particle counts and mass-based measurements.
4. If EC analysis method is to remain the main measure for exposure to diesel exhaust, a more extensive study to establish the relationship between nanoparticle number concentration and EC concentration should be conducted. Noting that such a method will only be relevant to average concentrations, and will not capture peak exposures or other temporal variation. The relationships presented here should be evaluated in other mines using a range of mobile plant and emissions controls.
5. Furthermore, CFD can be employed to optimize the ventilation flow rates in desired regions depending on the intended activities for a period of time. This can aid in greater control over the DPM and exhaust gas composition in the underground environment, and hence the occupational exposure to underground miners.
6. It is often challenging to design appropriate primary ventilation intakes and exhaust airways while expanding an existing mine for underground operations and while ensuring that these airways are sufficiently far from each other to avoid any re-circulation of DPM into the stream. CFD analysis of the existing AST1900 region of Sunrise Dam Gold Mine shows no significant DPM

re-circulation back into the intake. However, a simple change such as interchanging the inlet and outlet vents results in significant re-circulation, due to the topography of the mine. On discussion with the mine vent officers, either this good design was accidental or the work of CFD consultants when the design was planned, as standard mine ventilation tools cannot simulate such external systems. Therefore it is recommended to conduct such CFD studies when planning external mine intake/exit locations.

7. As mines become deeper and Selective Catalytic Reduction becomes more widespread, it is important to ensure no sources of ozone or UV light are present in the mine, to ensure formation of secondary organic aerosols does not occur.

## INTRODUCTION

Underground mining in Western Australia is heavily reliant upon diesel-powered equipment. This is likely to remain so for some time to come, especially when expanding the mining envelope to deeper mines. This is largely because cost and production efficiencies offered by diesel-powered equipment are unrivalled by any evolving technologies (e.g. battery-electric or plug-in electric equipment). Mining in the Eastern Goldfields is progressively getting deeper as shallow orebodies are depleted. The economics of underground mining will progressively become more reliant on larger diesel fleets as tramming distances increase with depth. Future green fields discoveries are likely to be under deep mineralogical cover in the east of the state and are likely to have dependence upon the cost and production efficiencies offered by using diesel equipment.

The use of diesel-powered equipment has been continuously increasing in underground metal/non-metal mines. This extensive utilization of diesel-powered equipment generates the potential for exposure of underground miners to diesel particulate matter (DPM), including nano diesel particulate matter (nDPM). The majority (by numbers) of the diesel particles are in the nano size range (<100 nm), hence the term nDPM. DPM has received considerable study, both in terms of emissions and health effects<sup>5-12</sup>. In 2012, the International Agency for Research on Cancer (IARC) classified diesel exhaust (DE, which includes DPM) as carcinogenic to humans (Group 1)<sup>1</sup>, largely based on data using EC as an indicator of DE and DPM/nDPM. It is well known that the modal diameter of diesel particulate emitted from a typical light or heavy vehicle exhaust is approximately 80 nm, which is therefore in the "nano" particle size range (<100 nm)<sup>8</sup>.

nDPM consists of an insoluble elemental carbon (EC) core and adsorbed/bound soluble organic carbon (OC). Whether the particles exist as a core-shell arrangement or a more amorphous structure are the subject of current research. Diesel particulate is a fractal agglomerate which is typically <300 nm when emitted from the exhaust, which is in the ultrafine or submicron particle size range and can therefore penetrate deeply into the lung. In addition to carcinogenic effects, DPM and related air pollutants have been linked to an extensive list of health effects ranging from short term irritation and headaches to smoking-like cardio-respiratory responses and systemic inflammation. It was reported that the exposure to nDPM for underground miners can be over 100 times than the normal environmental concentrations and over 10 times than that measured in other environments where the use of diesel engines are common. This makes the nDPM exposure level highest for underground mining and construction among other industries.

The exact components of DPM are not well understood, but are known to consist mainly of elemental carbon (EC), with adsorbed (or otherwise bound) organic carbon species, as well as a range of nano-metal oxides. It has not yet been confirmed conclusively which components of DPM cause cancer. Synergistic toxicological effects between gases and particles have however been reported<sup>13</sup>. However, the composition of DPM (size and ratio of components) is changing with improved engine technology, which leads to reductions in EC by mass. However, the changes in overall particle number (suspected to have increased significantly in the nDPM fractions) and chemical composition are still not clear and less well regulated, especially in Australia.

Emissions levels and exhaust aftertreatment technology to remove/reduce DPM and gaseous emissions are specified by the US (Tier) specifications for off-highway plant and the EU (Euro)

specifications for light vehicles and on-highway vehicles such as concrete Agi-trucks. Current specifications (at the time of this study) for new vehicles are Tier 4i and Euro 5 respectively. Many older plant are still in use, however many of these vehicles have been fitted with aftermarket treatment systems consisting of a diesel particulate filter (DPF) with or without a Diesel Oxidation Catalyst (DOC). Diesel particulate filters (DPFs) that are in use potentially have reduced filtration efficiencies at smaller particle sizes<sup>14</sup>, however have a high DPM removal efficiency overall. In order to comply with Euro 5/Tier 4i, many manufacturers have fitted selective catalytic reduction (SCR) to control NO<sub>x</sub> emissions. This technology is highly effective, however has been shown to release free ammonia from the exhaust, and in-turn generate "new" nanoparticles through nucleation<sup>15</sup>. Photocatalytic processes have also been found to generate new nanoparticles through similar processes (so called secondary aerosol or secondary organic nanoparticle formation)<sup>16</sup>. To our knowledge, this effect has not yet been studied in underground mines, where elevated pressure may allow catalysis of such particles (in lieu of photocatalysis).

There are critical gaps of knowledge on the character of nDPM and its behaviour in underground hard rock mine environments. No studies could be found by the authors that have properly evaluated size and concentrations of nDPM in underground mines, as existing studies have focussed on EC mass concentration measurements only.

The health implication of nDPM is believed to extend beyond the human lungs and the particles are small enough to diffuse into the blood stream through the alveoli and stress other parts of the body<sup>2-4</sup>.

To ensure the continued availability of using diesel equipment into the future as an option for operations in underground mines as the mining envelop expands with deeper mines, understanding and characterising nDPM is critical as it will need good management and controls going forward.

There is no national occupational standard for exposure to diesel emissions but the Australian Institute for Occupational Hygienists (AIOH) recommends an average mass based exposure limit of 100 µg/m<sup>3</sup> over eight hours. However, this reduces to 67 µg/m<sup>3</sup> for a 12 hour exposure and further reductions should be applied for a work week longer than 5 days in every 7 (AIOH). It should be noted that the reduced levels are not being routinely applied in industry. Underground production workers, including diesel loader operators and shotcreters, potentially face the highest risk of exposure if there is no regulatory requirement for use of personal protective equipment.

A few countries have set an exposure limit for diesel exhaust, such as the USA and Germany, and they generally recommend a higher limit than the AIOH<sup>17</sup>. However, there has been growing calls for a reduction in those guidelines. The Finnish Institute of Occupational Health announced, in December 2015, that it was recommending an underground limit of 20 µg/m<sup>3</sup>. Emissions standards for diesel engines are moving to number-based (as well as mass-based) emissions limits. Such number based standards may be imposed in occupational settings in future.

There are also calls for diesel machinery to be replaced with near-zero-emission electric equipment. However, it should be noted that electric motors have been found to emit metal-carbon nanoparticles.

In 2013, the WA Department of Mines and Petroleum (DMP) issued guidelines on the management of diesel emissions<sup>18</sup>, recommending for the industry to conduct regular sampling, implement

controls and develop an emissions management plan. The guideline also noted "some sites have not effectively controlled emissions" to below the AIOH guideline of  $100 \mu\text{g}/\text{m}^3$ .

A sampling program of 29 mine sites conducted by DMIRS<sup>19</sup> that same year found 10 of the sites exceeded the accepted exposure standard.

In order to address critical knowledge gaps on the character and behaviour of nDPM in an underground mine environment, this project will undertake a pilot study of one underground hard-rock mine to develop near-complete data on all processes involved in nDPM generation in an underground mine, from emission, through transport, physico-chemical changes post emission and exposure.

This pilot research study therefore aims to trial and develop a methodology of near-complete data on all processes involved in nDPM generation in one underground mine, from emission, through transport, physico-chemical changes post emission and exposure. The finalised methodology will then be implemented at other hard-rock mines in Western Australia.

The project objectives were to:

- Generate datasets on size, number concentration, mass concentration and EC concentration of nDPM at representative locations in one mine (including personal monitoring of representative tasks);
- Measure Real-Time ambient concentrations of gaseous components (CO, CO<sub>2</sub>, NO<sub>x</sub>, SO<sub>x</sub>, VOCs);
- Use tracer gas technology to study the diesel exhaust flow behaviour and relative source contribution to exposure of nearby equipment operators;
- Study the dispersal of gaseous and ultrafine particulate emissions from diesel exhaust, i.e. particularly nDPM, and the dilution efficiency of the mine ventilation with particular focus on the auxiliary ventilation at the face of development headings;
- Study physico-chemical composition of nDPM and changes post emission in an underground mine;
- To determine the impact of ventilation practises on the exposure levels and physico-chemical composition of particles;
- Perform chamber studies of simulated mine environments to investigate the physico-chemical composition of nDPM and changes post emission in existing mines;
- Improve the understanding of the impact of nano-diesel particulate matter (nDPM) on air quality; and
- Better inform nDPM exposure assessments in existing and future deeper mines.

This project also aimed to deliver the following potential benefits to industry and the community;

- Generate critical data and validated methodologies to better understand the behaviour of nDPM generation in an underground mine, from emission, through transport, physico-chemical changes post emission and exposure;
- More informed industry and government on the behaviour and characteristics of nDPM emitted by diesel equipment in real underground hard rock mines in Western Australia;

- Enable informed industry and government assessment and management of nDPM in underground mines in Western Australia; and
- To better inform management options for the cost effective running of underground mines into the future as the mining envelope expands with deeper mines.
- Better informed risk assessments and provision controls.

## REFERENCES

1. WHO Press Release: [http://press.iarc.fr/pr213\\_E.pdf](http://press.iarc.fr/pr213_E.pdf).
2. Nemmar, A., Al-Salam, S., Zia, S., Dhanasekaran, S., Shudadevi, M., Ali, B.H. Time-course effects of systemically administered diesel exhaust particles in rats (2010) *Toxicology Letters*, 194 (3), pp. 58-65.
3. Oberdörster, G., Sharp, Z., Atudorei, V., Elder, A., Gelein, R., Lunts, A., Kreyling, W., Cox, C. Extrapulmonary translocation of ultrafine carbon particles following whole-body inhalation exposure of rats (2002) *Journal of Toxicology and Environmental Health - Part A*, 65 (20), pp. 1531-1543.
4. Heidari Nejad S., Takechi R., Mullins B. J., Giles C., Larcombe A. N., Bertolatti D., Rumchev K., Dhaliwal S., and Mamo J. (2014), The effect of diesel exhaust exposure on blood–brain barrier integrity and function in a murine model, *J. Appl. Toxicol.*, 35, 41–47.
5. S. Saarikoski, K. Teinila, H. Timonen, M. Aurela, T. Laaksovirta, F. Reyes, Y. Vasques, P. Oyola, P. Artaxo, A. S. Pennanen, S. Junntila, M. Linnainmaa, R. O. Salonen, 48 R. Hillamo, Particulate matter characteristics, dynamics, and sources in an underground mine, *Aerosol Science and Technology* 52 (1) (2018) 114-122.
6. E. A. Lutz, R. J. Reed, V. S. T. Lee, J. L. Burgess, Comparison of personal diesel and biodiesel exhaust exposures in an underground mine, *Journal of Occupational and Environmental Hygiene* 14 (7) (2017) D102-D109.
7. M. Debia, C. Couture, P.-E. Njanga, E. Neesham-Grenon, G. Lachapelle, H. Coulombe, S. Halle, S. Aubin, Diesel engine exhaust exposures in two underground mines, *International Journal of Mining Science and Technology* 27 (4) (2017) 641-645.
8. E. A. Lutz, R. J. Reed, V. S. T. Lee, J. L. Burgess, Occupational exposures to emissions from combustion of diesel and alternative fuels in underground mining—a simulated pilot study, *Journal of Occupational and Environmental Hygiene* 12 (3) (2015) D18-D25.
9. A. D. Bugarski, E. G. Cauda, S. J. Janisko, J. A. Hummer, L. D. Patts, Effects of a diesel particulate: Filter regeneration process on aerosols in an underground mine, *Mining Engineering* 64 (12) (2012) 57-63.
10. K. C. Kimbal, L. Pahler, R. Larson, J. Vanderslice, Monitoring diesel particulate matter and calculating diesel particulate densities using grimm model 1.109 real-time aerosol monitors in underground mines, *Journal of Occupational and Environmental Hygiene* 9 (6) (2012) 353-361.
11. D. Bertolatti, K. Rumchev, B. J. Mullins, Assessment of diesel particulate matter exposure among underground mine workers, *WIT Transactions on Biomedicine and Health* 15 (2011) 11-20.

12. [8] P. A. Stewart, J. B. Coble, R. Vermeulen, P. Schlei\_, A. Blair, J. Lubin, M. Att\_eld, D. T. Silverman, The diesel exhaust in miners study: I. overview of the exposure assessment process, *Annals of Occupational Hygiene* 54 (7) (2010) 728-746.
13. S. Steiner, C. Bisig, A. Petri-Fink, B. Rothen-Rutishauser, Diesel exhaust: current knowledge of adverse e\_ects and underlying cellular mechanisms, *Archives of Toxicology* 90 (2016) 1541-1553.
14. B. J. Mullins, R. Mead-Hunter, S. Abishek, A. J. C. King, Diesel Particulate Filter - Dynamometer Test Results, Contract research report for Mammoth equipment and exhausts (Copy available from author), Mammoth Equipment and Exhausts (1974).
15. S. Amanatidis, L. Ntziachristos, B. Giechaskiel, A. Bergmann, Z. Samaras, Impact of selective catalytic reduction on exhaust particle formation over excess ammonia events, *Environmental Science and Technology* 48 (19) (2014) 11527-11534.
16. S. Samy, B. Zielinska, Secondary organic aerosol production from modern diesel engine emissions, *Atmospheric Chemistry and Physics* 10 (2010) 609-625.
17. <http://www.abc.net.au/news/2016-11-18/study-shows-miners-face-high-lung-cancer-risk-from-diesel/8035798>
18. DMIRS (Department of Mines, Industry Regulation and Safety) - Management of diesel emissions in Western Australian mining operations – Guideline, MIAC WA Department of Mines and Petroleum. 2013.
19. [http://www.dmp.wa.gov.au/Documents/Safety/RS\\_RSM\\_Mag\\_Jan14.pdf](http://www.dmp.wa.gov.au/Documents/Safety/RS_RSM_Mag_Jan14.pdf), p8-11.

## ACKNOWLEDGEMENTS

The research teams and authors of this report wish to acknowledge the funding support for this study from the Department of Mines, Industry Regulation and Safety (DMIRS) and from the Mineral Research Institute of Western Australia (MRIWA).

Also acknowledged is the in-kind support provided by AngloGold Ashanti, Barminto and the staff at the Sunrise Dam Gold Mine and from DMIRS, the Mining Industry Advisory Committee (MIAC) nDPM Work Group, and the Australian Institute of occupational Hygienists (AIOH) by providing scientific staff to participate in the scientific advisory panel for this project.

In-kind contribution to this project is also appreciated from ChemCentre, Curtin University, BBE Consulting Australasia and Queensland University of Technology. This work was also supported by the Pawsey Supercomputing Centre, Perth, Western Australia with funding from the Australian Government and the Government of Western Australia, through the use of its advanced computing facility and resources.

## **PART A: CHEMCENTRE/BBE STUDY**



BBE CONSULTING  
AUSTRALASIA



ChemCentre  
EXPERT SOLUTIONS

# A Study of Nano Diesel Particulate Matter (nDPM) Behaviour and Physico-chemical Changes in Underground Hard Rock Mines of Western Australia

## Part A: ChemCentre Study

MRIWA PROJECT M495

SILVIA BLACK, STEVE WILKINSON, MICHAEL PEARCE, YANG LIU, LEON VAN DEN BERG AND KATIE MANNIS

FINAL REPORT

13 June 2019

PREPARED FOR

MRIWA

100, Plain Street

East Perth WA 6004

## TABLE OF CONTENTS

TABLE OF CONTENTS.....	2
LIST OF FIGURES.....	3
LIST OF TABLES.....	4
1 SCOPE.....	5
2 PROCEDURE .....	5
2.1 Charging Activity, 22-10-17.....	10
2.2 Bogging Activity, 21-10-17 .....	12
2.3 Hydro-scaling Activity: (1) 19-10-17 and (2) 23-10-17 .....	13
2.4 Shotcreting Activity: (1) 20-10-17 and (2) 23-10-17 (after hydro-scaling).....	13
2.5 Truck Activity, 24-10-17 .....	17
2.6 Traverse Exercise, 23-10-17 .....	17
2.7 WATU WSX Portal interaction, 23-10-17 .....	18
3 RESULTS AND DISCUSSION .....	19
3.1 Air Sampling Results.....	19
3.2 Charging .....	22
3.3 Bogging.....	24
3.4 Hydro-scaling and Shotcreting .....	26
3.5 Truck Activity.....	32
3.6 Traverse Exercise.....	33
3.7 WATU WSX Portal Interaction .....	35
4 SUMMARY AND CONCLUSIONS .....	36
4.1 Key Findings and Recommendations .....	36
4.2 Conclusions .....	37
5 RECOMMENDATIONS FOR FUTURE WORK .....	38

## LIST OF FIGURES

Figure 1:	Tracer gas release at the Agi truck exhaust. ....	6
Figure 2:	Schematic of the ventilation air circuits at Cosmo decline, Astro 1900 of SDGM. ....	7
Figure 3:	Mine schematic showing the location of the WATU portals.....	9
Figure 4:	Tracer gas study during the Charging activity.....	10
Figure 5:	Particle size monitoring during the Charging activity. ....	11
Figure 6:	Map of tracer gas study during the Charging activity.....	11
Figure 7:	Tracer gas study of the Bogging activity.....	12
Figure 8:	Map of tracer gas study during the Bogging activity .....	12
Figure 9:	Tracer gas study during Hydro-scaling and Shotcreting activities.....	14
Figure 10:	Air sampling during the Shotcreting activity .....	14
Figure 11:	Map of tracer gas study during the Hydro-scaling and Shotcreting activities.....	15
Figure 12:	Tracer gas study during the Truck activity .....	16
Figure 13:	Map of tracer gas study during the Truck activity .....	16
Figure 14:	Map of tracer gas study during the Traverse Exercise. The Mirans are shown at position 1 ready to traverse across the heading from left to right.....	17
Figure 15:	Tracer gas study during the Traverse Exercise .....	18
Figure 16:	WATU WZX Portal interaction activity. Left picture: vent inlet. Right picture: vent outlet.....	18
Figure 17:	Tracer gas study during Charging activity .....	22
Figure 18:	Particle size distribution data during the Charging activity .....	23
Figure 19:	Tracer gas study data uring the Bogging activity .....	24
Figure 20:	Tracer gas study data during sequential Hydro-scaling and Shotcreting activity on 23-10-17. M1 = blue line, M2 = orange line, M3 = grey line and M4 = green line. ....	26
Figure 21:	Relative exposures (extracted form Figure 20) to the Spraymec and Agi truck operators during the Hydro-scaling activity .....	27

Figure 22: Relative exposures (extracted form Figure 20) to the Spraymec and Agi truck operators during the Hydro-scaling and Shotcreting activities, normalised to the same time scale. ....28

Figure 23: Relative exposures (extracted form Figure 20) to the Spraymec and Agi truck operators during the Shotcreting activity .....29

Figure 24: Tracer gas study data during Hydro-scaling activity on 19-10-17.....31

Figure 25: Tracer gas study data during Shotcreting activity on 20-10-17 .....31

Figure 26: Tracer gas study data during Truck activity .....32

Figure 27: Tracer gas study data during Traverse exercise.....33

Figure 28: Particle size distribution data during the Traverse exercise at Miran 1 position .....34

Figure 29: Tracer gas study data at the WATU WSX Portal .....35

**LIST OF TABLES**

Table 1: Ventilation conditions .....19

Table 2: Air sampling results for VOCs (ppb) during bogging, hydro-scaling and shotcreting activities .....20

Table 3: Air sampling results for ammonia, nitrogen dioxide and sulfur dioxide (ppm) during bogging, hydro-scaling and shotcreting activities .....21

Table 4: Air sampling results for CO and CO<sub>2</sub> (%) during bogging, hydro-scaling and shotcreting activities .....21

Table 5: Relative exposures calculated from integrated peak areas (extracted form Figure 20) experienced by the Spraymec and Agi truck operators during the hydro-scaling and shotcreting activities .....30

## 1 SCOPE

There are critical gaps of knowledge on the character of nDPM and its behaviour in underground hard rock mine environments.

The mine ventilation system plays an important role in mitigating human exposure to diesel particulate matter (DPM) emissions, exhaust gases and heat in underground mines. The mine's secondary ventilation systems are critical for diluting contaminants when working at the face of a heading.

It is important to understand the localized flow profiles on a "micro scale" to identify areas of improvement and ensure that the ventilation system is optimized to maximise dilution of exhaust gases. The application of tracer gas technology enables reliable measurements of flow behaviour and differentiation between the contribution of various contaminant sources including nano DPM (nDPM).

Previous studies performed by ChemCentre and in collaboration with USA researchers (confidential work not published) showed that the smaller the particle size (< 80 nm) the more likely the particle would behave like a gas. Hence, tracer gas technology is an appropriate tool for studying nanoparticles, such as nDPM.

The scope of this report and project component was to assess the applicability of tracer gas technology as a tool to study diesel exhaust flow behaviour and source contribution in an underground hard rock mine.

The objectives of this project component were to:

- Study the diesel exhaust flow behaviour and source contribution relative to proximate equipment operators using tracer gas technology;
- Study the dispersal of gaseous and ultrafine particulate emissions from diesel exhaust, particularly nDPM, and the dilution efficiency of the mine ventilation with particular focus on the auxiliary ventilation at the face of development headings;
- Measure Real-Time concentration of gaseous components (CO, CO<sub>2</sub>, NO<sub>x</sub>, SO<sub>x</sub>, VOCs) at the tracer gas monitoring sites;
- To determine the impact of ventilation practises on the exposure levels; and
- Improve the understanding of the impact of nano-diesel particulate matter (nDPM) on air quality from diesel exhaust emissions.

## 2 PROCEDURE

The project team aimed to undertake a study of diesel exhaust flow behaviour and source contribution in the underground mine at Sunrise Dam Gold Mine (SDGM) using tracer gas technology.

On-site tracer Gas study on the transport of nDPM between source and proximate equipment operators was performed to assess the real-time exposure of mineworkers (e.g. Service crews, Shotcreters, Jumbo drill operators, Bidders and Supervisory staff) and the efficiency of secondary

ventilation systems at each worksite over similar extended periods of time. The key benefit of tracer gas studies is that they enable differentiation between different potential nDPM sources and allow accurate characterisation of air flow behaviour.

The tracer gas sulfur hexafluoride ( $\text{SF}_6$ ) was released (from a pressurised cylinder) via Teflon tubing directly into the exhaust stream at the exhaust outlet pipe of the diesel engine under study (Figure 1). The aim was to achieve the best possible mixing of tracer gas with the exhaust as is practically possible and taking in consideration the high temperature of the exhaust within the exhaust pipe. Close mixing of the tracer gas with the exhaust gas would then allow the tracer gas to behave in a similar manner to the exhaust gases and nDPM in the heading. Measurements of the concentrations of  $\text{SF}_6$  were taken in real time at various receiving sites using Fourier-Transform Infrared Spectrometers (FTIR). Thus, the tracer gas was used as a surrogate to characterise and “visualise” the flow profile and the build-up and decay of nDPM in the development heading and other relevant areas in the mine.

The ChemCentre team performed tracer gas study (19<sup>th</sup> - 24<sup>th</sup> October 2017), air sampling (19<sup>th</sup> - 21<sup>st</sup>, 23<sup>rd</sup> October) and particle size monitoring (22<sup>nd</sup> and 23<sup>rd</sup> October) in the development heading at Cosmo decline, Astro 1900 of SDGM to study the behaviours and characteristics of nDPM. Figure 2 shows a schematic of the ventilation air circuits of the study site.



Figure 1: Tracer gas release into the Agi truck exhaust.

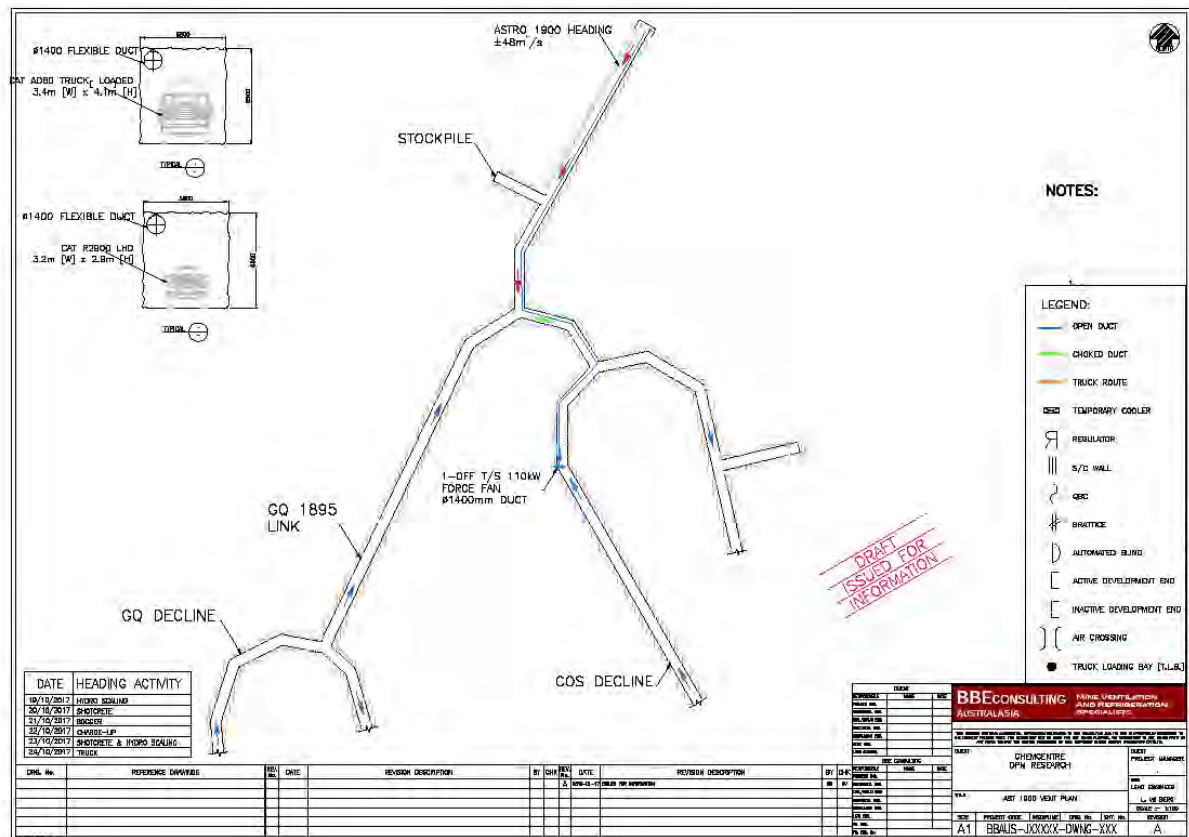


Figure 2: Schematic of the ventilation air circuits at Cosmo decline, Astro 1900 of SDGM.

The ventilation arrangement in Astro 1900 where the study was undertaken comprised of a typical twin stage 110kW axial flow fans, force ventilation at the development heading via 1400mm duct. The secondary fans were located in the trucking decline. The distance from the fans to the face was approximately 200 m. The fans typically supply about 45m<sup>3</sup>/s with approximately 35m<sup>3</sup>/s supplied to the face after leakage. This yields an air speed of 1.4m/s. The duct discharge end was located approximately 25 m from the working face.

The tracer gas study, air sampling and particle size monitoring activities are detailed below.

- a) Tracer gas study – four MIRAN FTIR units (MIRAN: M1, M2, M3 and M4) were utilised to study the typical development heading sequence of activities, which are described below with the respective figures demonstrating the work done and location of tracer release, monitoring and sampling sites.
  1. **Charging** (Figures 4, 5 and 6) - the tracer gas was released at the exhaust pipe outlet while the diesel engine was running and it was switched off while the engine was not running. As a result the gas was released while the charge up rig drove into and out of the level.
  2. **Bogging** (Figures 7 and 8) - the tracer gas was released into the loader exhaust while it was bogging the dirt from the development face into the stockpile.

3. **Hydro-scaling** (Figures 9, 10 and 11) - the tracer gas was released into the exhaust of the Spraymec machine while it was scaling the loose rock with water and compressed air.
4. **Shotcreting (Agi truck and Spraymec)** (Figures 9, 10 and 11) - the tracer gas was released first into the Agi truck exhaust while the machine was unloading shotcrete as the spraymec was in operation. Then the tracer gas was moved to release from the Spraymec exhaust while the machine was spraying.
5. **Truck** (Figures 12 and 13) - the tracer gas was set up to release into the tailpipe of the truck while the truck travelled from surface, down the decline past the fan that feeds the test level, got loaded and travelled back up past the test level again to surface.

In Addition to the mining activities, the following was also studied;

6. **Traverse exercise** (Figures 14 and 15); This relates to the heading that was used for the tracer gas analysis of each activity. The objective of this particular experiment was to determine if the fresh air supplied by the duct is distributed uniformly (or not) along the heading cross section (left to right). For example does the fresh air form a 'layer' along the sidewall where the duct is positioned or is it effectively distributed along the entire heading width. A second objective was to determine the penetration distance of fresh air into the blind heading from the duct discharge. For example, with the distance to the face does the fresh air reach the end of the heading or does the end experience a 'blind spot'.
7. **WATU WSX Portal interaction** (Figures 3 and 16). While the research team were working underground, an opportunity arose to apply trace gas technology to study the WATU WSX Portal interaction. This study was undertaken at the exhaust portal which is located on opposite side of the pit to the intake portal inside the open pit. The objective of this study was to determine if any of the contaminants in the exhaust will recirculate back into the mine via the intake portal which is about 100m away from the exhaust. **Note:** This should be not be confused with the Astro Daniel portals where the intake and returns are directly adjacent to each other. There was no time during the site visit to also study this portal interaction.

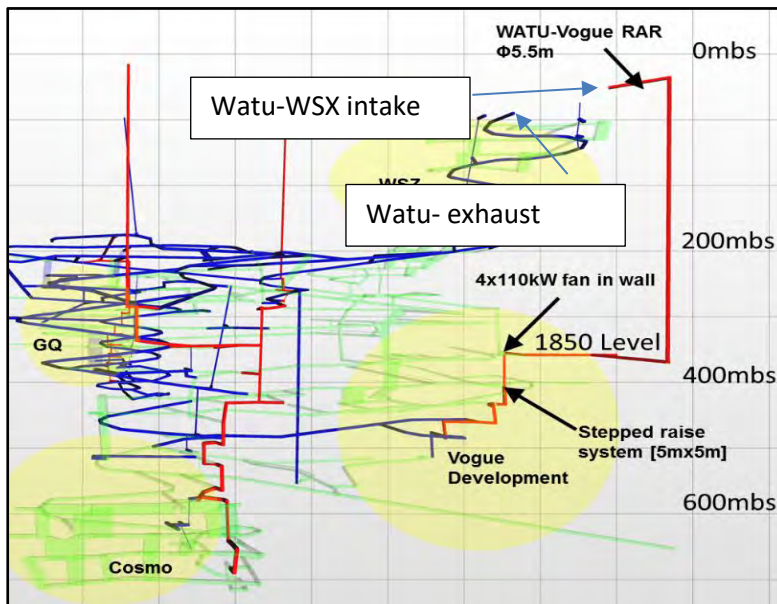


Figure 3: Mine schematic showing the location of the WATU portals.

- b) Air sampling – Summa canisters were used to collect samples for VOCs, CO, CO<sub>2</sub>, and NH<sub>3</sub> analysis. Pumps, tubes and filters were used to collect separate atmospheric samples for NO<sub>x</sub> and SO<sub>x</sub> as per the NIOSH methods. The air sampling was performed during the following activities:
- Bogging;
  - Hydro-scaling; and
  - Shotcreting - Agi truck and Spraymec (Figure 10).
- c) Particle size monitoring – A Palas Frog analyser was used for monitoring mass fractions of PM<sub>1</sub>, PM<sub>2.5</sub>, PM<sub>4</sub>, PM<sub>10</sub> and TSP during the following activities:
- Charging (Figure 5); and
  - Traverse exercise.
- Note: the Palas Frog analyser was borrowed while on-site from the Curtin research team for a trial run during the tracer gas study.

Passive sampling tubes were supplied by ChemCentre and used to collect personal samples for VOCs and for SO<sub>x</sub> and NO<sub>x</sub> analysis during the study part done by the Curtin Uni group.

## 2.1 Charging Activity, 22-10-17

The SF<sub>6</sub> gas release box was strapped to the charge up rig on the railing and the gas tube was extended down to the tailpipe under the vehicle. SF<sub>6</sub> release began at the intersection of COS decline and GQ link. The charge-up rig drove into the heading and when stationary during the activity the diesel engine kept running. SF<sub>6</sub> was then turned off at end of heading. Overall SF<sub>6</sub> was released for 59 min at 2.0 L/min. The Mirans M1, 2 and 3 were positioned as described below; M1 nearest face of heading, ~ 5m from end of vent bag. M2 in open charge-up cabin with PSA on driver's seat. M3 at the stockpile Cos Decline and M4 hang opposite electrical cuddy (GQ Link). Charge-up drive into heading (activity started).

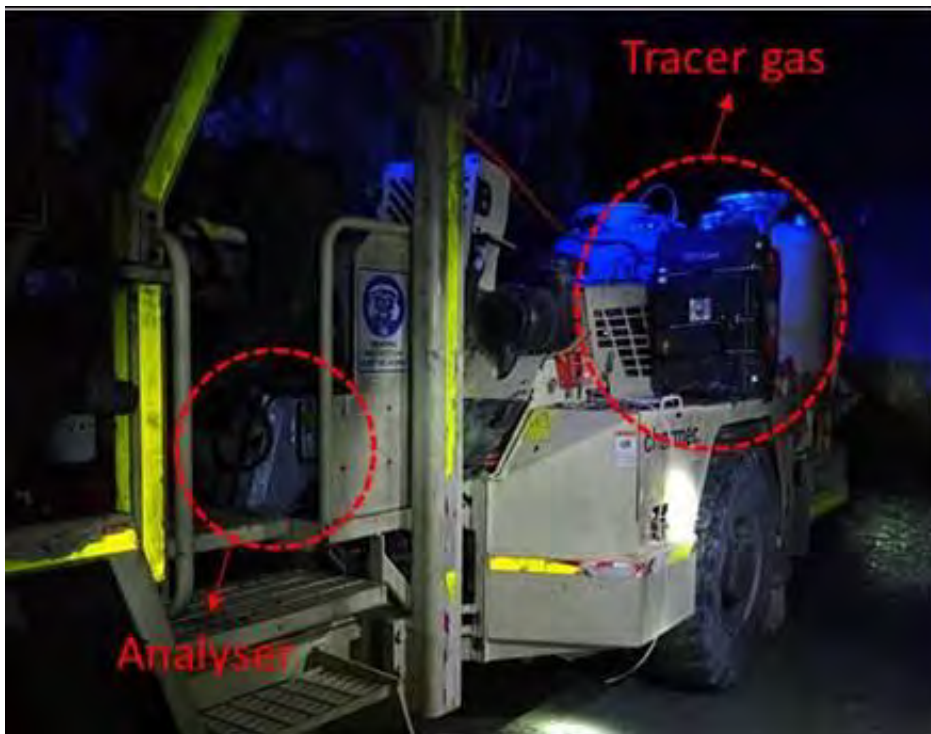


Figure 4: Tracer gas study during the Charging activity.



Figure 5: Particle size monitoring during the Charging activity.

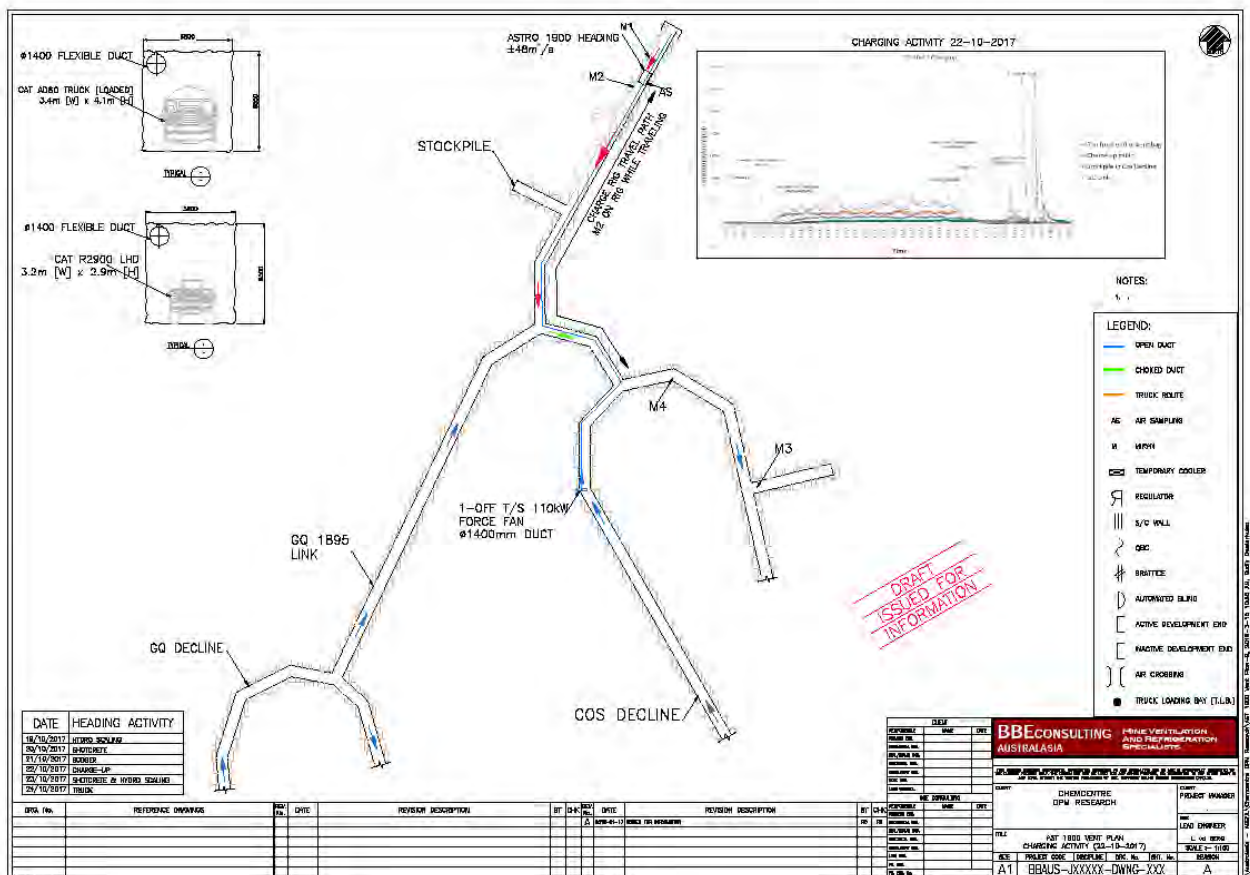


Figure 6: Map of tracer gas study during the Charging activity.

## 2.2 Boggging Activity, 21-10-17

SF<sub>6</sub> was released from the boggger at the tailpipe under the vehicle using 2 canisters in parallel (bracketed to the boggger) and gas tube was extended down to the tailpipe. Overall, SF<sub>6</sub> was released for 42 min at 2.0 L/min. The Mirans M1, 2 and 4 were positioned as described below; M1 and particle size analyser (PSA) at rope-line. Air sampling also at this M1 position. M2 in cabin with boggger operator. M3 at the stockpile Cos Decline. M4 hang in electrical cuddy (GQ Link). No readings were obtained from M4.



Figure 7: Tracer gas study on the Boggging activity.

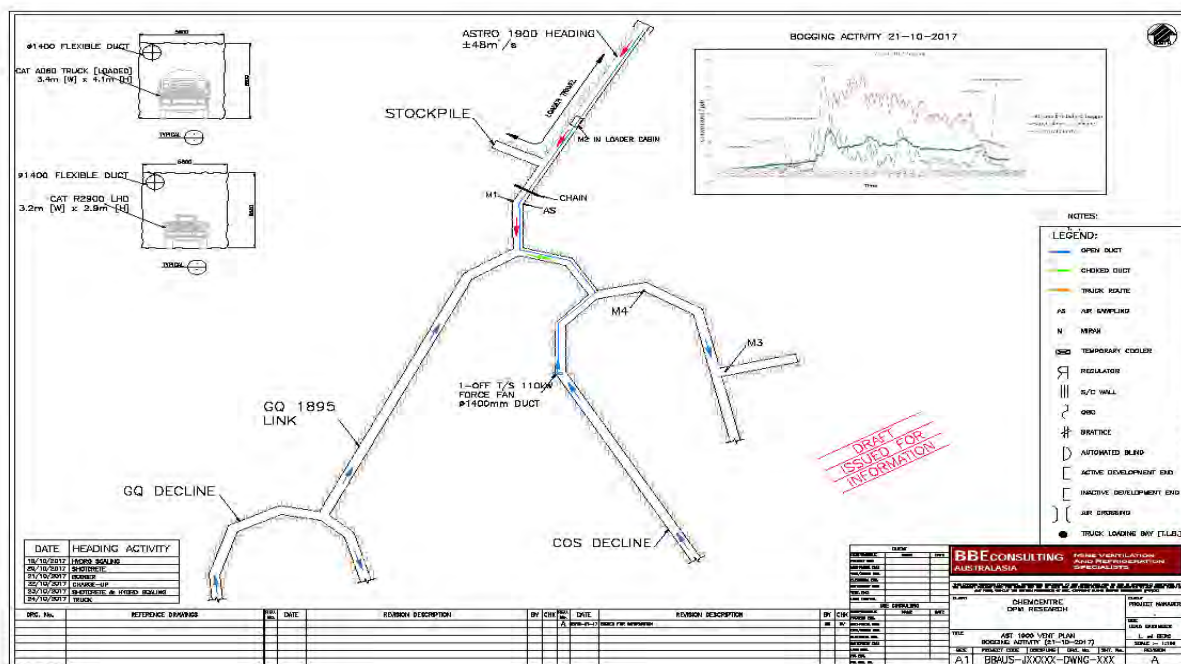


Figure 8: Map of tracer gas study during the Boggging activity.

## 2.3 Hydro-scaling Activity: (1) 19-10-17 and (2) 23-10-17

**During (1):** M1 at spraymec operator.

Noted increase in M1 readings as operator moved Hydroscale from right to left of tunnel.

M2 at Agi truck operator. M3 at the stockpile Cos Decline and M4 hang in electrical caddy in GQ Link.

No readings were obtained from M4. Air sampling at M1 for VOCs, CO, CO<sub>2</sub> and NH<sub>3</sub>.

**During (2):** Didn't reach steady state due to hydro-scaling activity finishing too soon (~ 10 min activity). No air sampling done.

M1 at spraymec operator. M2 at Agi truck operator. M3 at the stockpile Cos Decline and M4 hanging opposite the electrical caddy in GQ Link.

## 2.4 Shotcreting Activity: (1) 20-10-17 and (2) 23-10-17 (after hydro-scaling)

Released SF<sub>6</sub> at Agi truck first. Once the SF<sub>6</sub> concentration had reached a steady state air samples were taken near Agi truck operator (M2 position). Spraymec operator stopped mid-activity. Then stopped SF<sub>6</sub> release & allowed to clear (~10 min). Resumed release of SF<sub>6</sub> at spraymec once shotcreting activity was resumed. Once the SF<sub>6</sub> concentration had reached a steady state air samples were taken near the Spraymec operator (M1 position). Air sampling at M1 and M2 for VOCs, CO, CO<sub>2</sub>, NH<sub>3</sub>, NO<sub>x</sub> and SO<sub>x</sub>. SF<sub>6</sub> was released at 2.0 L/min.

**During (1):** M1 at spraymec operator.

M2 at Agi truck operator. M3 at the stockpile Cos Decline and M4 hang in electrical caddy in GQ Link. No readings were obtained from M4.

08:18 (8.20) spraymec false start (small SF<sub>6</sub> release)

08:20 Spraymec false start end

(8.21) SF<sub>6</sub> released at Agi truck

08:24 Noted broken filter on SF<sub>6</sub> Release Box, Moved box close to Agi exhaust. Began work to bypass filter and release into the exhaust

08:27 completed filter bypass, releasing to the exhaust. Regulator pressure 60 psi

(8.30) shotcrete activity stopped at mid-activity

08:32 SF<sub>6</sub> released stopped

(8.37) shotcrete activity re-started

08:37 SF<sub>6</sub> on

08:45 shotcrete activity stopped

08:45 SF<sub>6</sub> off

08:53 truck reversed out of the tunnel

08:56 walk M1 back down tunnel

08:57 M1 in stockpile

M1 & M2 still on when back to the LV & values went up from ~100 to ~500.

**During (2):** M1 at spraymec operator. M2 at Agi truck operator. M3 at the stockpile Cos Decline and M4 hang in electrical caddy in GQ Link.



Figure 9: Tracer gas study during the Hydro-scaling and Shotcreting activities.



Figure 10: Air sampling during the Shotcreting activity.

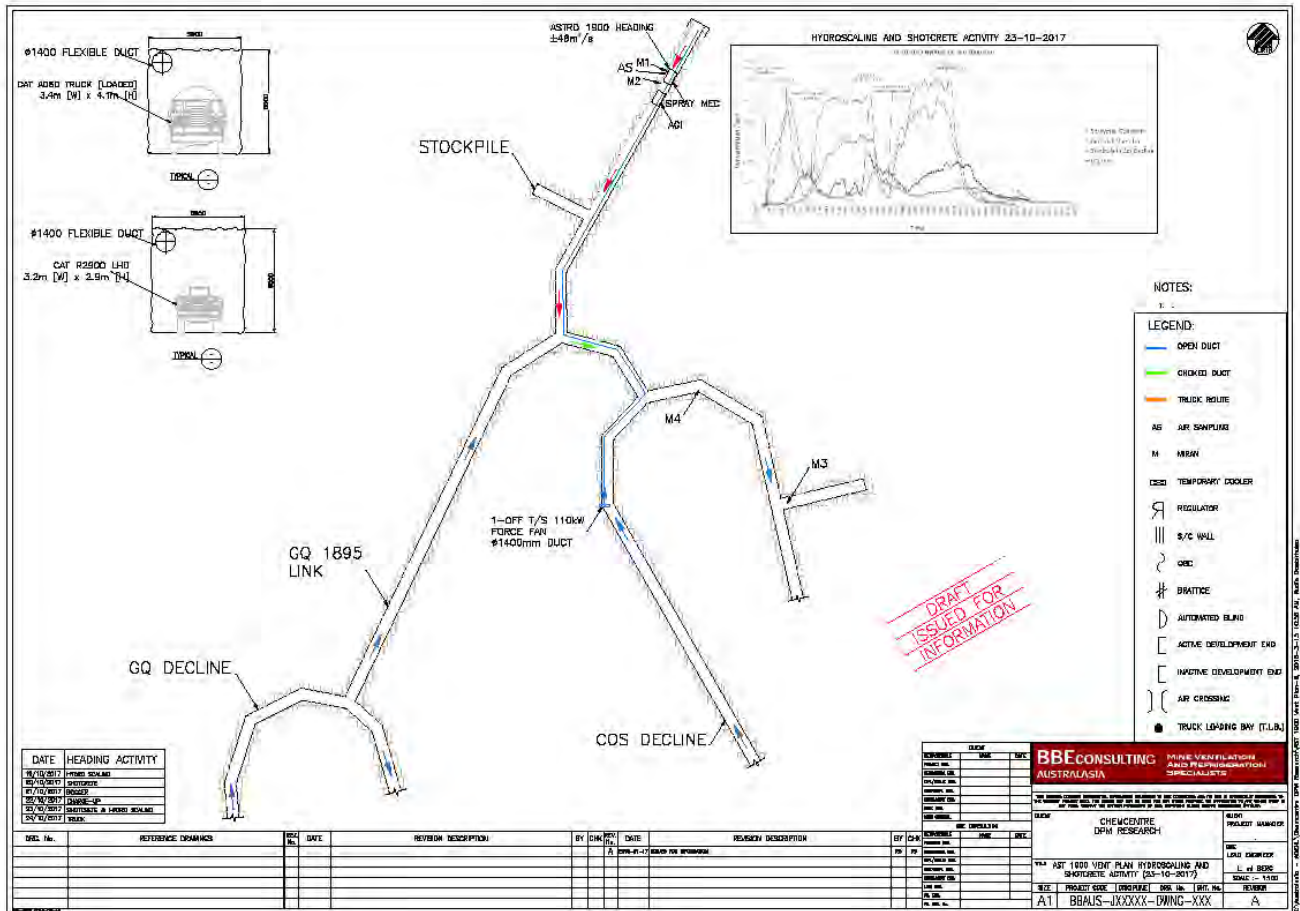


Figure 11: Map of tracer gas study during the Hydro-scaling and Shotcreting activities.

## 2.5 Truck Activity, 24-10-17

The SF<sub>6</sub> release box was fixed to the truck with a sturdy bracket (see Fig 12) supplied by the SDGM workshop. SF<sub>6</sub> release started at the portal and continued whilst the truck drove into the mine and from the loading area. M1 was positioned in the cabin behind the driver under the control of research staff.

M2 in the development heading, M3 at the stockpile Cos Decline and M4 hang in Cos decline, just below the Hammer head (Figure 13).



Figure 12: Tracer gas study during the Truck activity.

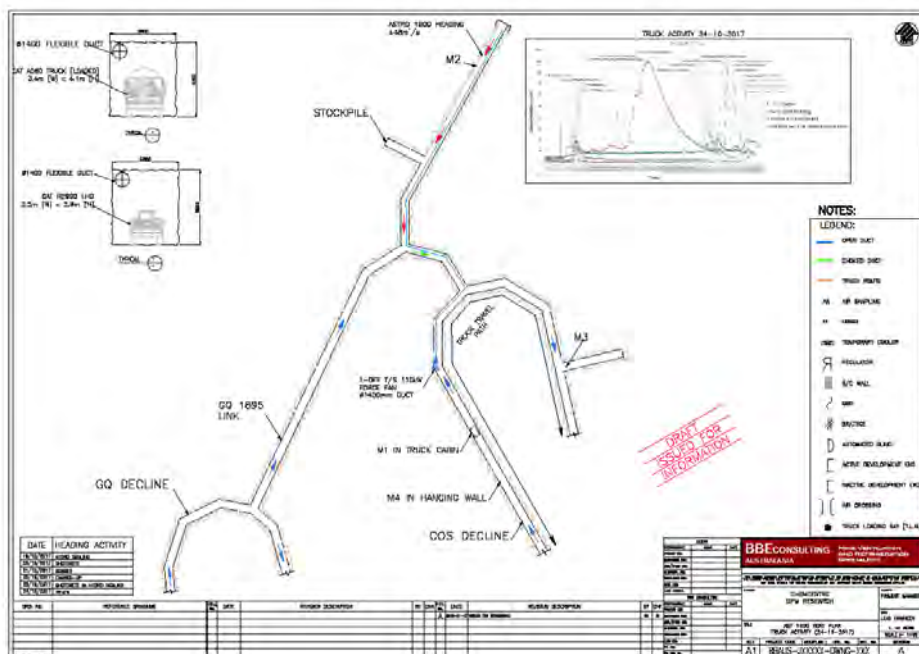


Figure 13: Map of tracer gas study during the Truck activity.

## 2.6 Traverse Exercise, 23-10-17

Vent bag 27 m from face.

M1 6.5 m from face, 5 m intervals for each MIRAN back from face.

SF<sub>6</sub> released from inside vent bag 15 m from end of bag.

Initial position left side of tunnel. Moving from left to right when facing the face of the heading (Figures 14 and 15). M1 (+ SPA)

08:50 SF<sub>6</sub> Release start.

08:57 Change Position to 1/3 of way across tunnel i.e. position 2 (Figure 14).

09:03 Change Position to 2/3 of way across tunnel i.e. position 3.

09:08 Change Position to right side of tunnel i.e. position 4.

09:10:30 Spraymec, Agi arrive in tunnel.

(09:12) Move MIRANs to clearance positions (M4 in front of vent bag, 11.5 m from face) (M1-3 across tunnel 6.5 m from face), turn of tracer gas.

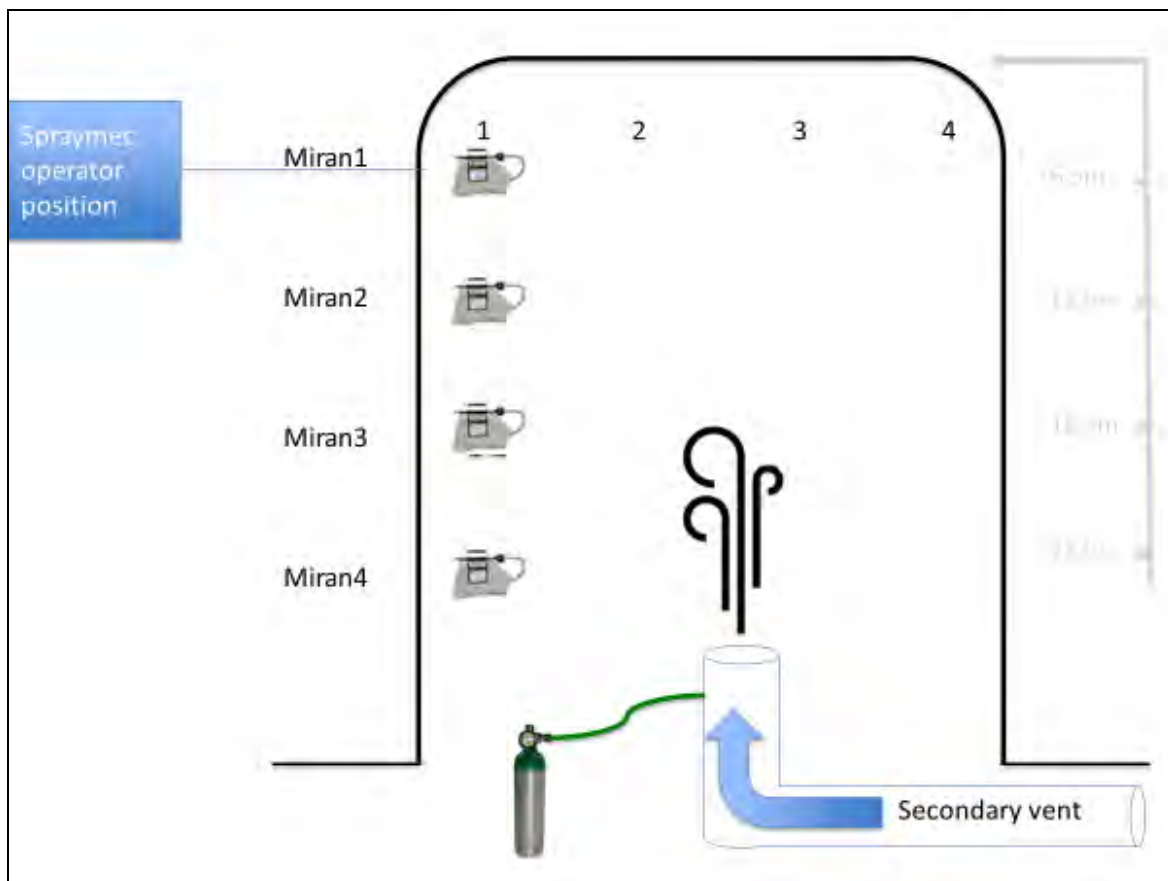


Figure 14: Layout of Mirans and tracer gas release during the Traverse exercise. The Mirans are shown at position 1 ready to traverse across the heading from left to right.



Figure 15: Tracer gas study during the Traverse exercise.

## 2.7 WATU WSX Portal interaction, 23-10-17

Released SF<sub>6</sub> at the vent exhaust and measured at the vent inlet with M1 & M2 (M3 & M4 battery run out & error message respectively).

SF<sub>6</sub> released at vent outlet (Figure 16, right picture) as a 5-min pulse at 92 L/min. Measured SF<sub>6</sub> at vent inlet.



Figure 16: WATU WSX Portal interaction activity. Left picture: vent inlet. Right picture: vent outlet.

### 3 RESULTS AND DISCUSSION

As mentioned earlier (Section 3), the ventilation arrangement in Astro 1900 where the study was undertaken (Figure 2) comprised of a typical twin stage 110kW axial flow fans (i.e. 2, force ventilation at the development heading via 1400mm duct. The secondary fans were located in the trucking decline. The distance from the fans to the face was approximately 200 m. The duct discharge end was located approximately 25 m from the working face.

A summary of the heading ventilation measurements taken during different activities is given in Table 1.

Table 1: Ventilation Conditions.

Activity at Heading	Size of drive	Rated kW	Required airflow	Measured airflow	Condition by visual inspection
Hydro-scaling	5.5 m x 6.0 m	90 kW	4.5 m <sup>3</sup> /s	30 m <sup>3</sup> /s	Very good
Shotcreting	5.5 m x 6.0 m	346 kW [90 +256 kW]	17.3 m <sup>3</sup> /s	31 m <sup>3</sup> /s	Good
Charging	5.5 m x 6.0 m	110 kW	5.5 m <sup>3</sup> /s	29 m <sup>3</sup> /s	Good
Bogging	5.5 m x 6.0 m	305 kW	15.25 m <sup>3</sup> /s	28 m <sup>3</sup> /s	Good

Note: The linear velocity was between 0.8 and 1.0 m/s.

Tracer gas study, air sampling and particle size monitoring results and charted data are presented below for each activity studied at the SDGM underground site.

#### 3.1 Air Sampling Results

Air samples for VOCs, CO, CO<sub>2</sub>, NH<sub>3</sub>, NO<sub>x</sub> and SO<sub>x</sub> were taken during the following activities;

- Bogging activity (21-10-17) at the M1 position (Figure 8), at the rope line together with particle size distribution data collection;
- Hydro-scale activity (19-10-17) at M1 position (Figure 11), next to the Spraymec operator;
- Shotcrete activity (20-10-17) at M1 position (Figure 11), next to the Spraymec operator;
- Shotcrete activity (23-10-17) at M2 position (Figure 11), next to the Agi truck operator; and
- Shotcrete activity (23-10-17) at M1 position (Figure 11), next to the Spraymec operator.

The air sampling data is displayed in Tables 2, 3 and 4. The levels measured for VOCs, CO, CO<sub>2</sub>, NH<sub>3</sub>, NO<sub>x</sub> (NO + NO<sub>2</sub> reported as NO<sub>2</sub>) and SO<sub>2</sub> were below both the Occupational Exposure Guidelines<sup>2</sup> for both the Short Term Exposure Limit (STEL) and the Time Weighted Average (TWA) levels, except for CO during hydro-scaling and NO<sub>2</sub> during the shotcreting and bogger activities.

Table 2: Air sampling results for VOCs (ppb) during bogging, hydro-scaling and shotcreting activities.

Analyte (ppb)	Occupational Exposure Guidelines		Hydro-scale 19-10-17	Shotcrete 20-10-17	Bogger 21-10-17	Agi truck 23-10-17	Spraymec 23-10-17
	TWA <sup>1,2</sup>	STEL <sup>3</sup>					
Benzene	1000	N/A	28	46	230	23	57
Benzene, 1,2,4-trichloro-	N/A	N/A	< 1.3	< 1.3	< 1.3	< 1.5	< 1.4
Benzene, 1,2,4-trimethyl-	25000	N/A	< 11	< 11	< 11	< 13	< 12
Benzene, 1,2-dichloro-	25000	N/A	< 11	< 11	< 11	< 13	< 12
Benzene, 1,3,5-trimethyl-	25000	N/A	< 1.2	< 1.2	< 1.2	< 1.4	< 1.3
Benzene, 1,3-dichloro-	N/A	50000	< 11	< 11	< 11	< 13	< 12
Benzene, 1,4-dichloro-	25000	50000	< 11	< 12	< 12	< 13	< 12
Benzene, chloro-	10000	N/A	< 1.2	< 1.2	< 1.2	< 1.4	< 1.3
Benzene, ethyl-	100000	125000	< 1.2	< 1.2	2.1	< 1.4	< 1.3
Buta-1,3-diene, 1,1,2,3,4,4-hexachloro-	20	N/A	< 12	< 12	< 12	< 14	< 13
Butadiene	10000	N/A	< 1.2	< 1.2	20	< 1.4	< 1.3
Carbon tetrachloride	100	N/A	< 1.2	< 1.2	< 1.2	< 1.4	< 1.3
Chloroform	2000	N/A	< 1.2	< 1.2	< 1.2	< 1.4	< 1.3
Ethane, 1,1,1,2-tetrachloro-	100000	200000	< 1.2	< 1.2	< 1.2	< 1.4	< 1.3
Ethane, 1,1,1-trichloro-	1000	N/A	< 1.2	< 1.2	< 1.2	< 1.4	< 1.3
Ethane, 1,1,2-trichloro-	10000	N/A	< 1.2	< 1.2	< 1.2	< 1.4	< 1.3
Ethane, 1,1,2-trichloro-1,2,2-trifluoro	1000000	1250000	< 1.2	< 1.2	< 1.2	< 1.4	< 1.3
Ethane, 1,1-dichloro-	100000	N/A	< 1.2	< 1.2	< 1.2	< 1.4	< 1.3
Ethane, 1,2-dibromo-	N/A	N/A	< 1.2	< 1.2	< 1.2	< 1.4	< 1.3
Ethane, 1,2-dichloro-	10000	N/A	< 1.2	< 1.2	< 1.2	< 1.4	< 1.3
Ethane, chloro-	1000000	N/A	1.8	< 1.2	< 1.2	< 1.4	< 1.3
Ethane, dichlorotetrafluoro-	1000000	N/A	< 1.2	< 1.2	< 1.2	< 1.4	< 1.3
Ethene, 1,1-dichloro-, (E)-	5000	N/A	< 1.2	< 1.3	< 1.3	< 1.4	< 1.3
Ethene, 1,2-dichloro-, (E)-	200000	N/A	< 1.2	< 1.2	< 1.2	< 1.4	< 1.3
Ethene, chloro-	5000	N/A	< 1.2	< 1.2	< 1.2	< 1.4	< 1.3
Ethylene, tetrachloro-	50000	150000	< 1.2	< 1.2	< 1.2	< 1.4	< 1.3
Ethylene, trichloro-	10000	40000	< 1.2	< 1.2	< 1.2	< 1.4	< 1.3
Methane, bromo-	5000	N/A	< 1.2	< 1.2	< 1.2	< 1.4	< 1.3
Methane, chloro-	50000	100000	< 1.2	< 1.2	< 1.2	< 1.4	< 1.3
Methane, dichlorodifluoro-	1000000	N/A	< 1.2	< 1.2	< 1.2	< 1.4	< 1.3
Methane, trichloromonofluoro-	N/A	N/A	< 1.2	< 1.2	< 1.2	< 1.4	< 1.3
Methylene chloride	50000	N/A	< 1.2	< 1.3	< 1.3	< 1.4	< 1.3
Prop-1-ene, 1,3-dichloro-, (E)-	1000	N/A	< 1.2	< 1.2	< 1.2	< 1.3	< 1.2
Prop-1-ene, 1,3-dichloro-, (Z)-	1000	N/A	< 1.2	< 1.3	< 1.2	< 1.4	< 1.3
Propane, 1,2-dichloro-	75000	110000	< 1.2	< 1.2	< 1.2	< 1.4	< 1.3
Styrene	50000	100000	3.5	2.1	23	1.6	5.6
Toluene	50000	150000	1.3	1.7	12	2.4	4.0
Xylene, m- & p-	80000	150000	< 2.3	< 2.4	< 2.4	< 2.7	< 2.5
Xylene, o-	80000	150000	< 1.2	< 1.2	< 1.2	< 1.4	< 1.3

N/A – not applicable - no guideline value available from Safe Work Australia Workplace Exposure standards for Airborne Contaminants.

Table 3: Air sampling results for ammonia, nitrogen dioxide and sulfur dioxide (ppm) during bogging, hydro-scaling and shotcreting activities.

Analyte (ppm)	Occupational Exposure Guidelines		Hydro-scale 19-10-17	Shotcrete 20-10-17	Bogger 21-10-17	Agi truck 23-10-17	Spraymec 23-10-17
	TWA <sup>1,2</sup>	STEL <sup>3</sup>					
Ammonia, NH <sub>3</sub>	25	35	0.3	<0.05	<0.05	<0.05	<0.05
Nitrogen dioxide, NO <sub>2</sub>	3	5	NS*	34*	7.3*	18*	11*
Nitrogen monoxide, NO	25	N/A					
Sulphur dioxide, SO <sub>2</sub>	2	5	NS	< 0.2	< 0.1	< 0.3	< 0.3

NS = not sample taken. \* NO + NO<sub>2</sub> (i.e. NO<sub>x</sub>) reported as NO<sub>2</sub>. N/A – not applicable - no guideline value available from Safe Work Australia Workplace Exposure standards for Airborne Contaminants.

Table 4: Air sampling results for CO and CO<sub>2</sub> (%) during bogging, hydro-scaling and shotcreting activities.

Analyte (%)	Occupational Exposure Guidelines		Hydro-scale 19-10-17	Shotcrete 20-10-17	Bogger 21-10-17	Agi truck 23-10-17	Spraymec 23-10-17
	TWA <sup>1,2</sup>	STEL <sup>3</sup>					
Carbon dioxide, CO <sub>2</sub>	0.5	3	< 0.3	< 0.3	< 0.3	< 0.3	< 0.3
Carbon monoxide, CO	0.003	N/A	0.2	< 0.05	< 0.05	< 0.05	< 0.05

N/A – not applicable - no guideline value available from Safe Work Australia Workplace Exposure standards for Airborne Contaminants.

<sup>1</sup> TWA = **Time Weighted Average** - The TWA for the exposure to a chemical can be used when both the chemical concentration and time for exposure varies over time. It is thus used as the average exposure to a contaminant to which workers may be exposed without adverse effect over a period such as in an 8-hour day or 40-hour week (an average work shift). They are usually expressed in units of ppm (volume/volume) or mg/m<sup>3</sup>

<sup>2</sup> Data taken from Safe Work Australia Workplace Exposure Standards for Airborne Contaminants. Date of Effect: 18 April 2013 and NIOSH International Chemical Safety cards <https://www.cdc.gov/niosh/ipcs/default.html>.

<sup>3</sup> STEL = **Short term exposure limit** – The STEL is the time-weighted average maximum airborne concentration of a substance calculated over a 15-minute period the STEL value is acceptable if the time-weighted average is not exceeded.

### 3.2 Charging

During the charging activity, the tracer gas was released at the exhaust pipe outlet during the whole charging activity including while the charge up rig drove into and out of the level (Figures 4, 5 and 6). The positions of the four Miran units during this activity are shown in Figure 6. The tracer gas concentration measured during the charging activity was charted versus time (Figure 17).

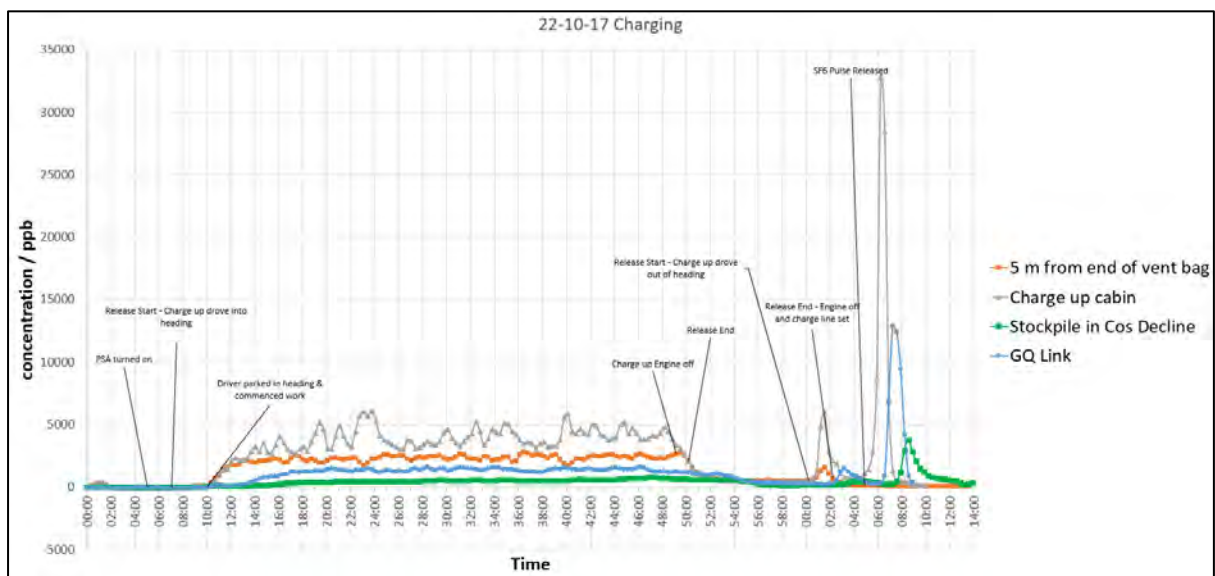


Figure 17: Tracer gas study data during Charging activity.

The variations in tracer gas concentration in the cabin (grey trace line in Figure 17) may correlate with varying engine loading from the charge up. These concentration variations are unlikely to be significant as they fall within experimental error ( $\pm 10\%$ ) of the Miran instrument. An interesting observation is that the tracer gas concentration in the cabin (which was open all the time, grey line) is higher when compared to the tracer gas concentration in the general heading (orange line). This is perhaps because the face is well ventilated by the secondary ventilation allowing the heading to be scoured and cleared of tracer gas. This reading suggests that the secondary ventilation may have less of an impact on the exhaust gasses at the machine's location and its ability to dilute the gasses that reach the cabin. It is anticipated that nDPM will behave similarly to the tracer gas. More data is required from further studies to inform how to best improve ventilation scouring in the charge up cabin. Note that no operator was in the cabin during the charging activity, during which time the operator was in the basket (charge up crew location).

Due to access limitations that apply to mine site visitors measurements could not be taken at the charge up crew location. However based on the effective scouring of the tracer gas by the secondary ventilation it is inferred that effective scouring at the crew location is achieved. Future studies should attempt some measurement of tracer gas levels at the face where the charge up crew is located.

The green line tracer gas reading (Figure 17) was taken downstream of the heading in through ventilation. The trend suggests that the mechanism by which  $\text{SF}_6$  is moving through the decline is

not by diffusion but mainly by active transport, thus moving relatively quickly through the decline with tracer gas levels being diluted quickly.

During the charging activity, a Palas Frog particle size analyser (PSA) was used for monitoring mass fractions of PM<sub>1</sub>, PM<sub>2.5</sub>, PM<sub>4</sub>, PM<sub>10</sub> and TSP (Figure 18) at position M2 (Figure 6), in the open charge-up cabin with the PSA on the driver’s seat, near Miran M2 (Figure 17).

Relatively higher concentrations (approximately 70 to 100 µg/m<sup>3</sup>) of PM 1 (< 1000 nm size, Figure 18) were measured between 18 and 40 minutes and constituted approximately 30% of the total particles measured. During this period the vehicle had been stationary and charging was in progress (Figure 17, M2 in charge up cabin).

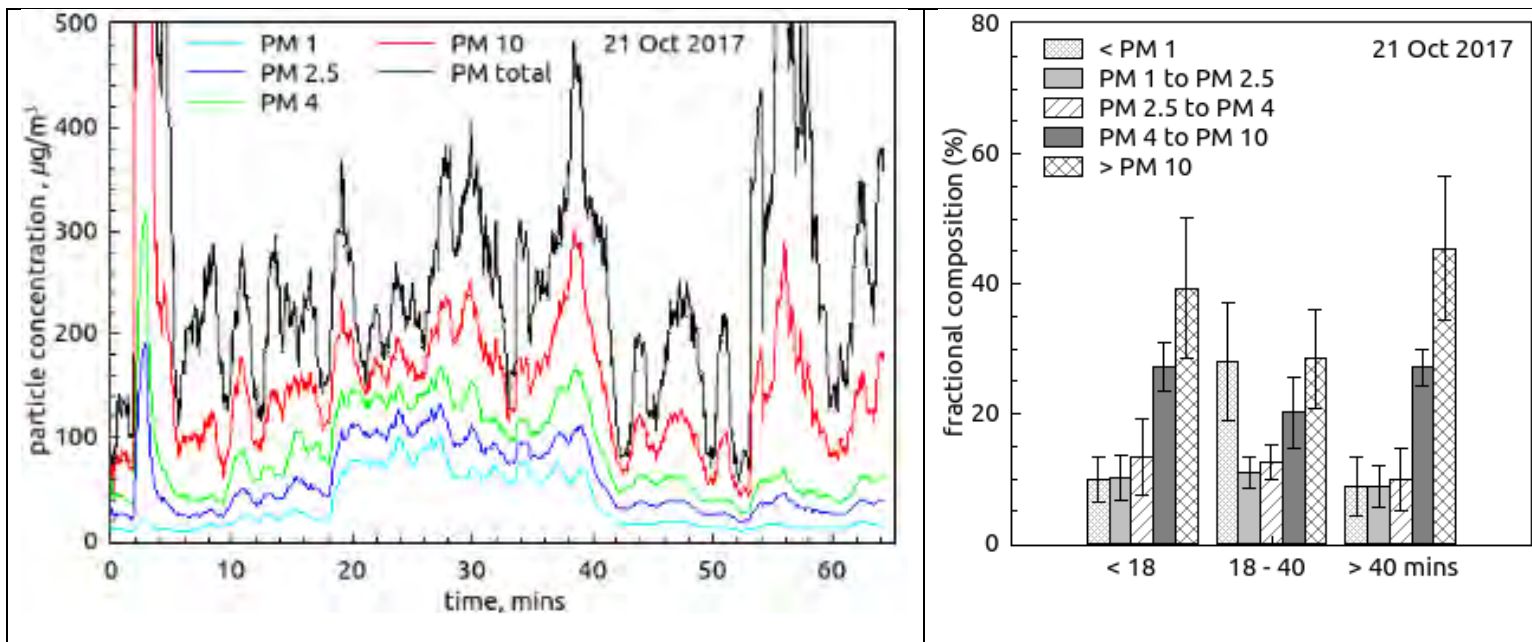


Figure 18: Particle size distribution data during Charging activity.

### 3.3 Boggging

During the boggging activity, the tracer gas was released into the loader exhaust while it was boggging the dirt from the development face into the stockpile (Figures 7 and 8). The positions of the three Miran units during this activity are shown in Figure 8. The tracer gas concentration measured during the boggging activity was charted versus time (Figure 19).

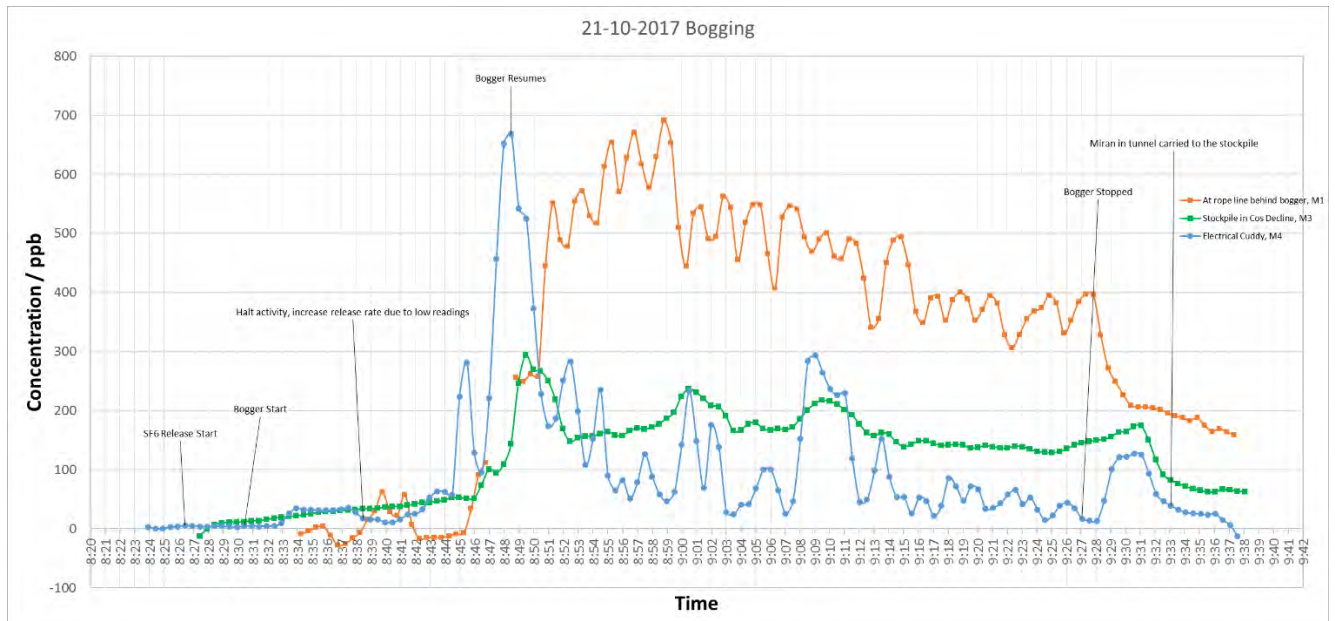


Figure 19: Tracer gas study data during Boggging activity.

No real time measurements could be taken in the bogger cabin because the Miran unit did not fit in the available cabin space. Hence, direct correlation of SF<sub>6</sub> to exposure to the bogger driver in the cabin was not possible. Measurements were however taken at; (i) the heading rope line behind the bogger (heading return air, M1 in Figure 8), (ii) the electrical cuddy and (iii) the stockpile on the decline, the latter two being located in through ventilation.

The tracer gas peaks and valleys shown in Figure 19 correlate with the bogger movement in the heading (i.e. moving to and from the face of the heading and the stockpile). This could possibly point to the impact of the ‘piston’ effect on the ability of the secondary ventilation to control SF<sub>6</sub> concentration. nDPM may behave in a similar manner. The heading in this instance was “force ventilated”. Future studies should consider a comparative assessment of a force versus exhaust arrangement to determine if a different secondary ventilation strategy would result in better dilution, i.e. damping of the peaks.

As mentioned earlier, the electrical cuddy is located (Figure 8) on the decline which is in through ventilation and thus it is located downstream of the heading. It is observed that the secondary ventilation dilutes the gasses in the heading from the bogger by approximately 50% to 60%. This will represent the exposure level for other activities downstream of the bogger. These observations are

specific for the location studied on this instance. The peaks and valleys experienced near the bogger “at the rope line” tend to “smooth out” as the SF<sub>6</sub> moves from the heading and enters the main airstream ventilation (primary ventilation air) in the decline, as observed by the SF<sub>6</sub> movement profile past the electrical cuddy and past the stockpile in the Cos decline.

In general the tracer gas concentration in the electrical cuddy is lower but still around 15-25% of the tracer gas just behind the loader. This suggests that an electrician undertaking any work in this cuddy directly downstream of the heading will experience relatively higher tracer gas concentrations. Administrative controls to limit work directly downstreams of loaders could be considered.

### 3.4 Hydro-scaling and Shotcreting

During Hydro-scaling (Section 2.3, Figures 9, 10 and 11), the tracer gas was released into the exhaust of the Spraymec machine while it was scaling the loose rock with water and compressed air. The four Miran positions are shown in Figure 11.

During shotcreting (Section 2.4), SF<sub>6</sub> was released at Agi truck first (Figure 11). Once the SF<sub>6</sub> concentration had reached a steady state air samples were taken near Agi truck operator (M2 position). Spraymec operator stopped mid-activity. Then stopped SF<sub>6</sub> release and allowed to clear (~10 min). Resumed release of SF<sub>6</sub> at spraymec once shotcreting activity was resumed. Once the SF<sub>6</sub> concentration had reached a steady state air samples were taken near the Spraymec operator (M1 position).

The tracer gas study observations (Figures 20, 24 and 25) are specific to the ventilation configuration and the distance of the secondary ventilation duct to the face for the duration of these particular hydro-scaling and shotcreting activities. The results may differ for other ventilation configurations and cannot necessarily be considered universal. In this instance there was good ventilation in the face with the ventilation duct close to the face and good mixing (Table 1).

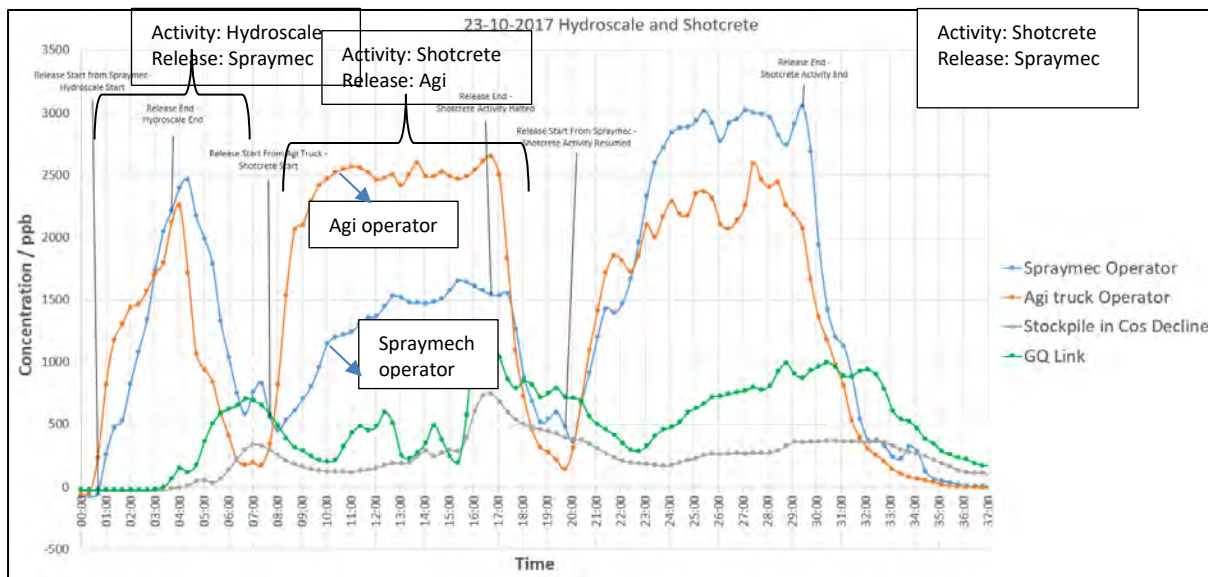


Figure 20: Tracer gas study data during sequential Hydroscale and Shotcrete activity on 23-10-17.

M1 = blue line, M2 = orange line, M3 = grey line and M4 = green line.

During hydro-scaling (Figure 21, extracted from Figure 20) the Spraymec and Agi operators received a similar SF<sub>6</sub> exposure from the Spraymec exhaust. Note: the Agi operator does not necessarily have to be present during this activity and this was merely a coincidence on the day.

During shotcreting the exhaust from the Agi truck mainly impacted the Agi operator with lower exposure to the Spraymec operator. In this instance the Spraymec operator exposure is only 60% of Agi operator exposure from the Agi truck. This suggests that having the ventilation duct close to the heading face ensures that the Spraymec operator benefits from the fresh air in the ventilation duct as it scavenges the Agi exhaust away from the heading face before it can impact the Spraymec operator.

However, during shotcreting the exposure from the Spraymec exhaust significantly impacted both the spraymec operator and Agi operator albeit slightly lower for the Agi operator.

The Agi operator received a similar exposure from both the Spraymec and Agi machines. Under the prevailing ventilation conditions, the Agi operator experienced approximately 10-15% more exposure compared to the Spraymec operator and would be at greater risk. It is worth noting that respiratory personal protective equipment is worn during shotcreting.

If further comparative studies can be undertaken with heading set-up in different ventilation configurations, the approach can be used to optimise airflow in the heading to reduce the exposure impact. Similarly to the bogger case (section 4.3) a comparative experiment with exhaust ventilation and force ventilation would be useful to determine if better secondary ventilation practises are possible.

In terms of the readings taken downstream of the heading in through ventilation, the following was observed:

- The stockpile is not significantly impacted by the activity. This is due to the small amount of fresh ventilation air entering the stockpile; and
- any exhaust entering the stockpile does so by diffusion rather than active ventilation.

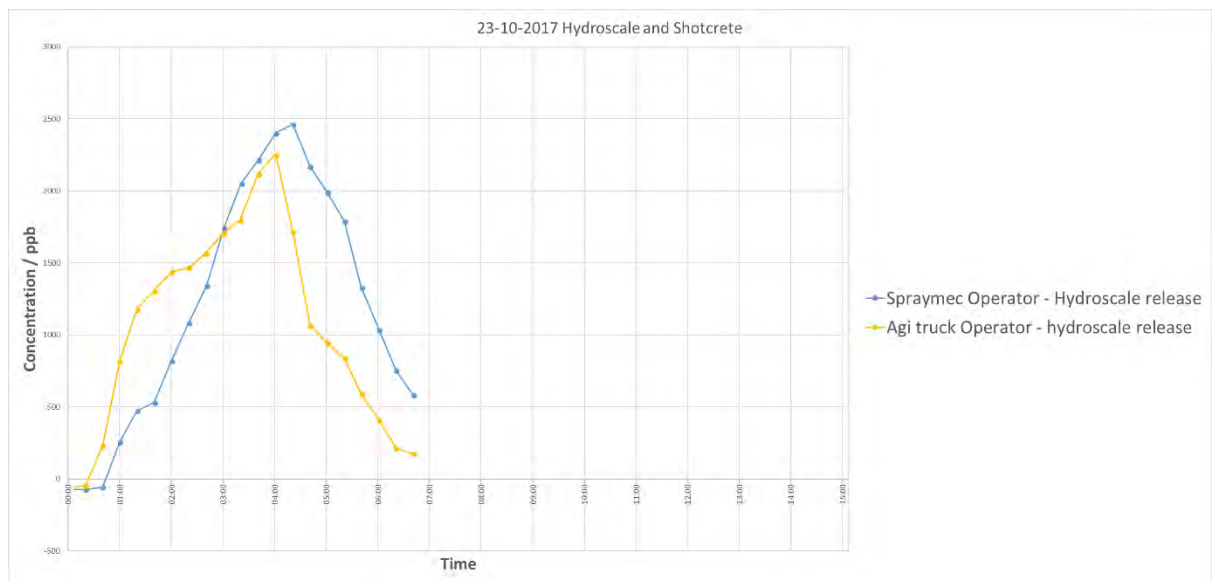


Figure 21: Relative exposures (extracted from Figure 20) to the Spraymec and Agi truck operators during the Hydro-scaling activity.

### Safe shelter area for observation personnel

It is worth noting that within the short timeframe of the activity the concentrations in the stockpile do not reach the peak values that are experienced by either operator and are also less than in the main return (GQ link). Because the stockpile was not actively ventilated at the time, the buildup of gas concentration relies on diffusion processes only and is therefore slow. This means that during a short duration activity an unventilated cuddy (as represented by the stockpile in this case) could be a

natural ‘place of safety’ or shelter area for personnel that are in the general area but not involved with the actual activity. The data also shows that after the diesel sources have left the heading, concentrations are quickly diluted. In the case of the experiment (shown by Figure 20) this occurs within 2-3 minutes. After this period the concentrations are lower than in the cuddy, which then take some time to clear. This perhaps provides an opportunity to have administrative controls in place to exploit this phenomenon. For example, shelter in a cuddy (stockpile) during activity but leave stockpile soon after the diesel machines have vacated the heading.

The peaks observed at the heading (Figure 20) occur 6 minutes later at the through ventilation within QC link and the levels are approximately 20% of the levels at the heading.

Figures 21, 22 and 23 represent the exposure of the Spraymec and Agi truck operators during the hydro-scale and shotcrete activities from both the Agi truck and the spraymec machine with the trace lines superimposed on top of each other.

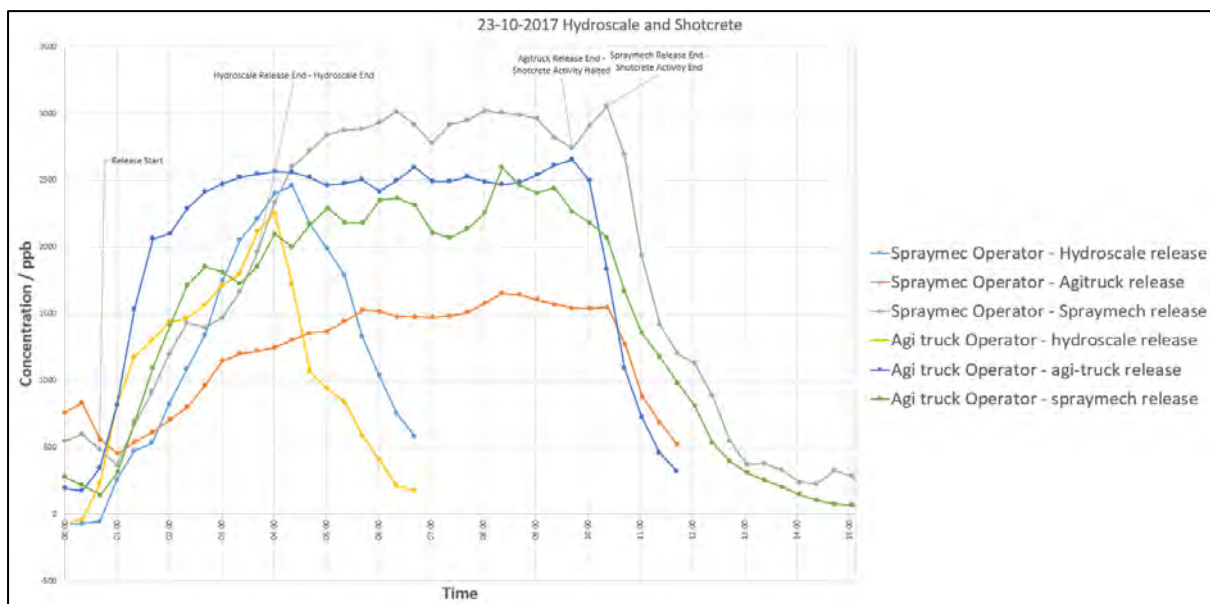
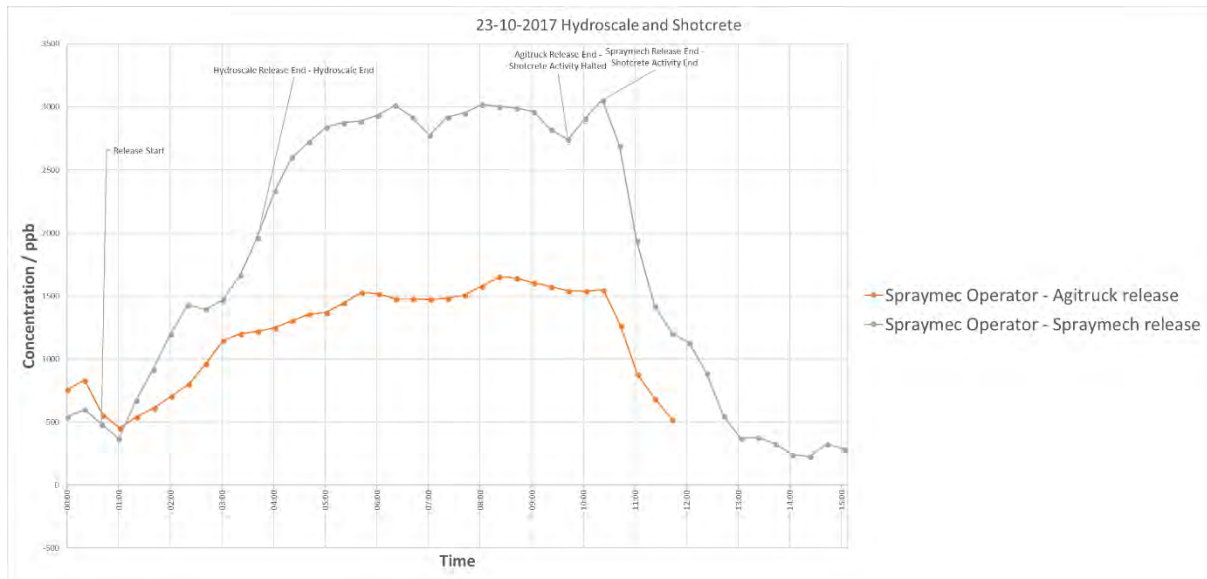


Figure 22: Exposures (extracted from Figure 20) to the Spraymec and Agi truck operators during the Hydro-scaling and Shotcreting activities, normalised to the same time scale.

(a) Exposure of spraymec (grey) and Agi (orange) exhaust on the spraymec operator.



(b) Exposure of spraymec (green) and Agi (blue) exhaust on the Agi truck operator

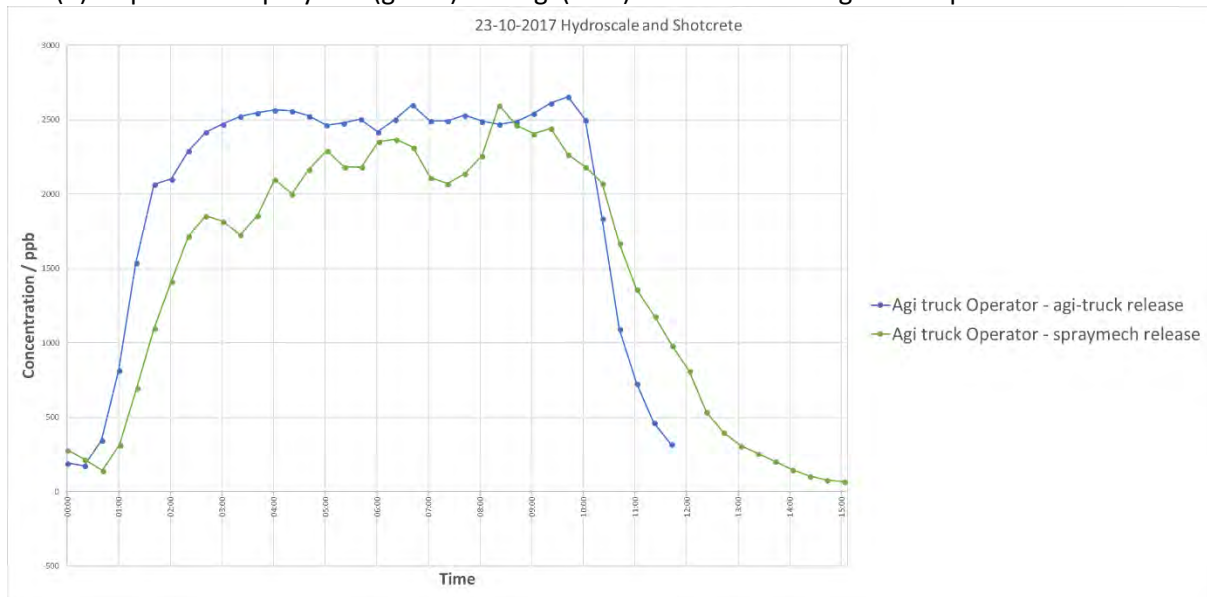


Figure 23: Relative exposures (extracted from Figure 20) to the Spraymec and Agi truck operators during the Shotcreting activity.

The tracer gas data (Figures 21, 22 and 23) shows that the Agi operator is exposed to similar amounts of SF<sub>6</sub> released from both pieces of equipment, which means he/she was at greater risk in this particular ventilation setup. The integrated total exposure to fumes is summarised in Table 5. This is the sum total from both exhausts over the exposure period. For this particular setup the Agi operator received approximately 12% more exposure to gas, but given the experimental errors from the Miran instruments ( $\pm 10\%$ ) this may not be significant.

Table 5: Relative exposure calculated from integrated peak areas (as shown in Figure 20) experienced by the Spraymec and Agi truck operators during hydro-scaling and shotcreting activities.

Release Activity	Peak from Figure 20	Spraymec Operator, M1	Agi truck Operator, M2
Hydro-scale (Agi release)	1	27,603	22,054
Shotcrete (Agi release)	2	43,090	72,113
Shotcrete (Spraymec release)	3	79,734	65,548
<b>Total</b>			
Shotcrete	2 + 3	122,824	137,661
Hydroscale	1	27,603	22,054

The spraymech operator receives almost 65% of his total exposure from his own machine and only 35% from the Agi truck. Therefore, any improvements to the Spraymec exhaust will be beneficial for the Spraymech operator. The Agi operator also gets as much as 50% of his exposure from the Spraymech. Thus, improvements to the Spraymech truck will have a beneficial impact to both operators. Hence, a focus firstly on the Spraymech will have the greatest initial return on investment. With effective ventilation in place the concentration of both machines are rapidly diluted at similar rates.

In summary it can be concluded that the two operators experience the same nominal amount of exposure with both being impacted by each of the two machines.

In comparison to Figure 20, Figures 24 and 25 show similar SF<sub>6</sub> flow profiles for the hydro-scaling and shotcreting activities respectively performed on separate days in the same development heading under similar ventilation conditions (Table 1). The results obtained on separate days are within the Miran instruments' experimental error of 10% and hence the SF<sub>6</sub> profile data was reproducible.

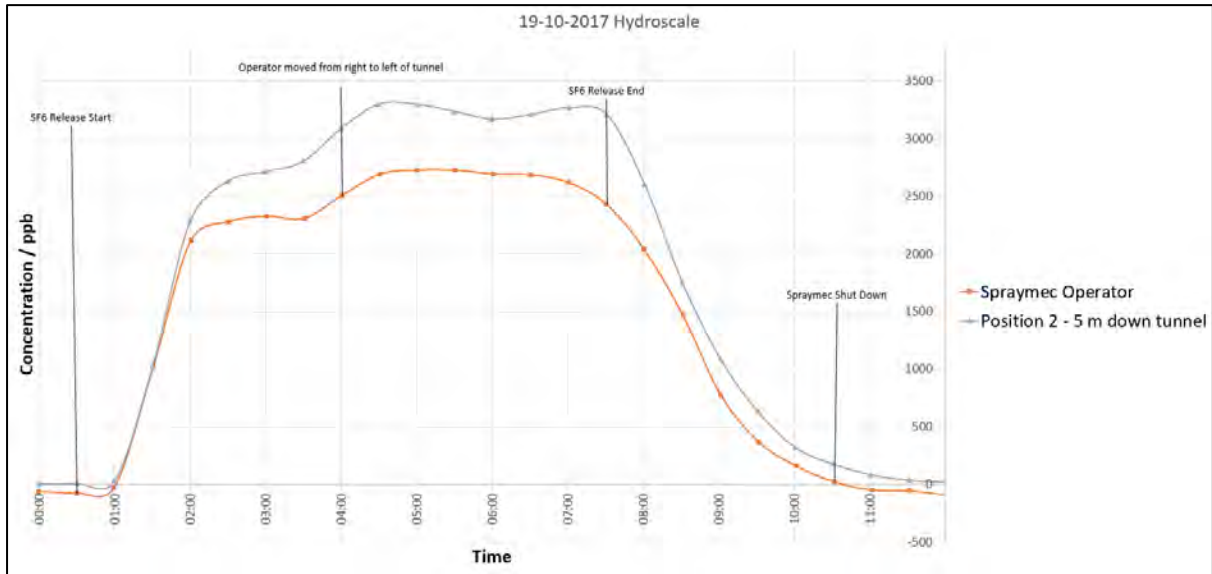


Figure 24: Tracer gas study data during Hydro-scaling activity on 19-10-17.

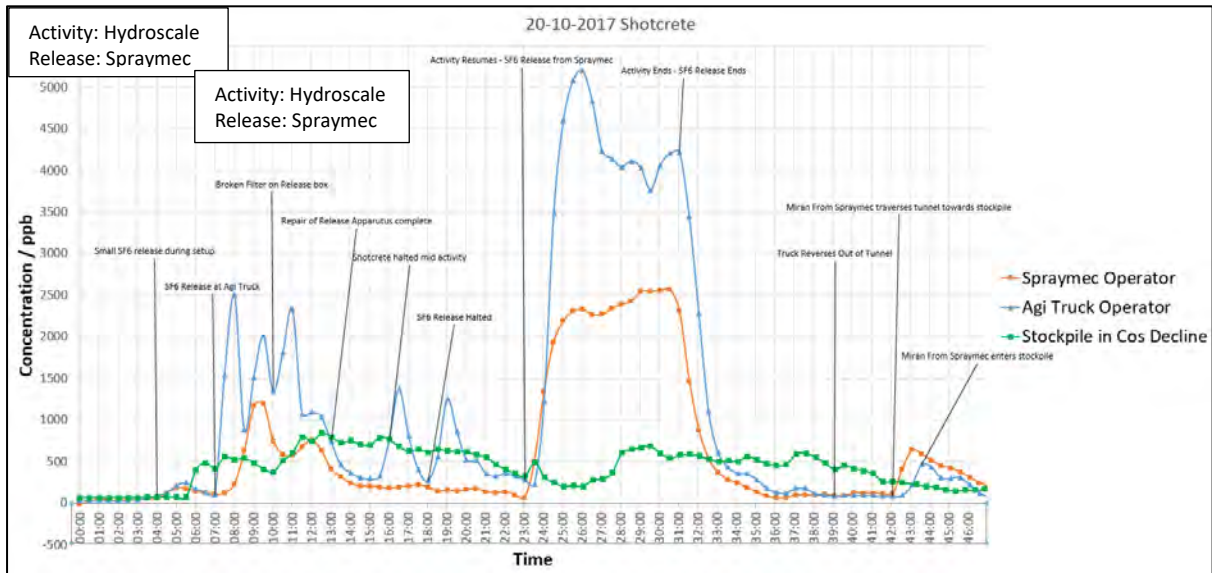


Figure 25: Tracer gas study data during Shotcreting activity on 20-10-17.

### 3.5 Truck Activity

During the truck activity, the tracer gas was set up to release into the tailpipe of the truck while the truck travelled from surface, down the decline past the fan that feeds the test level, got loaded and travelled back up past the test level again to surface (Figures 12 and 13).

The truck experiment (Figure 26) shows that SF<sub>6</sub> exposure levels to the truck driver are much lower when compared to operator exposure levels during shotcreting activities (Figures 20 and 25). However care should be taken in comparing these directly since the SF<sub>6</sub> release rate would be constant whilst in reality exhaust rates between different pieces of equipment will be different. Subsequent studies should calibrate SF<sub>6</sub> release rates relative to exhaust rates of different diesel engine equipment to enable direct comparisons.

The levels of exhaust gas entering the truck cabin is only approximately 5% of that observed during the shotcreting activity. During the truck experiment, the truck driver opened the window (for a few minutes) while the truck was stationary during loading and this resulted in a 9-fold increase in truck exhaust gas entering the cabin. It is worth noting that it took approximately 20 minutes after closing the window again before the levels in the cabin reached those prior to opening the window. This means that not only does the exposure levels increase, but period of exposure also increases when a window is opened. The benefits of ensuring the cabin remains isolated is clear.

A recommendation from this study is that if the truck driver needs to open the cabin window while stationary during loading, it is best that the window is left open while driving away for a certain amount of time to ensure faster clearance of exhaust from the cabin.

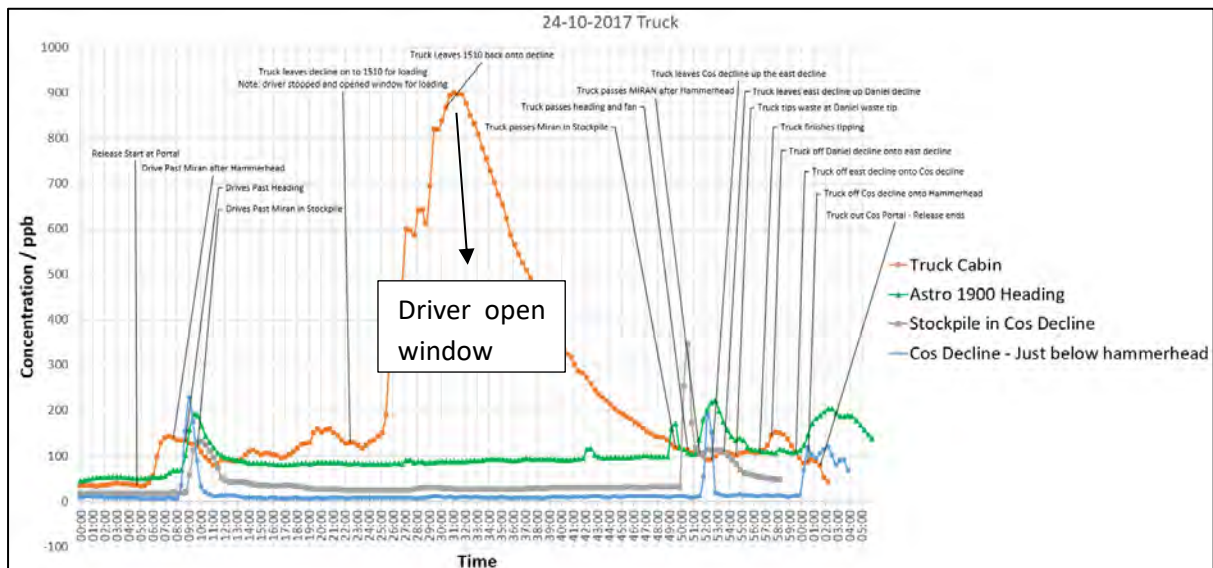


Figure 26: Tracer gas study data during Truck activity.

### 3.6 Traverse Exercise

This study relates to the heading that was used for the tracer gas analysis of each activity described earlier. The objective of this particular experiment was to determine if the fresh air supplied by the duct is distributed uniformly (or not) along the heading cross section (left to right). For example does the fresh air form a ‘layer’ along the sidewall where the duct is positioned or is it effectively distributed along the entire heading width. A second objective was to determine the penetration distance of fresh air into the blind heading from the duct discharge. For example, with the distance to the face does the fresh air reach the end of the heading or does the end experience a ‘blind spot’.

During the traverse exercise, tracer gas was released into the secondary ventilation system near the outlet in the development heading in order to test the system effectiveness and side to side stratification. The 4 Miran detectors were placed at varying distances from the heading face with Miran 1 being closest to the face, 6.5 m from the face (Figures 14 and 15). The other Mirans were placed at 5 m intervals from each other back from the face. Over a period of time the 4 Mirans were moved from one side of the heading to the other.

As expected the Miran M1 which is closest to the face recorded the lowest concentration (Figure 27) and indicates that only about 83% of the fresh air from the vent bag reaches the face. The full amount of ventilation in the bag probably reaches a position of about 11.5m. Thus there is a very rapid drop-off between 11.5m and 6.5m which also means that areas much closer to the face will probably have far less effective ventilation. Over time measurements were taken across the width of the heading. The similar concentrations suggest that there is little horizontal stratification across the heading despite the vent bag being near the right hand side of the heading wall.

Future studies should look into different ventilation configurations to determine if better scouring is possible.

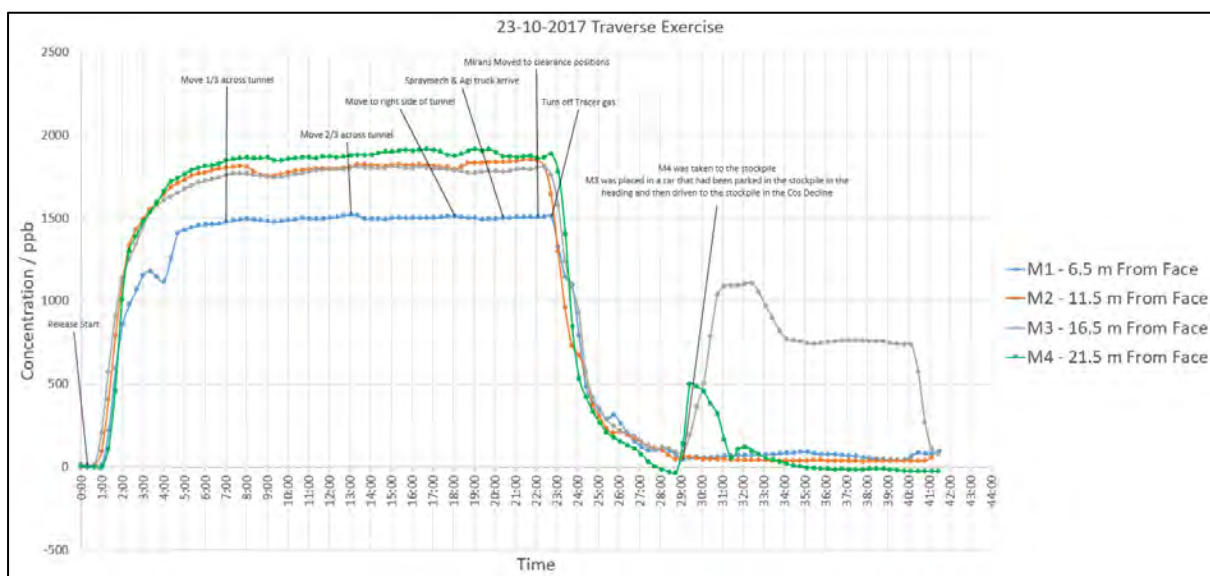


Figure 27: Tracer gas study data during a Traverse exercise.

During the traverse exercise, a Palas Frog particle size analyser (PSA) was used for monitoring mass fractions of PM<sub>1</sub>, PM<sub>2.5</sub>, PM<sub>4</sub>, PM<sub>10</sub> and TSP (Figure 28) at position M1 (Figure 14), closest to the face of the heading i.e. 6.5 m from the face. During this study, there were no diesel vehicles present or operating in the heading and ventilation was operating as usual (Table 1).

Overall, approximately 20 to 25 % of the particles measured were under PM 1 (< 1000 nm size, Figure 28) with the particle concentrations not exceeding 50 µg/m<sup>3</sup>. Position 1 (from 1 to 7 minutes) showed a constant low count of PM 1 and PM 2.5. Position 2 (from 7 to 13 minutes) showed a peak for PM 1, PM 2.5 and PM<sub>4</sub>. Positions 3 (from 13 to 18 minutes) and 4 (from 18 to 22 minutes) showed higher peaks for PM<sub>10</sub>. The latter observations are in accordance with the vent bag being positioned off centre to the right of the heading with larger particles being mobilised by the ventilation flow path.

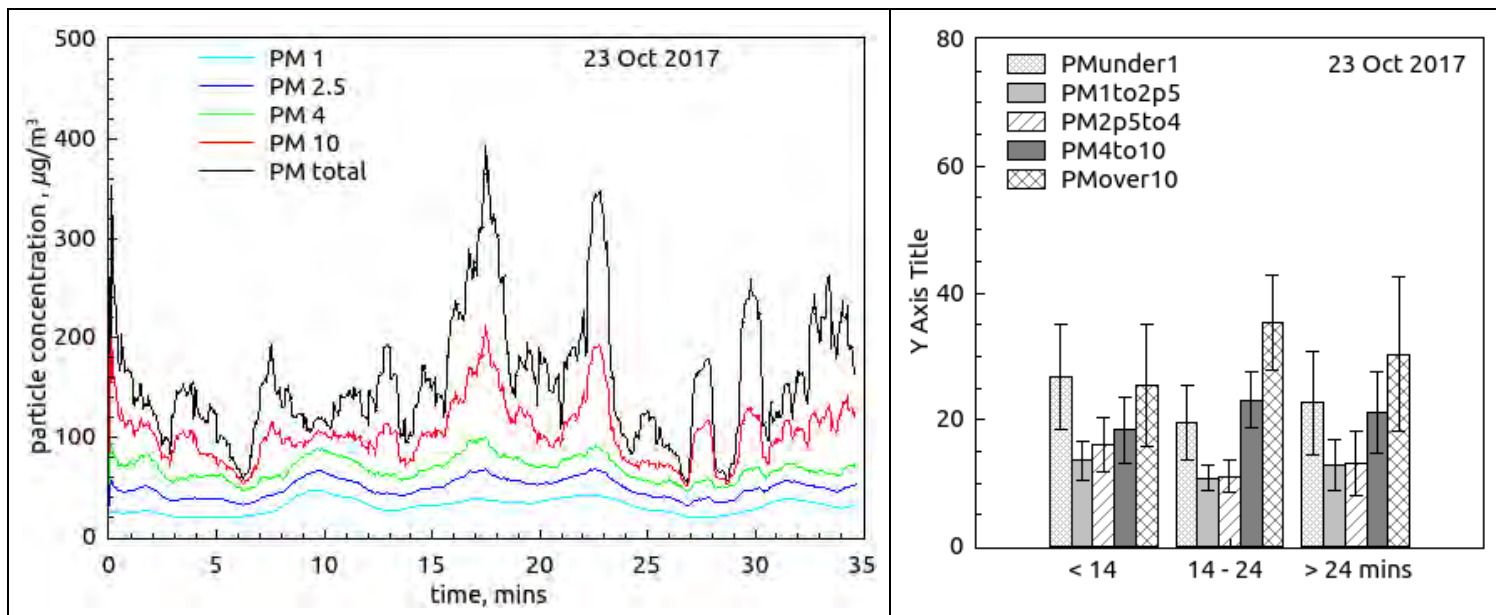


Figure 28: Particle size distribution data during the Traverse exercise at Miran 1 position.

### 3.7 WATU WSX Portal Interaction

This study was undertaken at the exhaust portal which is located on opposite side of the pit to the intake portal inside the open pit (Figures 3 and 16). The objective of this study was to determine if any of the contaminants in the exhaust will recirculate back into the mine via the intake portal which is about 100m away from the exhaust. Note: This should not be confused with the Astro Daniel portals where the intake and returns are directly adjacent to each other. There was no time during the site visit to also study this portal interaction.

Figure 29 shows the amount of gas measured in the intake portal after being released in the exhaust portal. The airflow that exhaust via the portal is about 280m<sup>3</sup>/s. The tracer gas release rate in the return was 92 l/min which gives an exhaust concentration in the portal of 5500 ppb. The concentration in the intake peaked at about 3 ppb from the baseline drift. This means the exhaust is diluted to 0.05% of the exhaust portal concentration and therefore not a contribution to fresh air intake concentrations. This is not surprising since there is a large distance between these portals and despite it being in an open pit there is sufficient dilution. There are other portals at Sunrise Dam where the intake and exhaust are closer and it may be worth repeating this experiment for this section of the mine. At the portals where the experiment was undertaken, it shows no material contamination of the intake portal by the exhaust portal.

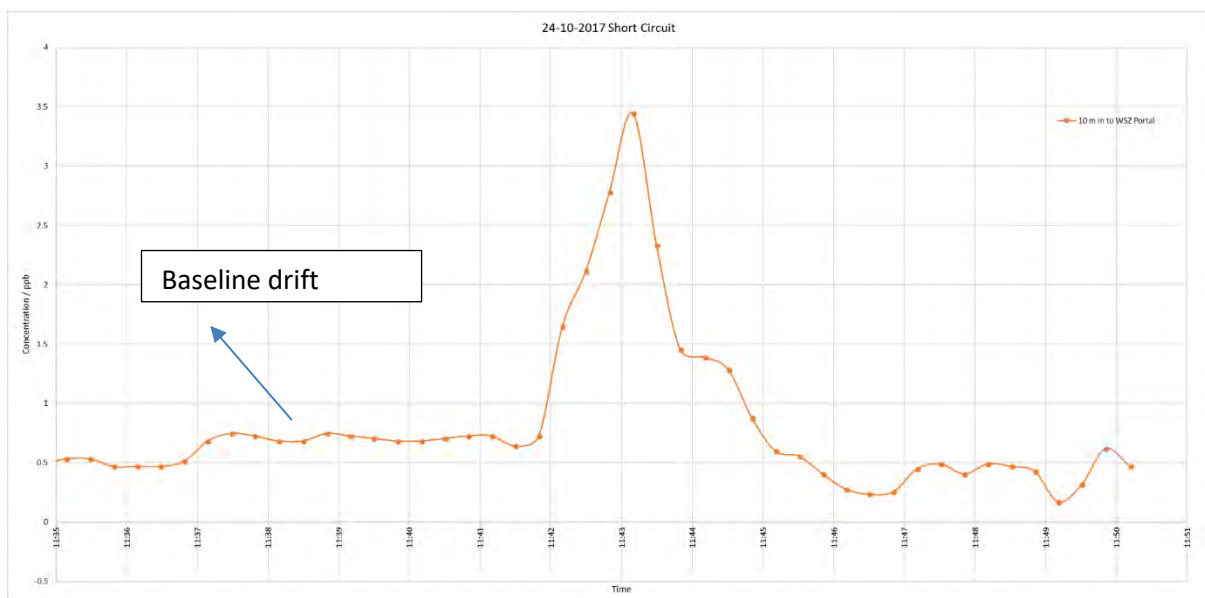


Figure 29: Tracer gas study data at the WATU WSX Portal.

## 4 SUMMARY AND CONCLUSIONS

### 4.1 Key Findings and Recommendations

The key finding should be considered in terms of the objective of the study which is to undertake a pilot study to show how SF<sub>6</sub> tracer gas techniques can be applied to improve ventilation for better nDPM dilution over time. The findings are as followed:

- The tracer gas study of a number of underground mining activities, such as charging, bogging, hydro-scaling, shotcreting and truck driving, demonstrated that during those activities there were consistently relatively higher SF<sub>6</sub> concentrations measured during the hydro-scaling and shotcreting activities.
- During shotcreting, the Agi truck operator experienced approximately the same exposure of SF<sub>6</sub> from the Agi truck and spraymec exhaust (Section 3.4). In contrast, the spraymec operator received almost twice the exposure from the spraymec exhaust than from the Agi truck exhaust. The Agi operator in this instance was at greater risk. Hence, because the spraymec is the more significant contributor of exhaust to the operators it is recommended that a focus on improving systems around the spraymec will give the greatest initial return on investment.
- During a short duration activity in a development heading, an unventilated cuddy (as represented by the stockpile in this study) could be a natural 'place of safety' or shelter area for personnel that are in the general area but not involved with the actual activity at a development heading. This information can be utilised to better inform the planning of administrative controls to manage activities around other major diesel activities.
- The SF<sub>6</sub> results from the truck study suggest that the enclosed airconditioned cabin is very effective in managing exposure levels. However, the level of SF<sub>6</sub> exposure to the truck driver increases significantly when a window is opened (a 9 fold increase). Once the window is closed the clearance time is very slow. Thus, the opening of the window not only results in increased levels but also results in prolonged exposure to higher levels once the SF<sub>6</sub> is inside the cabin. The benefits of ensuring the cabin remains isolated is clear and some administrative controls need to be considered.  
A recommendation from this study is that the truck driver should keep the window closed while stationary during loading. However, if the truck driver needs to open the window to communicate with the loader driver it is best that the window is left open while driving away for a certain amount of time to ensure faster clearance of exhaust from the cabin.
- A traverse exercise performed in a well ventilated development heading demonstrated that there was little horizontal stratification across the heading despite the vent bag being near the right hand side of the heading wall (Figures 14 and 27). However, there was a very rapid drop-off in ventilation flow between 11.5m from the face and 6.5m from the face which means that areas much closer to the face will probably have far less effective ventilation.

- At the portals where the experiment was undertaken (Figures 3 and 16), it showed no material significant contamination of the intake portal by the exhaust portal. However, there are other portals at Sunrise Dam where the intake and exhaust are closer and thus it would be worthwhile repeating the portal interaction experiment for these sections of the mine to identify if there is any material contamination of the intake portal by the exhaust portal.
- Tracer gas effectively identified anomalies and concentration differences for different activities. Controlled experimental set-ups with different secondary ventilation configurations should be considered to allow comparative studies that will enable ventilation optimisation. e.g. 1: different distances of end ducting to the face of heading; e.g. 2: comparison study between three secondary ventilation systems (force system, exhaust system and force-exhaust system).
- .

## 4.2 Conclusions

Tracer gas technology was applied successfully at Sunrise Dam underground gold mine to better understand and inform the following;

- SF<sub>6</sub> flow behaviour as a surrogate for diesel exhaust and relative source contribution to exposure of nearby equipment operators;
- The dispersal of gaseous and ultrafine particulate emissions from diesel exhaust, i.e. particularly nDPM, and the dilution efficiency of the mine ventilation with particular focus on the auxiliary ventilation at the face of a development heading;
- The impact of ventilation practises on the exposure levels; and
- The potential impact of nano-diesel particulate matter (nDPM) on air quality.

## 5 RECOMMENDATIONS FOR FUTURE WORK

It would be possible to correlate SF<sub>6</sub> tracer gas measurements with dispersal of nanoparticles if particle characterisation data is available from the sites studied using tracer gas. This would require particle analysers to be co-located with the tracer gas detectors. The unavailability of suitable power supplies precluded this activity being undertaken in the current study.

The tracer gas study performed at the underground SDGM focused on a development heading that was not serviced by an electricity supply and hence the Curtin Uni. team could not perform particle characterisation measurements at or in the vicinity of this heading.

Previous studies performed by ChemCentre in collaboration with USA researchers (confidential work not published) showed that the smaller the particle size (< 80 nm) the more likely the particle would behave like a gas.

It is recommended that future research on nDPM in underground mines includes both tracer gas study and particle characterisation at the same location.

## **PART B: CURTIN UNIVERSITY/QUT STUDY**

# **Draft Report: MRIWA M495 - A Study of Nano Diesel Particulate Matter (nDPM) Behaviour and Physico-chemical Changes in Underground Hard Rock Mines of Western Australia**

## **Part B. Personal and Stationary Monitoring, Ventilation Modelling and Deeper Mines Study**

Authors: Benjamin Mullins<sup>1,2</sup>, Abishek Sridhar<sup>1,2</sup>, Guang Xu<sup>3</sup>  
Ping Chang<sup>2</sup>, Ryan Mead-Hunter<sup>1,2</sup>, Sam Spearing<sup>3</sup>

### **Appendix 2 – Deeper Mines Study – Influence of elevated pressure and ammonia concentration on diesel exhaust particulate matter**

Authors: Reece Brown<sup>4,5</sup>, Joel Alroe<sup>4,5</sup>, Benjamin Mullins<sup>1,2</sup>, Zoran Ristovski<sup>4,5</sup>

- 1 Occupation, Environment and Safety, School of Public Health, Curtin University, Australia
- 2 Fluid Dynamics Research Group, Curtin Institute for Computation, Curtin University, Australia
- 3 WA School of Mines: Minerals, Energy and Chemical Engineering, Curtin University, Australia
- 4 Biofuel Engine Research Facility, Queensland University of Technology, Australia
- 5 International Laboratory for Air Quality and Health, Queensland University of Technology, Australia

#### **Corresponding Author:**

Benjamin Mullins, b.mullins@curtin.edu.au, 08 9266 7029.

**June 27, 2019**

# CONTENTS

<b>1</b>	<b>Methods - In-situ and Ex-situ Measurements and Analysis</b>	<b>6</b>
1.1	Personal Monitoring . . . . .	6
1.2	Stationary Monitoring . . . . .	7
1.3	Analytical Methods . . . . .	7
1.3.1	Elemental Carbon . . . . .	7
1.3.2	Metals . . . . .	8
1.3.3	Volatile Organic Compounds (VOCs) . . . . .	8
1.3.4	Poly-aromatic Hydrocarbons (PAHs) . . . . .	9
1.3.5	Nitrogen Dioxide (NO <sub>2</sub> ) and Sulphur Dioxide (SO <sub>2</sub> ) . . . . .	9
<b>2</b>	<b>Methods - Ventilation Simulations using Computational Fluid Dynamics</b>	<b>10</b>
2.1	CFD Domain - Simulation of the Migration of Diesel Particulates from Vehicle Exhausts and SF <sub>6</sub> (tracer gas) in Confined Regions of the Underground Mine . .	10
2.1.1	Shotcreting Activity . . . . .	12
2.1.2	Bogging/Loading Activity . . . . .	12
2.1.3	Charging Activity . . . . .	13
2.2	CFD Domain - Simulation of DPM Re-circulation into Ventilation Intake due to Proximity with Exhaust . . . . .	14
2.3	Computational Technique . . . . .	16
<b>3</b>	<b>Methods - Chamber Study</b>	<b>17</b>
<b>4</b>	<b>Results and Discussion</b>	<b>17</b>
4.1	Personal Monitoring . . . . .	17
4.2	Stationary Monitoring . . . . .	22
4.3	Optical Particle Measurements . . . . .	23
4.4	Gas Measurements . . . . .	24
4.5	Ultrafine/nano Particle Spectrometry . . . . .	25
4.6	Watu Exhaust Shaft . . . . .	27
4.7	Traverse Measurements . . . . .	27
4.8	Summary of Key Findings - Personal Monitors, Stationary and Mobile Measurements . . . . .	28
4.9	CFD - DPM and SF <sub>6</sub> (tracer) Migration in Confined Regions of the Underground Mine . . . . .	28
4.9.1	Shotcreting Activity . . . . .	28
4.9.2	Bogging Activity . . . . .	32
4.9.3	Charging Activity . . . . .	36
4.9.4	Summary of Key Findings - Simulation of DPM and SF <sub>6</sub> Migration in Confined Regions . . . . .	39

4.9.5	Comparison of Tracer Gas and CFD Results . . . . .	39
4.10	CFD - DPM Re-entrainment into Ventilation Inlets due to Proximity with Outlets	41
4.10.1	Summary of Key Findings - Simulation of DPM Re-entrainment into Vent-Stream . . . . .	44
4.11	Chamber Study (Deeper Mines) . . . . .	44
<b>5</b>	<b>Summary</b>	<b>44</b>
5.1	Limitations . . . . .	45
5.2	Recommendations . . . . .	46
	<b>References</b>	<b>46</b>
	<b>Appendix-1: Personal Monitoring Data</b>	<b>48</b>
	<b>Appendix-2: Chamber Study - Deeper Mines</b>	<b>60</b>

**List of Tables**

1	Operating conditions for the CFD involving Shotcreting Activity . . . . .	12
2	Operating conditions for the CFD involving Bogging Activity . . . . .	14
3	Operating conditions for the CFD involving Charging Activity . . . . .	14
4	Physical properties of materials used for the CFD simulations . . . . .	16
5	Summary statistics for individual monitoring for (nano)particles and gases re- lated to diesel exposure . . . . .	20
6	Mean elemental carbon concentrations at stationary monitoring sites . . . . .	20
7	Comparison between CFD predictions and measurements during shotcreting . .	29
A1:	Personal sampling results for metals . . . . .	48
A2:	Personal sampling results for NO <sub>2</sub> and SO <sub>2</sub> . . . . .	51
A3:	Personal sampling results for VOCs (alkanes and chlorinated alkanes and alkenes)	53
A4:	Personal sampling result for VOCs (aromatic hydrocarbons) . . . . .	55
A5:	Personal sampling results for VOCs (ethers, sulphides and terpenes) . . . . .	57
A6:	Stationary monitoring results for PAHs . . . . .	59

**List of Figures**

1	Computational domain comprising of the AST-1900 mine development and the ventilation channels . . . . .	11
2	Computational domain and surface mesh of the underground AST-1900 region with a Spraymec positioned in a representative location . . . . .	12
3	Computational domain and surface mesh of the underground AST-1900 region with a Loader positioned in three representative locations . . . . .	13
4	Computational domain and surface mesh of the underground AST-1900 region with a Charmec positioned in a representative location . . . . .	14

5	Satellite topography of the Western Shear / Watu ventilation regions of Sunrise Dam gold mine, and geometry and representative surface mesh used for CFD analysis . . . . .	15
6	Typical realtime personal monitoring data for underground workers (designated Uxx), compared with Surface worker data (designated control or Axx); (a) Particle number concentration over time, (b) particle mean diameter over time, (c) frequency histograms of particle diameter (probability of exposure to a given particle diameter over the period of work) . . . . .	18
7	Shift average DPM (EC) vs shift average (nano)particle number concentration for matched worker exposures. Nanoparticle counts are averaged from 11 hours of continuous measurement data for each worker. . . . .	19
8	Optical Particle Counter measurements, (a) Cosmo 1815, (b,c) Astro 1930 . . .	21
9	Gas measurements in the mine; temporal variation on different days/ locations .	22
10	Gas measurements in the mine; proportional data on different days/ locations .	23
11	Average nano/ultrafine particulate spectrum measured in the mine (AST 1930) .	24
12	Diameter, mass and number concentration data for SMPS measurements . . . .	25
13	Correlation between average EC level and average number concentration and calculated mass concentration . . . . .	25
14	Measurements at WATU vent outlet; (a) mass concentration measurements using Palas-Frog, (b) mass concentration measurements using Pinssar, (c) proportional gas measurements over 24 hours, and (d) instantaneous gas measurements at certain intervals that recorded high CO and NO <sub>x</sub> levels . . . . .	26
15	Mine traverse measurements of particulate and gas concentrations at different altitudes underground; (a) gas monitor data, (b) particle concentration . . . . .	28
16	Velocity vectors at a height of 3 m from the ground in the mine region during shotcreting activity . . . . .	29
17	Contours of DPM concentration in the mine region during shotcreting activity .	30
18	Regions where DPM concentrations are greater than 0.1 mg/m <sup>3</sup> in the mine region during shotcreting activity . . . . .	30
19	Contours of SF <sub>6</sub> concentration in the mine region during shotcreting activity . .	31
20	Comparison of SF <sub>6</sub> and DPM concentrations along the length of the heading, during shotcreting activity . . . . .	31
21	Velocity vectors at a height of 3 m from the ground in the mine region during bogging activity . . . . .	33
22	Contours of DPM concentration in the mine region during bogging activity . . .	34
23	Regions where DPM concentrations are greater than 0.1 mg/m <sup>3</sup> in the mine region during bogging activity . . . . .	35
24	Velocity vectors at a height of (a) 3 m and (b) 5 m, from the ground in the mine region during charging activity . . . . .	36
25	Contours of DPM in the mine region during charging activity . . . . .	37

26	Regions where DPM concentrations are greater than 0.1 mg/m <sup>3</sup> in the mine region during charging activity . . . . .	37
27	Contours of SF <sub>6</sub> concentration at (a) 3 m from the ground and (b) 3 m from the side walls in the mine region during charging activity . . . . .	38
28	Comparison of SF <sub>6</sub> and DPM concentrations along the length of the heading, during charging activity . . . . .	38
29	Comparison of tracer gas and CFD results for the Hydrosaling (Spraymec) activity	40
30	Comparison of tracer gas and CFD results for the Loading (Bogging) activity . .	40
31	Comparison of tracer gas and CFD results for the Charging activity . . . . .	40
32	Comparison of streamlines and iso-surfaces of DPM concentrations corresponding to 0.5 % and 4 % of that at the Watu outlet, between flow rates of 100 and 50 m <sup>3</sup> /s. The WATU outlet can best be seen in (e) located at the base of the yellow streamlines, while the Western Shear portal is located at the concentration of blue streamlines to the left. . . . .	42
33	Comparison of streamlines and iso-surfaces of DPM concentrations corresponding to 0.5 % and 4 % of that at the Watu outlet, between flow rates of 100 and 50 m <sup>3</sup> /s . . . . .	43

# 1 Methods - In-situ and Ex-situ Measurements and Analysis

## 1.1 Personal Monitoring

Personal monitoring was conducted to measure diesel exhaust particulate (DEP) exposure (as elemental carbon (EC)), as well as realtime (nano)particle spectrometry and passive gas sampling. Sampling equipment was fitted at the commencement of each work shift and removed shortly prior to the end. The average sample time for all participants was  $\approx 11$  hrs per person. A sample size of  $n = 20$  controls (surface/office workers) and  $n = 80$  underground workers were monitored. Underground workers were split evenly between day and night shifts, while controls were only day shift due to insufficient numbers of night shift workers in surface/office locations).

*Gravimetric:* Monitoring equipment consisted of a sample pump (SKC Inc, Eight Four, PA) connected to a respirable sampler with cyclone (SKC Inc), fitted with a 25 mm quartz filter (Whattmann, GE Life Sciences, Chicago, IL). Filters were prepared pre and post sampling according to the NIOSH 5040 protocol [1], with EC analysis conducted by the ChemCentre WA (method detailed in analytical section below). One field blank per day (per 5 measurements) was also prepared. Post NIOSH 5040 analysis, the residual sample on each filter was analysed for metals via Inductively Coupled Plasma Mass Spectrometry (ICP-MS). Sample pumps were calibrated before each use and the calibration checked at the end of each measurement.

*Particle Spectrometry:* Monitoring equipment consisted of a nanoparticle spectrometer (DiSCMini, Testo, Lenzkirch, Germany). This instrument measures (nano)particles via electrical charge. It consists of a corona charger, ion trap (to remove ions unattached to particles), followed by a diffusion battery connected to an electrometer [2, 3, 4]. The instruments were serviced and calibrated pre and post measurement, with instrument accuracy checked against an electrometer (Charme, Palas, Karlsruhe, Germany) and condensation particle counter (3775, TSI, Shoreview, MN) periodically. The instruments were also fitted with additional batteries to ensure a run-time greater than a full 12 hr working shift.

*Gas Monitoring:* One  $\text{NO}_2/\text{SO}_2$  passive sampling tube and one VOC sampling tube was fitted to each worker (Radiello, Padua, Italy).

*Protocol:* After consent forms, surveys and biometric data had been completed by each worker, each worker (5 per shift) was fitted with 1x particle spectrometer, 1x gravimetric sampler, 1x  $\text{NO}_2/\text{SO}_2$  passive sampling tube and 1x VOC sampling tube. Pumps and DiSCMinis were belt mounted. The Gravimetric sampler was located in the breathing zone and connected via a tube to the pump. Passive samplers were initially fitted to the breathing zone of the worker as per protocol, however due to the arduous physical nature of the work, breakage of the flimsy plastic mounts for the devices were experienced. Therefore for the underground workers it was necessary to mount the passive samplers to the rear of the safety helmet, in order to minimise breakages. Some difficulties were also experienced with the DiSCMinis. Again due to the arduous nature of the work, some workers inadvertently stopped the device recording,

either via bumping the record/power buttons or dislodging the SD data storage card. This was despite the device being inside the manufacturer's case and additional tape added to cover the buttons and the SD card slot.

## 1.2 Stationary Monitoring

Two stationary monitoring rigs were assembled to monitor (nano)particulates and gases at suitable locations within the mine. *Rig 1*: A scanning mobility particle sizer (SMPS) consisting of a 3081 DMA, 3018 classifier and 3775 CPC (TSI, Shoreview, MN); Two optical particle counters (Frog, Palas, Karlsruhe, Germany and DPMreader, Pinssar, Brisbane, Australia); A gas spectrometer (Testo 350 XL, Lenzkirch, Germany); An impactor (nanoMoudi II 125B, MSP, MN); A respirable sampler for EC and pump (SKC Inc); An XAD tube sampler, prefilter and pump (SKC Inc).

*Rig 2*: A scanning mobility particle sizer (SMPS) consisting of a DEMC, NanoDMA(1000) and Charme Electrostatic Classifier (Palas, Karlsruhe, Germany); An optical particle counter (Frog, Palas, Karlsruhe, Germany); A gas spectrometer (Testo 350, Lenzkirch, Germany); An impactor (nanoMoudi II 125B, MSP, MN); A respirable sampler for EC and pump (SKC Inc); An XAD tube sampler, prefilter and pump (SKC Inc).

The apparatus were moved to suitable locations (previously identified at approximately 24-hr intervals, then set to monitor at 5 minute intervals (apart from the SMPS systems which monitored every 30 minutes and the pumps which sampled continuously). The locations were (using mine region and elevation designation):

- |                 |                              |
|-----------------|------------------------------|
| i) Cosmo 1815   | iv) Cosmo East 1510          |
| ii) Astro 1965  | v) Vogue 1600                |
| iii) Astro 1930 | vi) WATU vent exhaust portal |

The gas analyzer and optical particle counter from Rig 2 were detached to permit monitoring by the ChemCentre during tracer gas studies and to undertake mobile traverses through the mine. All equipment was serviced and calibrated according to manufacturer specifications prior to use. Some equipment malfunctions were experienced due to the harsh mine environment, resulting in some missing data.

## 1.3 Analytical Methods

Chemical analysis of the filters, Radiello cartridges and XAD tubes were performed by the ChemCentre, using the procedures detailed in the following sections.

### 1.3.1 Elemental Carbon

Levels of elemental carbon collected on filters, either through personal sampling or sampling in fixed locations, were analysed using a NIOSH 5040 compliant method. This method yields both organic and elemental carbon levels, with the elemental component being used to indicate diesel particulate matter (DPM). The analysis was performed using a Lab OC-EC Aerosol Analyser

(Sunset Laboratory Inc., Tigard, Oregon, USA). A standard punch was taken from the filter and placed in a quartz oven. Following a Helium purge, a stepped temperature ramp increases the oven temperature to 870 °C thermally desorbing organic compounds into a manganese dioxide (MnO<sub>2</sub>) oxidising oven. As the carbon fragments flow through the MnO<sub>2</sub> oven they were quantitatively converted to CO<sub>2</sub> gas. The CO<sub>2</sub> was then swept out of the oxidising oven in a helium stream and mixed with hydrogen gas. This mixture then flowed through a heated nickel catalyst where it was converted to methane. The methane was subsequently measured using a flame ionisation detector (FID).

After the initial ramp in the quartz sample oven was completed, the oven was cooled to 550 °C and the flow stream switched to an oxidising helium/oxygen carrier gas mixture. A second temperature ramp was then initiated in the oxidising gas stream and any elemental carbon was oxidized off the filter and into the oxidizing oven. The elemental carbon was then detected in the same manner as the organic carbon.

### 1.3.2 Metals

Filters were placed into a digest vial and had a digestion mix of 4 mL 1:1 (50%) high purity (HP) Nitric acid, 1 mL concentrated Hydrochloric acid and 5 mL de-ionised (DI) water added to it. Samples were digested for 2 hours at 85 °C with a reflux cap. Digests are then filtered undiluted through acid (1% HNO<sub>3</sub>) washed Whatman 541 filter papers, with the filter squeezed with a glass rod. Filters are then rinsed twice with small portions of DI water (add DI water to tube, cap, shake, sit for 10 minutes to allow metals to desorb and then filter off) and make up to 20 mL in a 30 mL polystyrene vial. The metals determination was performed on both an Inductively Coupled Plasma–Atomic Emission Spectrometer (ICP-AES) (Agilent Vista Pro Axial, Santa Clara, California, USA) and an Inductively Couple Plasma–Mass Spectrometer (ICP-MS) (Agilent 7500, Santa Clara, California, USA) with a Collision Cell, with the metals reported off the instrument that provided the most confident result.

### 1.3.3 Volatile Organic Compounds (VOCs)

VOC samples were analysed based on the US EPA TO17 method, utilising thermal desorption and gas chromatography-mass spectrometry (GC-MS). The Radiello cartridge (code RAD-145) is a stainless-steel net cylinder, with 3x8 µm mesh opening and 4.8 mm diameter, packed with 350 ± 10 mg of graphitised charcoal (Carbograph 4), particle size is 35-50 mesh.

Volatile organic compounds are trapped by adsorption and recovered by thermal desorption, analysis is performed by capillary gas chromatography and mass spectrometer (GC-MS) detection. Thermal desorption is achieved using a thermal desorber (Markes Unity Series 2 with Markes 50/50 Ultra, Llantrisant, UK) coupled to a gas chromatograph (GC) (Agilent 7890N, Santa Clara, California, USA) with a mass selective detector (Agilent 5977A, Santa Clara, California, USA).

After sampling, the tubes are placed in stainless steel thermal desorption tubes, sealed with brass transport caps and are returned to the laboratory. Once received they were placed

on the Markes 50/50 Ultra instrument, the tubes were heated to 300 °C and the analytes swept onto the Markes Unity Series 2 thermal desorber cold trap, this trap is used to focus the target compounds. After the primary desorption has been completed the secondary trap is heated and part of the sample is directed onto the GC column, the rest is either re-adsorbed onto a tube or is sent to a split line. The GC then separates the mixture and the MS analyses its components. The GC was equipped with a DB5 MS (60 m x 320  $\mu\text{m}$  x 1 $\mu\text{m}$ ) capillary column for separation, using helium as the carrier gas with a constant flow of 3.5 mL/min. The GC temperature program ranged from 35-280 °C with a run time of 24 minutes. The mass spectrometer was operated in electron impact mode at 70 eV, scanning the range  $m/z$  33–350.

Average airborne concentrations ( $c$ ,  $\mu\text{g}/\text{m}^3$ ) of individual VOC species were calculated based on the obtained masses in each sample, using the following expression;

$$c = m/(Q_K t) \times 10^6 \quad (1)$$

In Eq. 1,  $m$  is the mass of analyte ( $\mu\text{g}$ ),  $t$  the total sampling time (minutes) and  $Q_K$  is the sampling rate for the specific analyte at 298 K [5]. Sampling rates were temperature corrected for the average temperature over the sampling period, using the following expression;

$$Q_K = Q_{298}(K/298)^{1.5} \quad (2)$$

#### 1.3.4 Poly-aromatic Hydrocarbons (PAHs)

The front and back sections of the XAD-2 resin tubes were split into separate vials for extraction. Filters were also placed into separate vials for extraction. All samples were extracted with 2 mL of dichloromethane and 30 minutes of ultra-sonication. During this time, PAHs desorb from the resin/filter and move into solution. After desorption, a small quantity of the extract is transferred to a vial and an internal standard is added. This vial is analysed for PAHs by gas chromatography – mass spectrometry (GC-MS) on a DB-5MS column. After analysis the results for the back sections of the tubes was checked for evidence of breakthrough—none was observed.

#### 1.3.5 Nitrogen Dioxide ( $\text{NO}_2$ ) and Sulphur Dioxide ( $\text{SO}_2$ )

The Radiello cartridge (code RAD 166) is made of microporous polyethylene coated with tri-ethanolamine (TEA). Nitrogen ( $\text{NO}_2$ ) and sulfur ( $\text{SO}_2$ ) dioxides are chemiadsorbed onto TEA respectively as nitrite and sulphite or sulphate ions. Nitrite was quantified by visible spectrophotometry while sulphite and sulphate were analysed by ion chromatography. Sampling is selective for gaseous molecules: any airborne nitrite, sulphite or sulphate will not cross the diffusive membrane. Both the tube and filters were extracted with laboratory water and then analysed for the target analyte.

*Nitrogen Dioxide:* Nitrite was analysed using a flow injection autoanalyser (Lachat QuikChem 8000, Loveland, Colorado, USA). The nitrite is determined by diazotization with sulfanilamide

under acidic condition to form a diazonium ion. The resulting diazonium ion is complexed with N-(1-naphthyl)-ethylenediamine dihydrochloride. The resulting pink dye absorbs at 540 nm.

Average airborne concentrations of  $\text{NO}_2$  ( $\mu\text{g}/\text{m}^3$ ) were then determined similar to VOCs, using Eq. (1), where  $m$  is the mass of  $\text{NO}_2$  ( $\mu\text{g}$ ) determined from the analysis,  $t$  is the total exposure time (minutes) and  $Q_K$  is the sampling rate (mL/min) at the average sampling temperature (K). The manufacturer quoted sampling rate of 78 mL/min at 298 K [6] was corrected for the sampling temperature using the expression;

$$Q_K = Q_{298}(K/298)^7 \quad (3)$$

*Sulphur Dioxide:* Sulphite was extracted from the filter in the laboratory and oxidized to sulphate using hydrogen peroxide and analyzed by ion chromatography using a conductivity detector.

The Chromatography system (Dionex DX 500, Sunnyvale, California, USA) consisted of: Model CP40 pump and system controller, Model 717 plus WISP autosampler, Model CD20 conductivity detector, Dionex AS411 anion column (4 mm) and AG11 anion guard column (4 mm), Dionex ASRS 300 (4 mm) Suppressor.

Average airborne concentrations of  $\text{SO}_2$  ( $\mu\text{g}/\text{m}^3$ ) were then determined using Eq. (1), similar to the VOCs, where the value of  $Q_K$  may be determined using Eq. 3, and the manufacturer quoted sampling rate of 119 mL/min at 298 K [6].

## 2 Methods - Ventilation Simulations using Computational Fluid Dynamics

### 2.1 CFD Domain - Simulation of the Migration of Diesel Particulates from Vehicle Exhausts and $\text{SF}_6$ (tracer gas) in Confined Regions of the Underground Mine

As outlined in the preceding section, DPM concentrations in underground mines are significantly higher than other working environments [7], and continuous or over-exposure to such high levels of nano particulates in addition to the exhaust gases from vehicle engines pose serious health risks to miners. Careful design and continuous monitoring of ventilation systems in underground mines has helped in controlling the overall levels of the diesel particulates and exhaust gases. However, regions typically undergoing shotcreting or bogging involve continuous operation of heavy machinery in confined spaces that inevitably lack the design level of ventilation. It is hence imperative to evaluate the typical distribution of diesel exhausts, particularly the nano-particulates, to evaluate and control the occupational exposure for underground miners. This can be accomplished (as per the previous report section) in mine sites by releasing a known concentration of a tracer gas – Sulfur hexafluoride ( $\text{SF}_6$ ) – near the vehicle and measuring it at desired locations in the mine to map the expected concentration distribution of diesel engine exhaust gases and particulates [8]. Computational fluid dynamics (CFD) is an alternate approach to allow similar mapping of pollutants (including DPM) within the mine, or specific regions of concern. The CFD approach (as with the tracer gas method) is considered more

accurate than 1D simulation tools which are conventionally used for mine ventilation design and management. The simulation of DPM migration and distribution in underground mines involves the modeling of two phases, air (with mixed exhaust gases) and the diesel particulates.

This section of the report summarizes the methodology adopted for CFD simulations of DPM and SF<sub>6</sub> distributions, during various activities including shotcreting, bogging and charging, in an underground development region AST-1900 in the Sunrise Dam Gold Mine (Western Australia). For activities such as bogging, that require the vehicle to be in constant motion, simulations with the vehicle placed at different locations are carried out to evaluate the influence of the location of the diesel exhaust sources on the dispersion and DPM in vicinity.

A range of diesel equipment was in use in the mine at the time of the study and this was captured as far as possible in the simulations. Most mobile plant had either original equipment (OE) or aftermarket diesel particulate filters fitted, apart from light vehicles. The average rating of equipment in use was Tier 3 or Euro 4 (equipment that is also supplied for on-highway use is rated under the EURO emissions regulations rather than Tier).

Figure 1 shows the schematic of the computational domain comprising of the underground mine region and ventilation channels. A 3D geometry of the region was obtained for the simulations from AngloGold Ashanti. As shown in the figure, the length of the development face considered for the study is 66.6 m, which has an average cross-section of about 6.5 m (height) × 5.5 m (width), and a 20.6 m long cuddy with an average cross-section of 6.5 m (height) × 6 m (width) is located orthogonal to the tunnel. A forcing duct system with a duct diameter of 1.2 m and an outlet diameter of 0.6 m (partially bocked – see photograph in Fig. 1) was used for ventilation in the region of the mine. The duct outlet was 15.2 m away from the heading face for shotcreting and bogging activities.

As mentioned above, three activities *viz.* shotcreting, charging and bogging with various locations of the vehicles in the underground mine are considered for this study. Details of the different configurations and operating conditions considered for the simulations are given below.

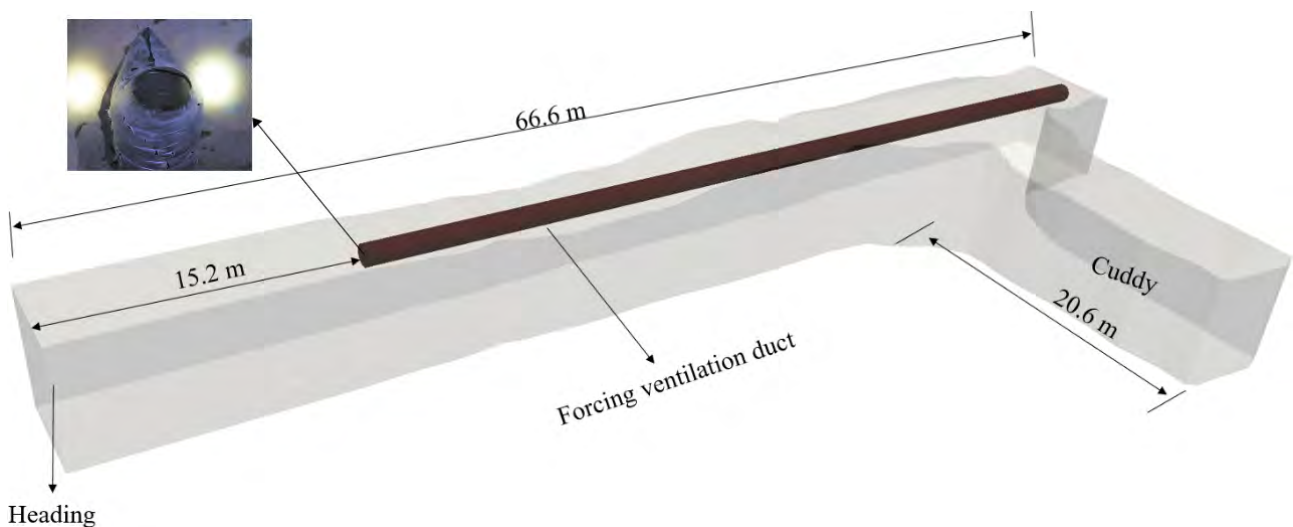


Figure 1: Computational domain comprising of the AST-1900 mine development and the ventilation channels

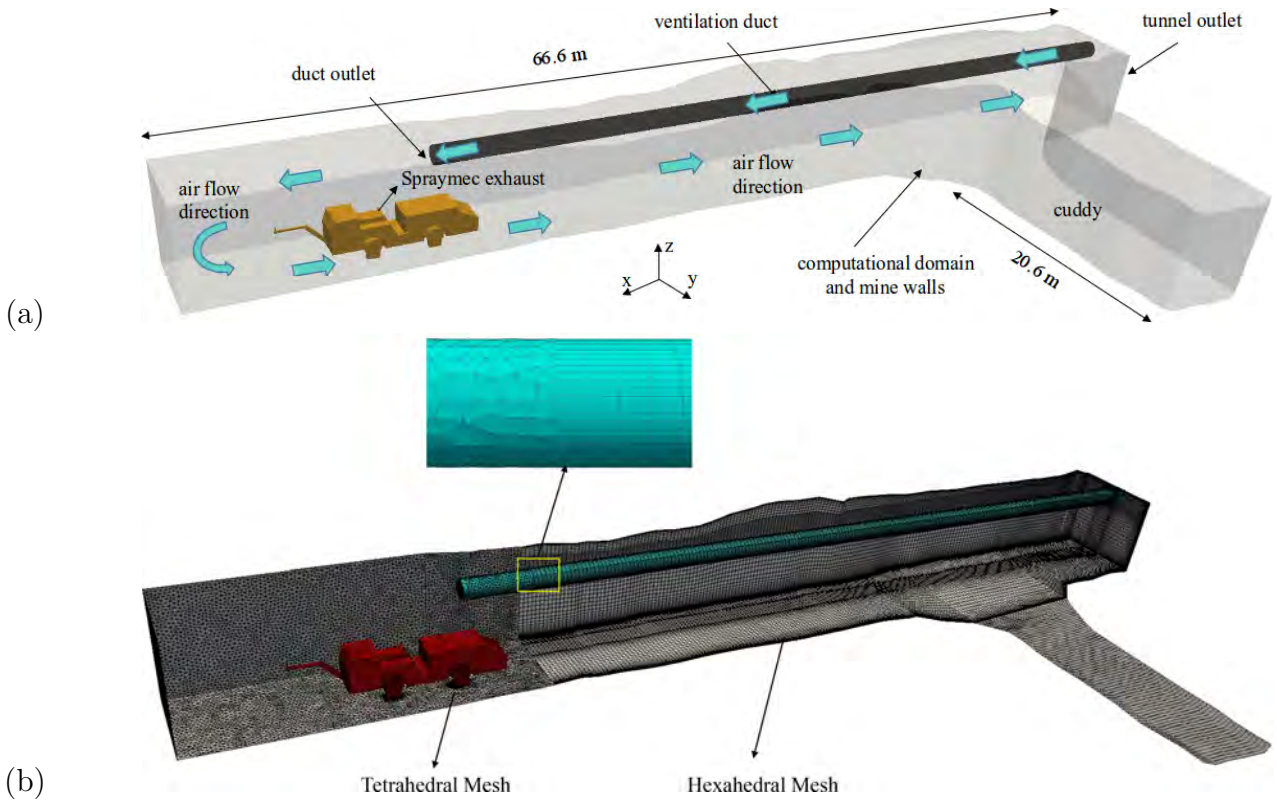


Figure 2: Computational domain and surface mesh of the underground AST-1900 region with a Spraymec positioned in a representative location

### 2.1.1 Shotcreting Activity

The vehicle model used for shotcreting was a Normet Spraymec 904 (90 kW). The Spraymec was positioned 8.5 m from the heading face, as shown in Figure 2(a). As shown in Fig. 2(b), a hybrid mesh with tetrahedral and hexahedral cells was generated using ANSYS ICEM was used for the simulations. The boundary conditions for the simulation are given in Table-1. The DPM emission rate of the Spraymec is based on Mine Safety and Health Administration (MSHA) data [9] and the exhaust flow rate is calculated according to the Product Guide [10].

### 2.1.2 Bogging/Loading Activity

The vehicle model used for the bogging activity was a Caterpillar Loader R3000H (305 kW). Unlike the shotcreting or charging activities that involve the vehicle to be at a particular location, bogging involves the vehicle to be in motion for most of the duration of work. Hence, three representative locations of the bogger in the vicinity of the confined underground mine

Table 1: Operating conditions for the CFD involving Shotcreting Activity

Boundary	Material	Flow rate	Units
Duct outlet	air	2.12	$\text{m}^3/\text{s}$
Spraymec exhaust	air	0.358	$\text{m}^3/\text{s}$
	DPM	$1.22 \times 10^{-6}$	$\text{kg}/\text{s}$
	$\text{SF}_6$	$3.58 \times 10^{-5}$	$\text{m}^3/\text{s}$

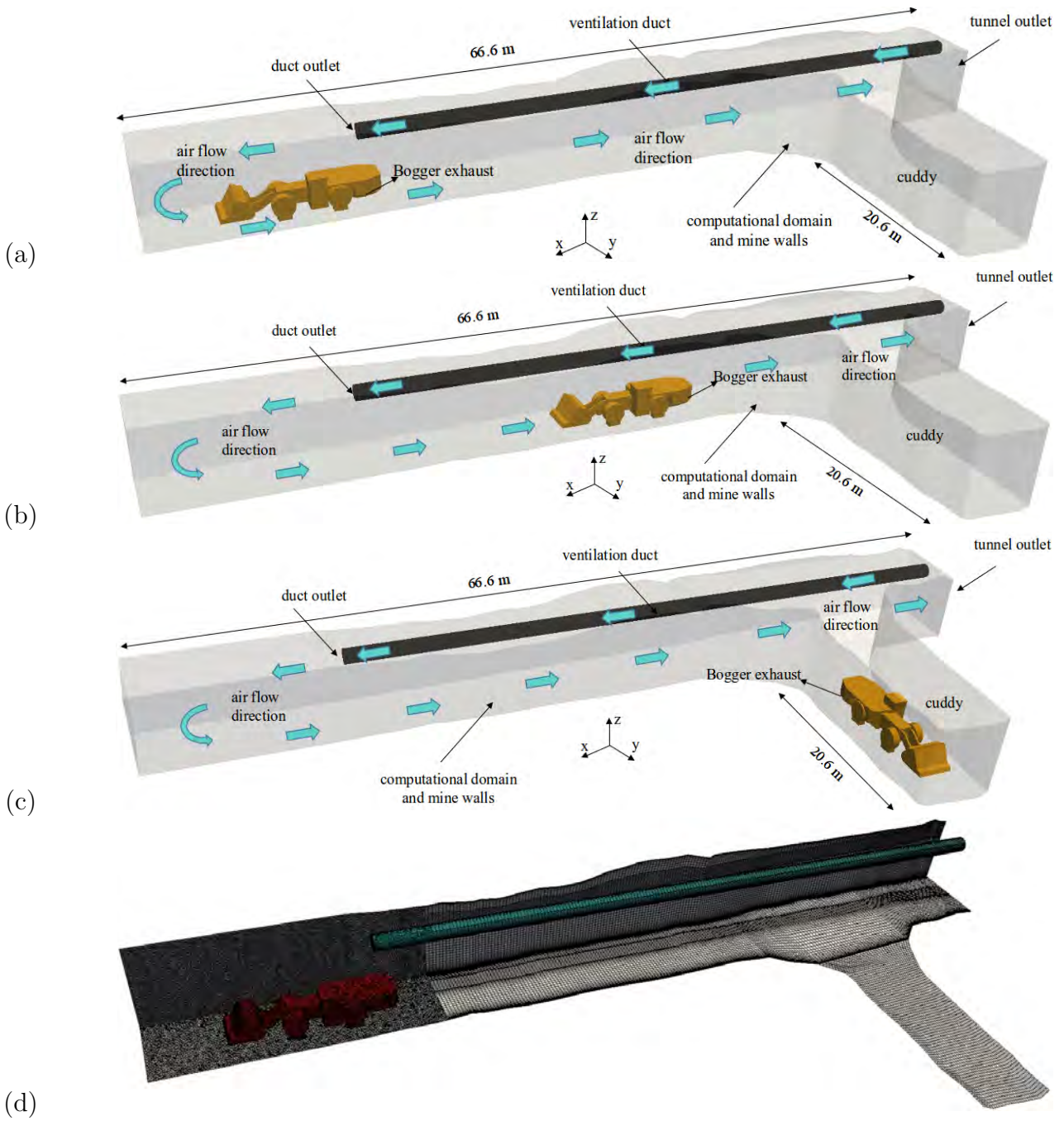


Figure 3: Computational domain and surface mesh of the underground AST-1900 region with a Loader positioned in three representative locations

regions were chosen for the simulation as shown in Fig. 3(a-c). As shown in the figure, the three chosen locations correspond to the bogger being 5 m and 30 m away from the heading face for cases 1 and 2 and 5 m from the cuddy heading for case 3. The boundary conditions for the simulation are given in Table-2. A hybrid mesh, as discussed in the preceding sections was employed for the simulations; a representative surface mesh for case-1 is shown in Fig. 3(d).

### 2.1.3 Charging Activity

The vehicle model used for charging activity was a Normet Charmec 1614B (110 kW Tier III). The Charmec was located at a distance of 5 m from the heading face for the simulations. Figure

Table 2: Operating conditions for the CFD involving Bogging Activity

Boundary	Material	Flow rate	Units
Duct outlet	air	2.12	m <sup>3</sup> /s
Bogger exhaust	air	1.215	m <sup>3</sup> /s
	DPM	$6.056 \times 10^{-6}$	kg/s
	SF <sub>6</sub>	$3.58 \times 10^{-5}$	m <sup>3</sup> /s

Table 3: Operating conditions for the CFD involving Charging Activity

Boundary	Material	Flow rate	Units
Duct outlet	air	2.12	m <sup>3</sup> /s
Charmec exhaust	air	0.437	m <sup>3</sup> /s
	DPM	$1.347 \times 10^{-6}$	kg/s
	SF <sub>6</sub>	$3.58 \times 10^{-5}$	m <sup>3</sup> /s

4(a,b) shows the computational domain and representative surface mesh of the underground AST-1900 region with a Charmec. Similar to the other cases considered for this study, A hybrid mesh with tetrahedral and hexahedral cells were employed for the simulation. Table-3 shows the boundary conditions used for the simulation.

## 2.2 CFD Domain - Simulation of DPM Re-circulation into Ventilation Intake due to Proximity with Exhaust

The second CFD analysis discussed in this report pertains to the evaluation of influence of relative proximity of the inlet ventilation portal and outlet shaft, on the re-circulation of DPM

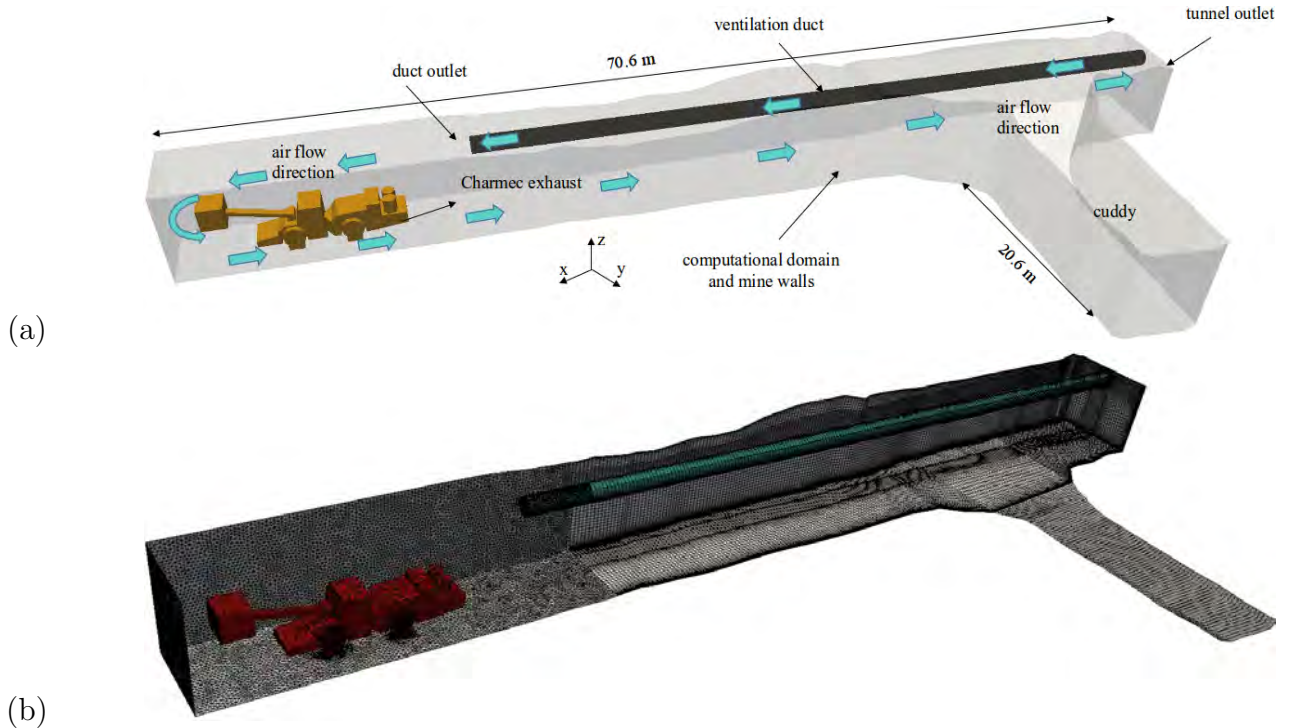
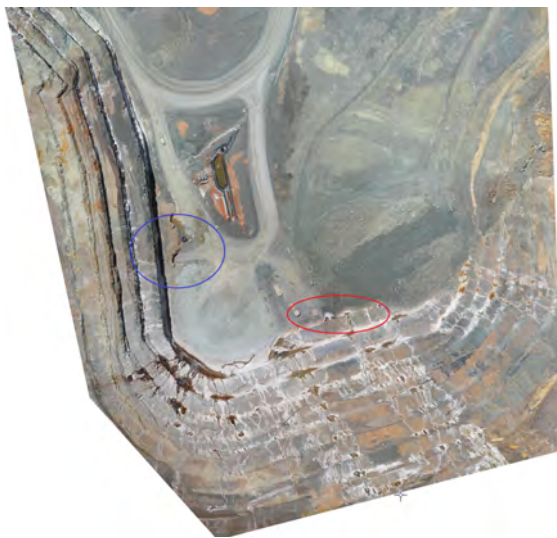


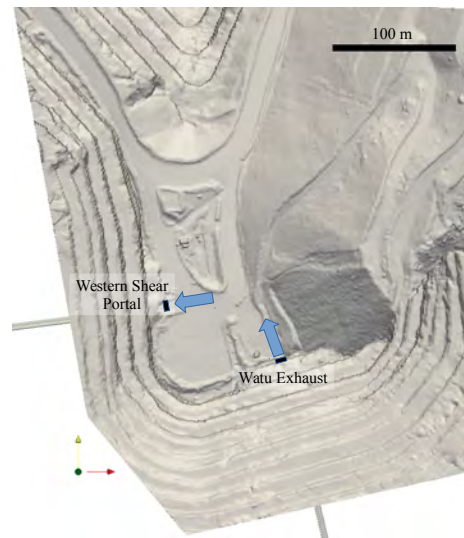
Figure 4: Computational domain and surface mesh of the underground AST-1900 region with a Charmec positioned in a representative location

into the ventilation stream. In many mines such [11] as Sunrise Dam Gold Mine, which have expanded from open-pit to underground mining, there is often limited space available to maintain adequate separation between the declines (that are also the ventilation inlets) from a given altitude and the outlet shafts. Careful design and placement of ventilation channels is paramount to for the efficacy of the underground ventilation system, and to avoid the build-up of DPM or exhaust gases ( $\text{NO}_x$ ,  $\text{SO}_x$ ,  $\text{CO}_x$ ) in the atmosphere of the underground mine.

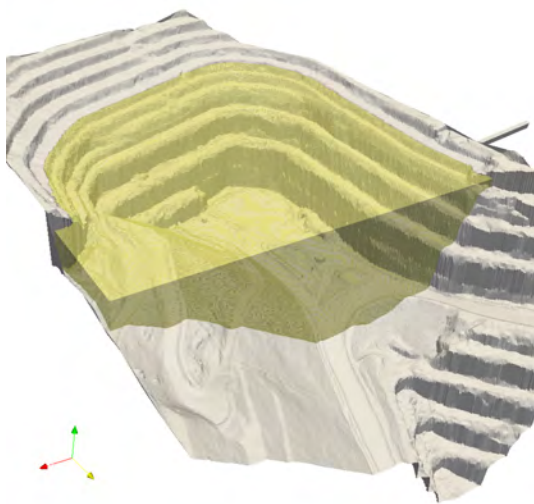
Figures 5(a,b) show the satellite and reconstructed 3D geometry of the open-pit section of the mine, indicating the Western Shear Portal and the Watu outlet (or return shaft) of Sunrise Dam Gold Mine, respectively. A computational mesh suitable for CFD was generated using the snappyHexMesh tool within OpenFOAM, with sufficient refinement in the vicinity of the walls to suit the turbulence models used. Figures 5(c,d) show the computational domain and



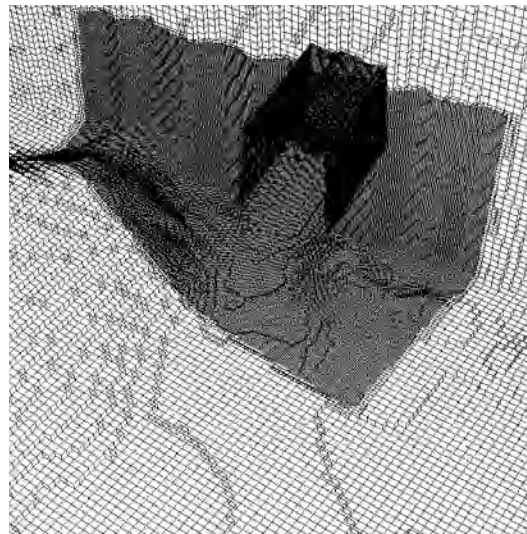
(a) satellite image of Western Shear portal (blue) and Watu exhaust (red)



(b) 3D reconstruction of mine pit showing ventilation inlet and outlet channels



(c) 3D image of the mine pit showing the region (yellow) used for CFD analysis



(d) representative surface mesh in the mine pit near Watu exhaust

Figure 5: Satellite topography of the Western Shear / Watu ventilation regions of Sunrise Dam gold mine, and geometry and representative surface mesh used for CFD analysis

representative surface mesh (at the outlet) used for the simulations. The mesh generated using this technique ensures surface-conformance, high mesh quality such as cell aspect ratios ( $\approx 1$ ), with predominantly hexahedral (96 %) cells in a structured distribution. The remaining elements are polyhedral (3 %) located near the ground and walls, which are 8-16 times smaller than the internal mesh. A mesh of size 8.98 million was used for the simulations.

The portal inlet and the return shaft each have a cross-section of about  $5 \text{ m} \times 6 \text{ m}$  (an area of about 28-30  $\text{m}^2$ ). Two cases corresponding to flow rates of 100 and 50  $\text{m}^3/\text{s}$  were considered for the simulations – representative of approximately full and 50% of the design flow rate given in the Ventilation plan for the area. Given the asymmetry in the topography of the region, an additional simulation was performed by reversing the flow directions in Watu and the Western Shear Portal, for 100  $\text{m}^3/\text{s}$ . Based on the field measurements made at the Watu outlet using Fidas Frog (Palas GmbH, Germany) a DPM concentration of  $200 \times 10^{-9} \text{ kg/s}$  was released at the outlet. The overall variation in the DPM concentrations at the outlet was measured to be between  $900\text{--}1500 \times 10^{-9} \text{ kg/s}$  over a period of 24 hours. Details of the computational methodology employed for the simulations are given in the following sections.

### 2.3 Computational Technique

The computational methodology employed for both the aforementioned CFD analyses discussed in Sections-(2.1,2.2) and is presented below. From a CFD standpoint, the volume fraction of DPM in air that is expected in such operating environments is low enough (typically  $\ll 10^{-4}$ ) for the particles to have any influence on the flow field. The migration of the particles is largely controlled by the surrounding mean flow, local turbulence and additionally, albeit to a much lower degree, molecular and Brownian diffusion. Given this, the species transport numerical technique within OpenFOAM is adopted for the simulations, which solves the conservation equations of mass, momentum and the concentration of DPM or  $\text{SF}_6$ . This is a two stage numerical procedure where – (i) the steady state flow field is initially evaluated using simpleFoam solver, and subsequently, (ii) the conversation of species is solved on the evaluated flow field using a customized (including dispersion due to turbulence) scalarTransportFoam solver. The material properties of air, DPM, and  $\text{SF}_6$  used in the simulations are listed in Table-4. All computational simulations reported here were carried out using 144-240 cores on the super-computing facility Magnus with a Cray XC40 system, located at the Pawsey Supercomputing Centre, Perth, Australia.

The governing equations for the conservation of mass, momentum and species concentration during steady incompressible flow are given below.

Table 4: Physical properties of materials used for the CFD simulations

Property	Units	Air	DPM	$\text{SF}_6$
density ( $\rho$ )	$\text{kg}/\text{m}^3$	1.2	1770	6.108
dynamic viscosity ( $\mu$ )	$\text{Pa}\cdot\text{s}$	$1.8 \times 10^{-5}$	-	-
diffusion coefficient in air ( $D$ )	$\text{m}^2/\text{s}$	-	$9.494 \times 10^{-6}$	$5.9 \times 10^{-6}$

$$\text{Continuity: } \nabla \cdot \vec{u} = 0 \quad (4)$$

$$\text{Momentum: } \nabla \cdot (\vec{u}\vec{u}) = -\frac{1}{\rho}\nabla p + \left(\frac{\mu}{\rho} + \nu_T\right)\nabla^2\vec{u} + \vec{g} \quad (5)$$

$$\text{Species: } (\vec{u} \cdot \nabla) C = \left(D + \frac{\nu_T}{Sc_T}\right)\nabla^2 C \quad (6)$$

where,  $\nu_T$  is the turbulence viscosity and  $Sc_T = 0.85$  is the turbulent Schmidt number. Turbulence is modeled in this study using the  $k - \epsilon$  model with standard wall functions. The equations for the conservation of turbulence scalars are given as:

$$\text{Turbulence kinetic energy: } \nabla \cdot (\vec{u} k) - (\vec{u} \cdot \nabla) k - \left(\frac{\mu}{\rho} + \nu_T\right)\nabla^2 k = G - \epsilon \quad (7)$$

$$\text{Turbulence dissipation rate: } \nabla \cdot (\vec{u} \epsilon) - (\vec{u} \cdot \nabla) \epsilon - \left(\frac{\mu}{\rho} + \alpha_\epsilon \nu_T\right)\nabla^2 \epsilon = \Omega_{\epsilon 1} \frac{\epsilon}{k} G - \Omega_{\epsilon 2} \frac{\epsilon^2}{k} \quad (8)$$

where,  $G = \nu_T^2 |S_{ij}|^2$ , the turbulence viscosity  $\nu_T = \Omega_\mu k^2 / \epsilon$  and the closure constants are  $\alpha_\epsilon = 0.76923$ ,  $\Omega_{\epsilon 1} = 1.44$ ,  $\Omega_{\epsilon 2} = 1.92$  and  $\Omega_\mu = 0.09$ .

Both the flow as well as the species transport simulations for all the cases were carried out at steady state using second order blended or central difference numerical schemes for all the variables. Pressure-velocity coupling was handled using the SIMPLE algorithm. Under-relaxation, typically 0.5-0.7 was applied to improve simulation stability.

### 3 Methods - Chamber Study

Refer to Appendix-2.

## 4 Results and Discussion

### 4.1 Personal Monitoring

Figure 6 (a-c) show the typical realtime monitoring data for selected workers. These were measured using the spectrometers (DiSCmini), which nominally measure all particles <700 nm. It can be seen that the surface or control workers had significantly different exposures to underground workers, with the former having a lower mass concentration but also a lower mean particle diameter. The number concentration for underground workers can be seen to be highly variable throughout the work shift.

Average nanoparticle exposures measured were found to correlate strongly with Elemental Carbon (EC) values monitored using the NIOSH 5040 protocol [1]. However some outliers with elevated nanoparticle exposure relative to EC were found which are being further explored. Figure 7 shows these data. Figure 7 shows a plot of the correlation between matched EC and (nano)particle exposures, the latter measured using the real-time diffusion spectrometer (discmini). A Pearson correlation demonstrated a highly significant correlation between EC and particle number concentration ( $R=0.82$ ,  $p<0.001$ ), however, a number of outliers exist with

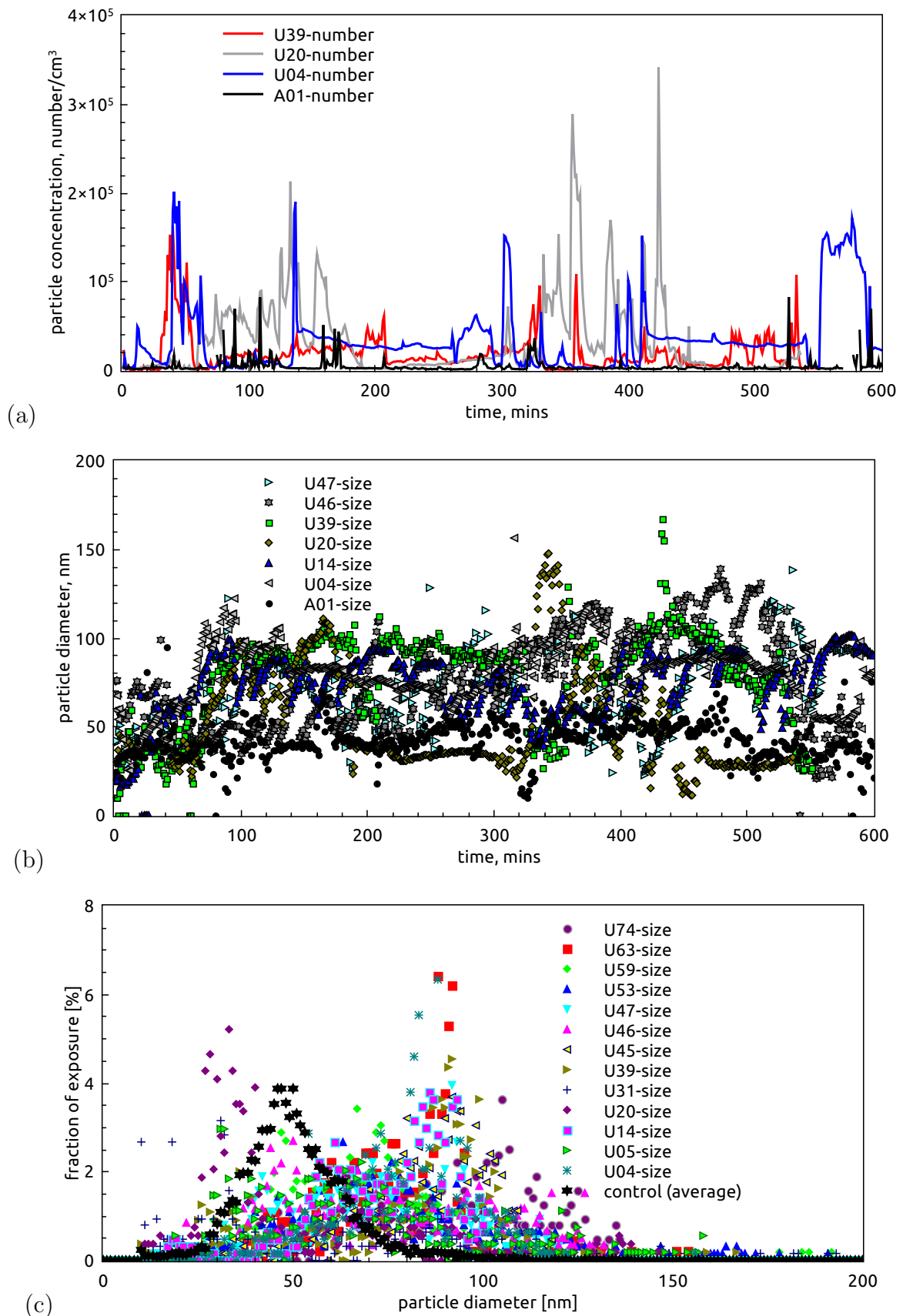


Figure 6: Typical realtime personal monitoring data for underground workers (designated Uxx), compared with Surface worker data (designated control or Axx); (a) Particle number concentration over time, (b) particle mean diameter over time, (c) frequency histograms of particle diameter (probability of exposure to a given particle diameter over the period of work)

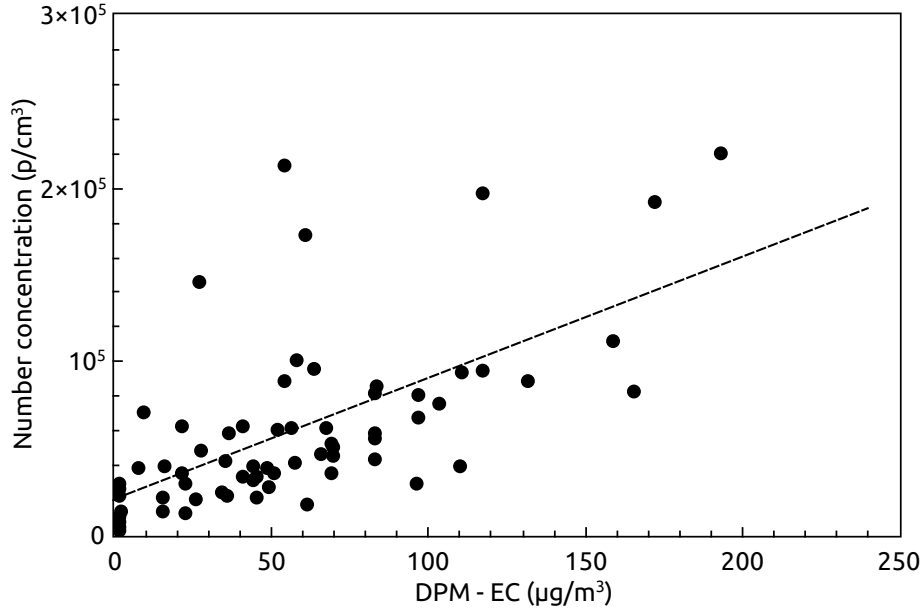


Figure 7: Shift average DPM (EC) vs shift average (nano)particle number concentration for matched worker exposures. Nanoparticle counts are averaged from 11 hours of continuous measurement data for each worker.

very high particle number exposure, without commensurate DPM values, such particles cannot be viewed as benign because they may not contain EC. During subsequent measurements post this main study, elevated particle counts (without commensurate DPM and PM1 (Frog) measurements, were found in the newly installed underground workshop which uses evaporative coolers. It is likely that residual salt/contaminant particles from the cooling water were contributing to the counts.

One of the questions for the research was whether nanoparticle exposure is captured sufficiently by current monitoring requirements which monitor mass based particle exposure (in the case of diesel particulate matter (DPM) exposure this is measured as elemental carbon (EC). It can be seen that this is generally the case, noting the comments above.

Approximately 5% of the workers, however demonstrate very high nanoparticle exposure but comparatively low EC levels. Whilst it is possible that these workers were exposed to high levels of nanoparticles not originating from diesel exhaust, this seems unlikely. The high temporal variability of the nanoparticle concentrations shown in Fig. 6 however lend weight to the potential need to monitor peak exposures and/or variability, rather than shift averages.

The approximate relationship between EC and particle concentration found during the personal monitoring can be given as,

$$C_N = 698.45 \times EC_\mu + B \quad (9)$$

where  $C_N$  is the particle number concentration (expressed as particles/cm<sup>3</sup>),  $EC_\mu$  is the elemental carbon concentration (in  $\mu\text{g}/\text{m}^3$ ) and B the baseline particle concentration in locations with no diesel sources (in this case  $\sim 20890$  particles per m<sup>3</sup>), which is expected to vary between mines. It should be emphasised that this relationship is only valid for the DiSCMini,

Table 5: Summary statistics for individual monitoring for (nano)particles and gases related to diesel exposure

Measure <sup>†</sup>	Unit	Control (n = 20) <sup>‡</sup>		Underground (n = 80)	
		Mean	Std. Dev.	Mean	Std. Dev.
EC / DPM	$\mu\text{g}/\text{m}^3$	3.1	5.3	63.0	41.1
Particle number	$\text{p}/\text{cm}^3$	14311	14206	67849	49274
Particle size	nm	50.1	6.3	58.94	12.7
NO <sub>2</sub>	ppm	0.000014	0.000007	0.000224	0.000163
SO <sub>x</sub>	ppm	0.000024	0.0	0.000045	0.000073

<sup>†</sup> Data for VOC species and metals are reported in the tables in Appendix-1. <sup>‡</sup> All values below detection limits are reported as the detection limit value. Control measures for DPM and NO<sub>2</sub> were generally below detection limits. Control values for SO<sub>2</sub> were all below the detection limit. Only 2 controls had EC values above the detection limit and were likely due to smoking rather than diesel exposure.

as other particle counters possess different upper and lower detection limits, which produce a shift in total particle counts if they were used to measure the same source.

Table-5 summaries gas and particulate measurements from control (surface workers not exposed to diesel particulate) and underground miner data. These results suggest that EC may generally be a reasonable indicator of nanoparticle concentration in an underground mine environment, and vice versa.

The results for personal samples collected from VOCs, SO<sub>2</sub>, NO<sub>2</sub> and Metals are provided in the Tables in Appendix-1, Tables-A1–A3. These are the calculated average airborne exposure concentrations for each substance for each worker. While there is some difference in exposures between the above ground and underground workers, there are no immediate causes for concern, with all workers being well below the OES values, even when accounting for the extended shift lengths.

Exposure to airborne metals were very low for all species tested. Exposure to iron (Fe) and calcium (Ca) appears consistent across both groups of workers. Measurable levels of potassium (K) were only recorded for underground workers. The only measurable levels of cadmium (Cd), lead (Pb) and lithium (Li) were recorded in above ground workers. The full results of the metals exposures are given in Table-A1, in Appendix 1.

Exposures to NO<sub>2</sub> were significantly higher in underground workers than in above ground workers, with minimal overlap between the two groups. The maximum recorded level of NO<sub>2</sub>

Table 6: Mean elemental carbon concentrations at stationary monitoring sites

Location	EC concentration, $\mu\text{g}/\text{m}^3$
Cosmo 1815	31.3
Astro 1965	72.3
Astro 1930	127.4
Cosmo East 1510	113.6
Cosmo East 1510	115.1
Vogue 1600	82.6
WATU Portal	33.1

was  $1.2 \text{ mg/m}^3$ . The majority of  $\text{SO}_2$  samples were below the detection level, with only 16% of underground workers having measurable  $\text{SO}_2$  exposures. There were no measurable exposures in above ground workers. The full results for  $\text{NO}_2$  and  $\text{SO}_2$  exposures are presented in Table-A2, in Appendix-1.

There were less differences in exposures between above ground and underground workers in terms of VOCs, with the majority of samples containing both alkanes and aromatic hydrocarbons. Exposure to BTEX chemicals (benzene, toluene, ethylbenzene and xylene) appears to be ubiquitous, though not at levels which pose serious concern. The highest exposure to benzene recorded was  $27 \text{ } \mu\text{g/m}^3$ , for example. For the majority of underground workers their main exposure to VOCs, was to the BTEX chemicals. The full results for VOC exposures are given in Tables-A3–A5, in Appendix-1. Subsequent data analysis and interpretation found significantly higher VOC exposure among jumbo and nipper operators that were using a solvent based glue to install bolts. Therefore in some cases the main VOC exposure is unlikely to have been due to diesel exhaust.

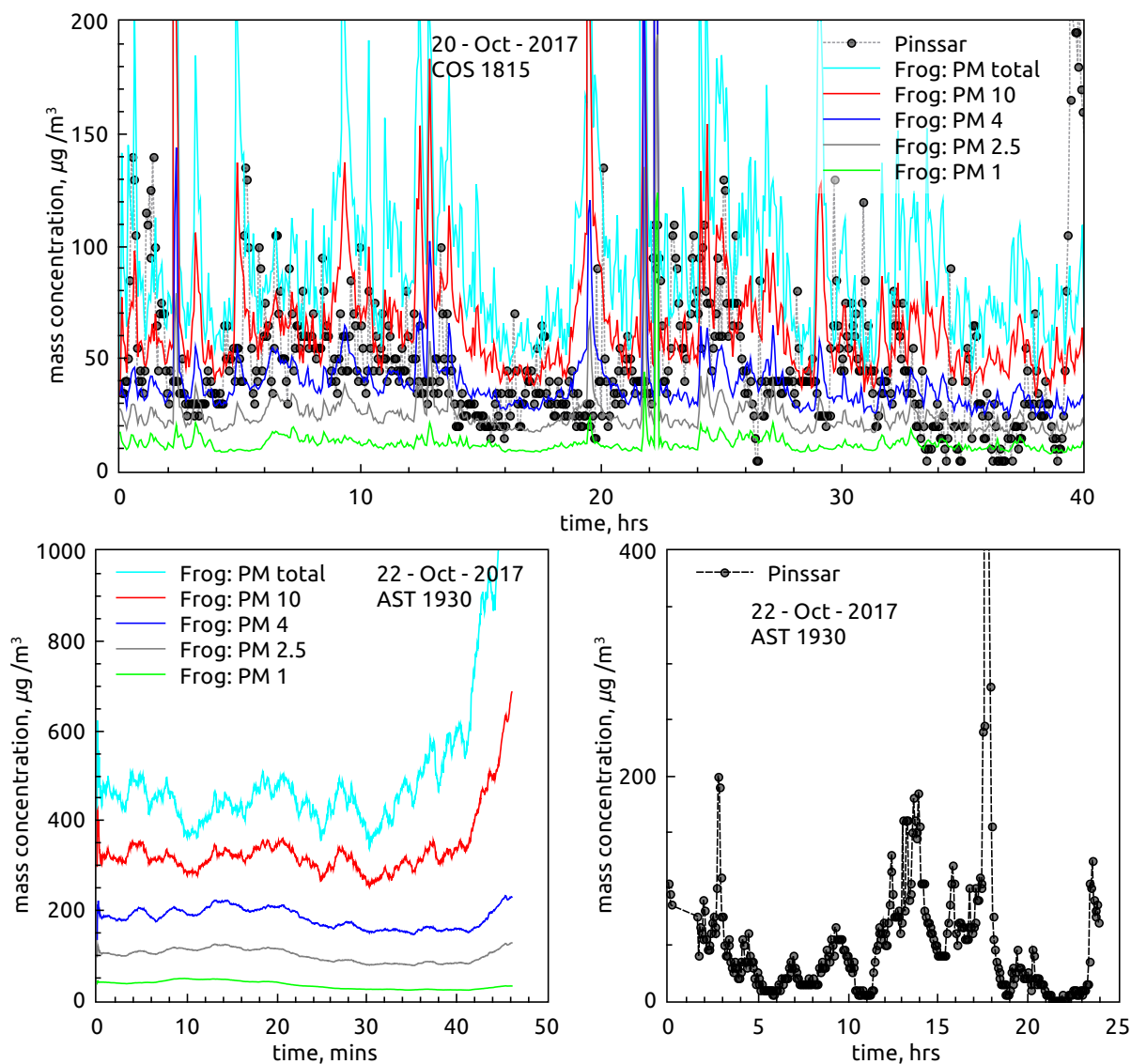


Figure 8: Optical Particle Counter measurements, (a) Cosmo 1815, (b,c) Astro 1930

## 4.2 Stationary Monitoring

Stationary monitoring sites were selected based on convenience, namely (a) proximity to suitable power transformers, (b) sufficient space to leave equipment for 24 hours, (c) proximity to active work areas. Ventilation regions of the mine are given a name (Cosmo etc.) and a number based on elevation relative to an arbitrary datum, with lower numbers being deeper in the mine. Table-6 shows the sites monitored and the mean EC concentrations at each site. The Cosmo East 1510 (COE1510 in some figures) site was the deepest point monitored in the mine. 2 sets of EC samples and PAH samples were taken at this site as sampling had to be discontinued one day because of imminent blasting at the sampling location, however the monitors were returned to the site the following day due to the high levels found. The WATU portal site was a vent

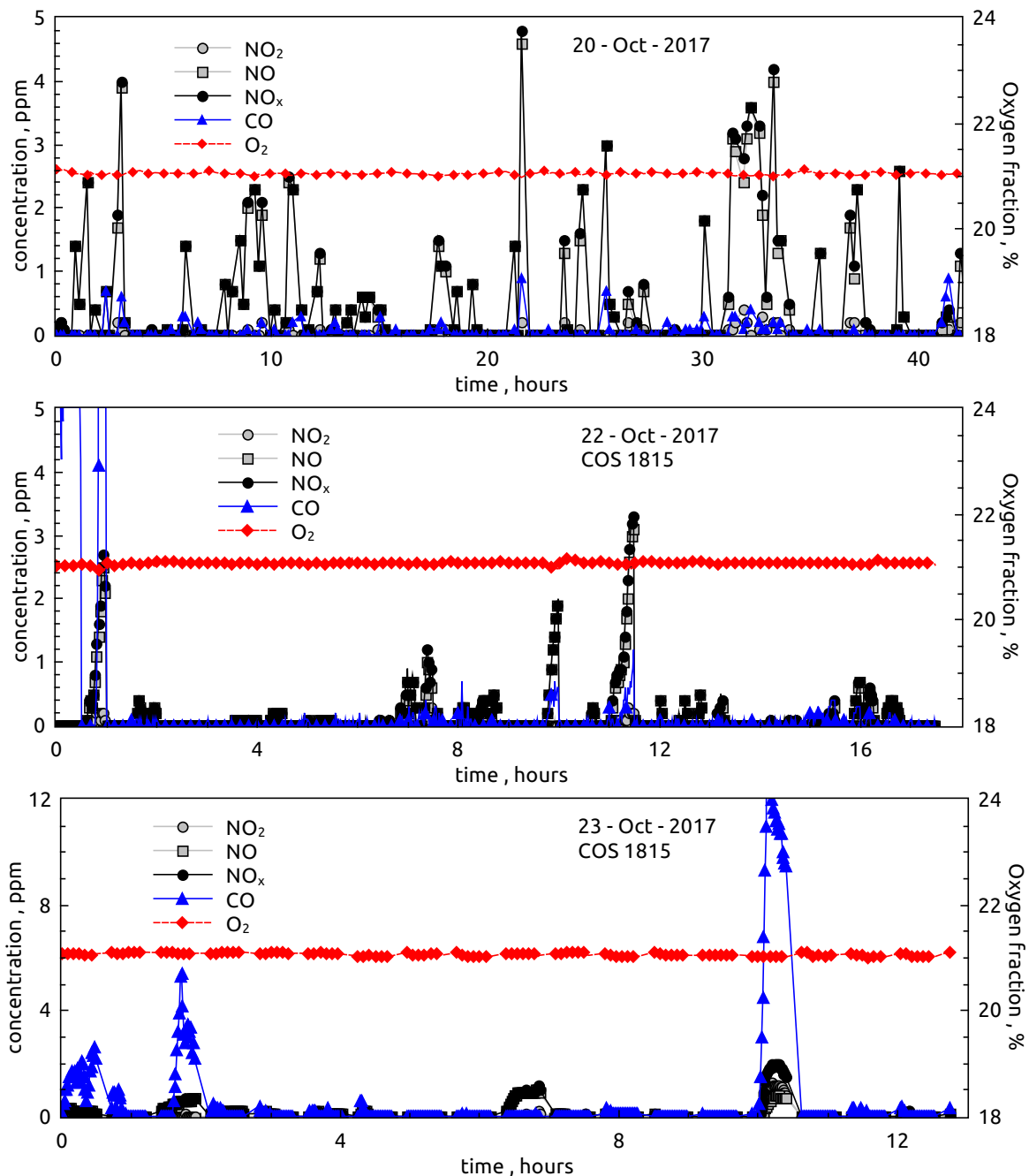


Figure 9: Gas measurements in the mine; temporal variation on different days/ locations

outlet located near a main portal/drive, at the bottom of the pit (refer Fig. 5 in Section-2.2). This site was selected to (a) measure outlet concentrations from the ventilation system and (b) measure/model potential short circuiting of gases from the outlet to the inlet combined with ChemCentre staff. It can be seen in Table-6 that two of the sites monitored had average EC concentrations above the guideline DPM level.

### 4.3 Optical Particle Measurements

Figure 8 shows the stationary optical particle counter (OPC) measurement data. Two different Optical particle counters were used, a 256-channel OPC (Palas) which measures size spectra from  $\approx 200$  nm to  $\approx 30$  microns and calculates mass based concentrations in the standard size classes used in occupational and environmental measurements of PM1, PM 2.5, PM4, PM10 and PMTotal ( $\approx$ PM30). The 2nd OPC (Pinssar) is designed for DPM measurement and uses

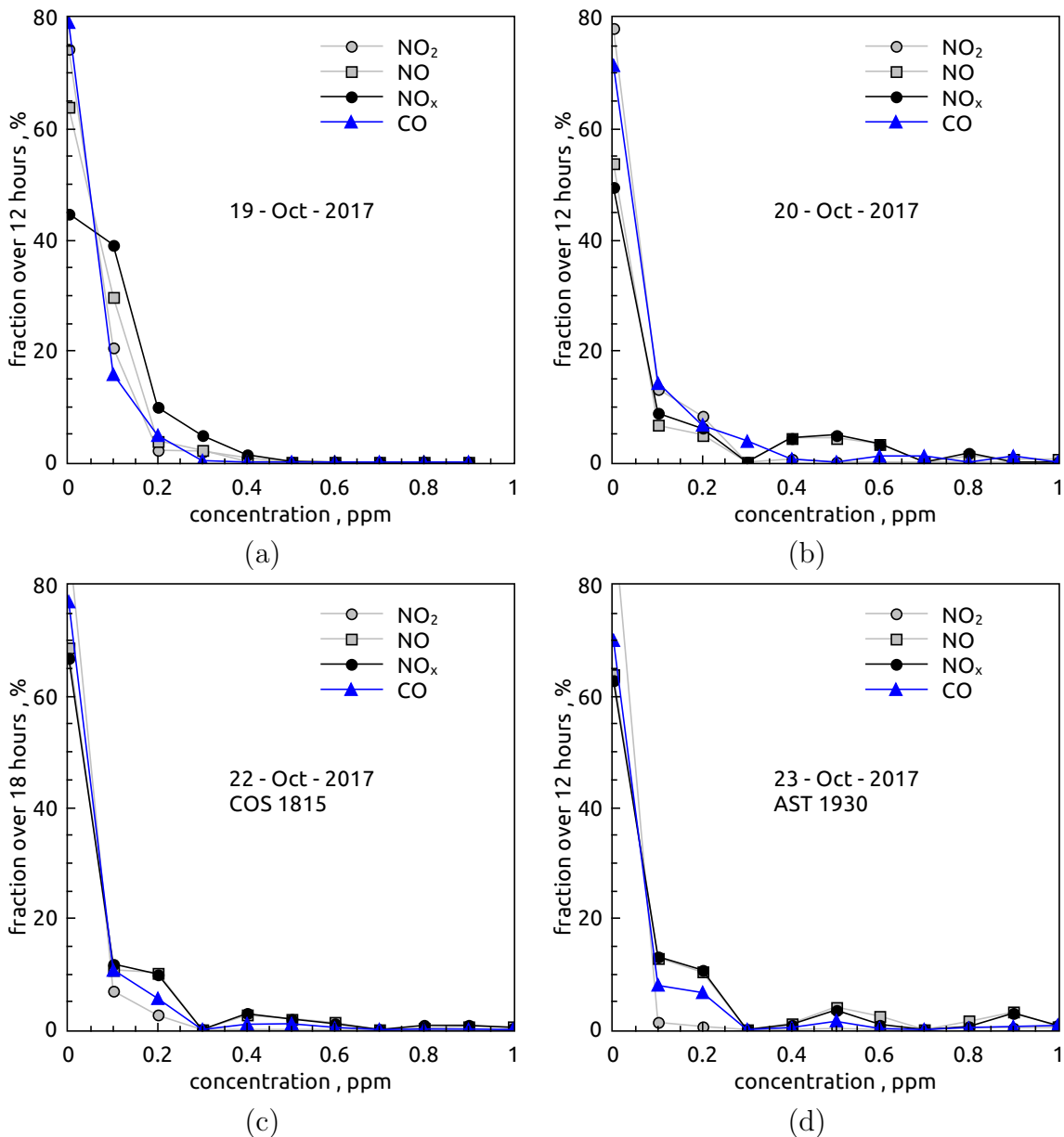


Figure 10: Gas measurements in the mine; proportional data on different days/ locations

an impactor with a cut size of  $\approx 800$  nm to ensure that only submicron particles are measured.

It can be seen that significant particulate of all sizes are present in the mine. The high velocity air in the main drive (Cosmo 1815) will ensure that large particles remain suspended. The Pinssar device is designed to measure particles from 200-800 nm (it includes a "sharp cut" impactor to remove larger particles) and convert the measured scattered light signal to a mass concentration. This size is considered to be representative of DPM. It was therefore surprising that the Pinssar results most closely correlate with the PM4 data from the Frog, rather than the PM1. The manufacturer however reported that they found some optical misalignment after the study was completed, which has since been corrected. As one Frog was loaned to the Chemcentre for use during the tracer gas experiments, we had limited data to compare PM1 and EC values, however generally found an approximate agreement.

#### 4.4 Gas Measurements

Figures 9(a-c) and Figs. 10(a-d) show the temporal gas data and proportional data respectively, on different days and locations in the mine. It can be observed that the values are highly transient, no doubt due to passing vehicles – especially in Cosmo 1815, which is a main drive. Blast flows may also have impacted results, however this could not be explicitly observed.  $\text{NO}_x$  values are calculated by oxidising NO to  $\text{NO}_2$ , as NO only have a short lifetime once emitted from an exhaust. However the conversion of NO to  $\text{NO}_2$  is often via photocatalytic processes, which are not present in an underground mine, resulting in longer lifetimes for NO.

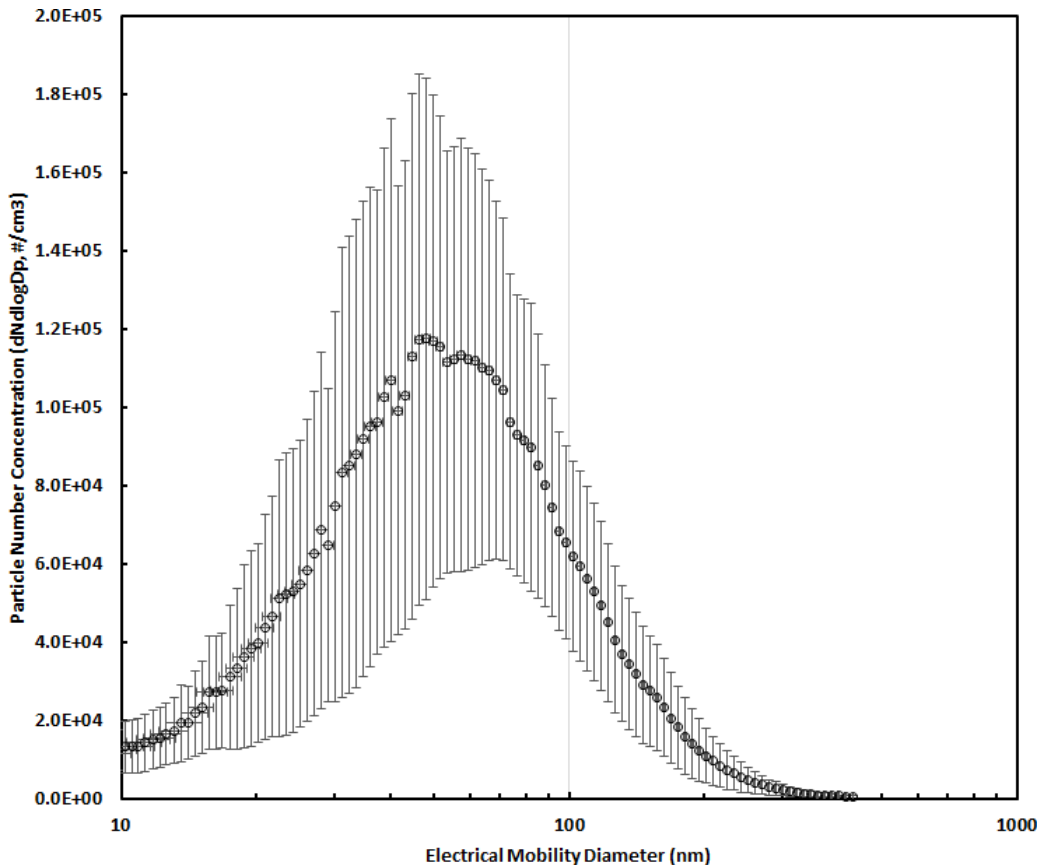


Figure 11: Average nano/ultrafine particulate spectrum measured in the mine (AST 1930)

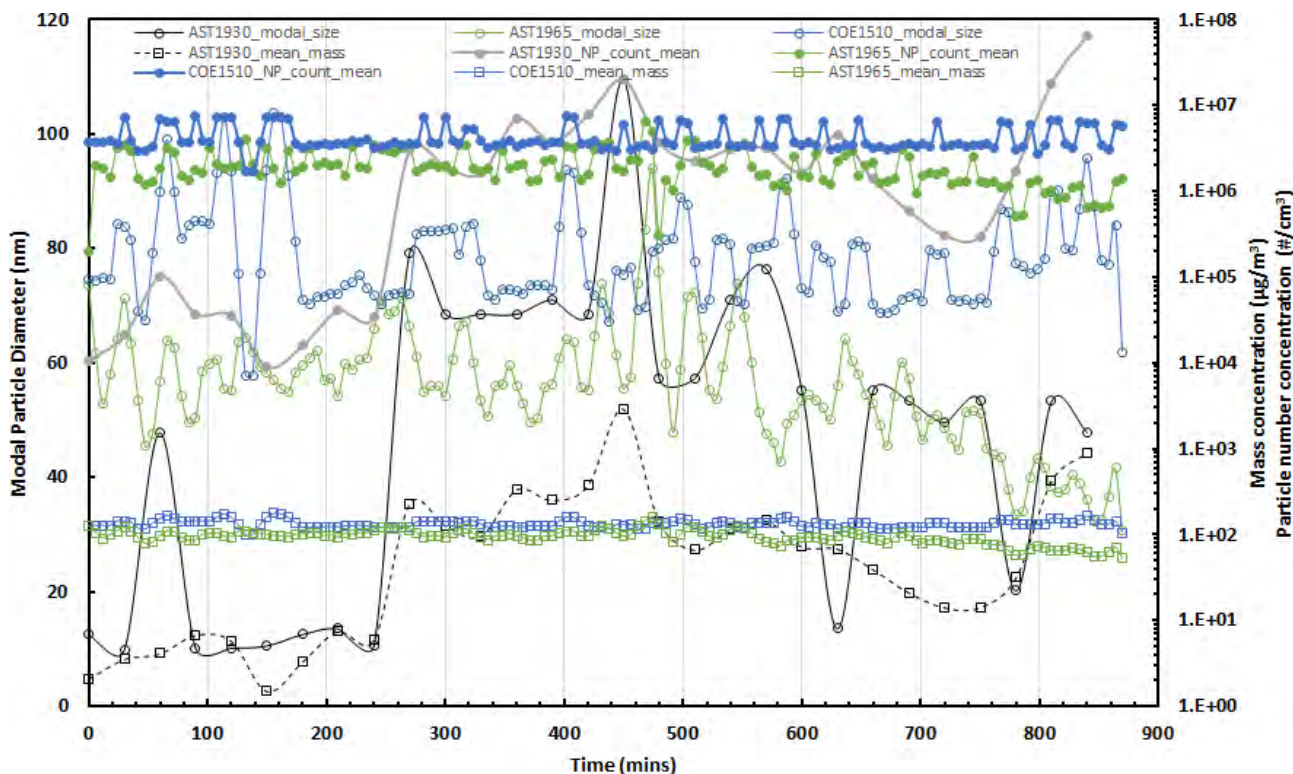


Figure 12: Diameter, mass and number concentration data for SMPS measurements

#### 4.5 Ultrafine/nano Particle Spectrometry

Figure 11 shows the nanoparticle spectrum measured in the mine at all the stationary sites. This represents a typical diesel soot (DEP) profile as found by previous studies, however the

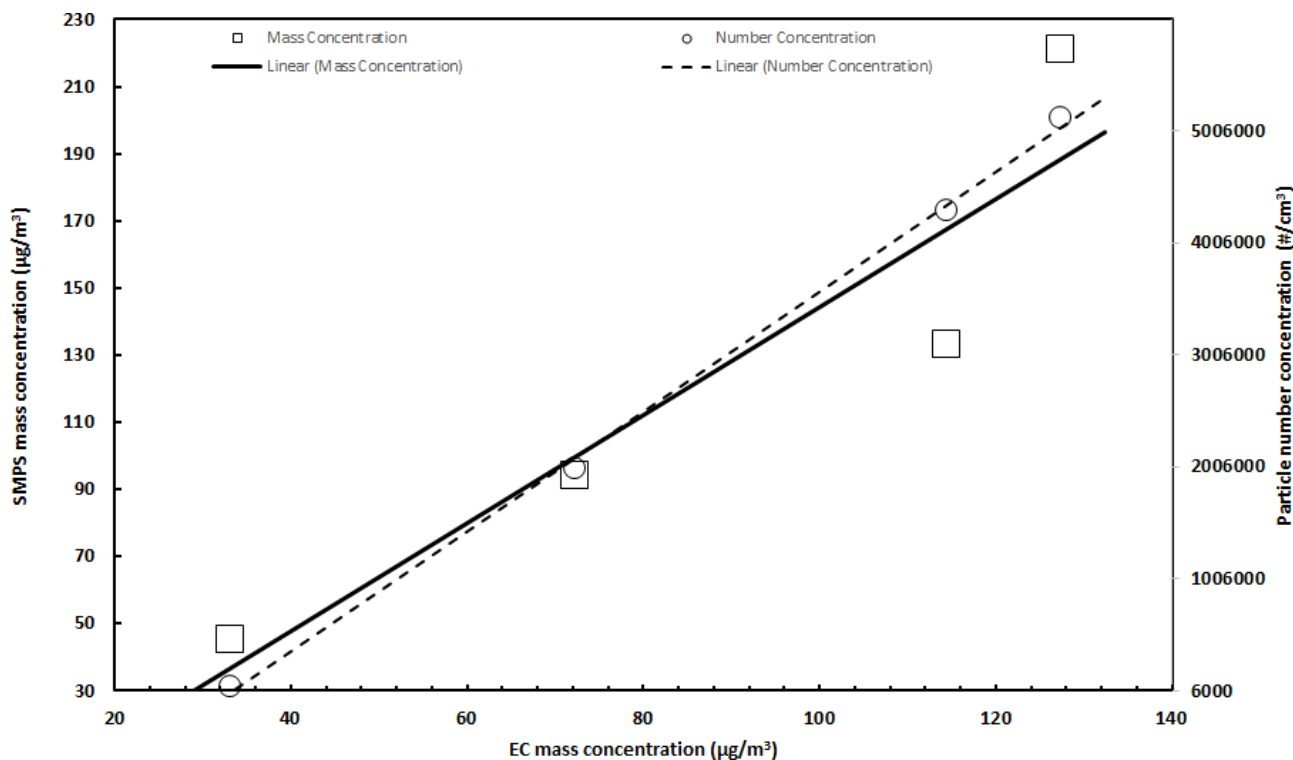


Figure 13: Correlation between average EC level and average number concentration and calculated mass concentration

peak is slightly shifted to the left (smaller) particle sizes compared to previous studies. This is possibly due to the fitment of diesel particulate filters, which may shift the peak particle size emitted to a smaller size (obviously though at a much lower concentration; see ref. [12]).

Figure 12 shows the particle number concentration found in each location measured. It can be seen that a significant number of nanoparticles were present in all cases, with mass and size changes temporally.

Figure 13 shows the correlation between mass-based filter EC values and measured ultra-fine particle concentrations using the SMPS systems. Data shown is for Astro 1930 and 1965, Cosmo East 1510 and Watu sites. Y-axis mass concentrations are calculated from number concentration data. The Watu data was measured using an SMPS and the mean particle size

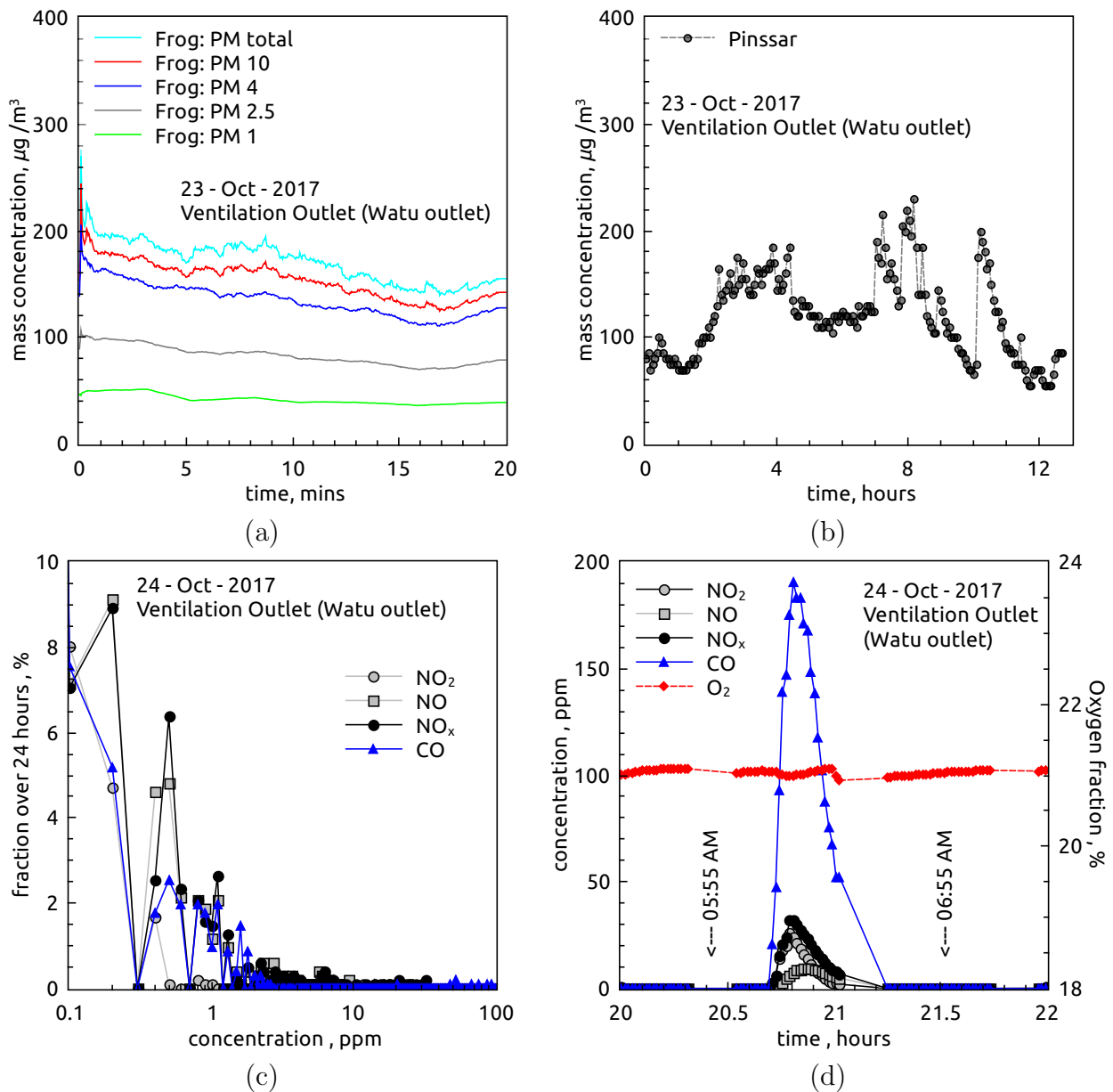


Figure 14: Measurements at WATU vent outlet; (a) mass concentration measurements using Palas-Frog, (b) mass concentration measurements using Pinssar, (c) proportional gas measurements over 24 hours, and (d) instantaneous gas measurements at certain intervals that recorded high CO and  $\text{NO}_x$  levels

from other sites used for calculations.

It can be seen that as with the personal monitoring data shown in Section 4.1, a good correlation exists between ultrafine/nanoparticle spectrometry and gravimetric EC values. The agreement appears to be improved for the stationary monitoring data, possibly due to the higher resolution of the SMPS over the DiSCmini, or the longer sampling time (and therefore greater statistics). It will be noted that the particle counts from the SMPS system shown in Figure 13 are higher compared the results in Figure 7 for the same EC level. This is likely due to the counting range and efficiency differences between the instruments, the SMPS systems used have been shown to measure reliably between 2-4 nm and up to 1000 nm (given a suitable DMA column). Although the DiSCMini is claimed to measure from 1-700 nm, a narrower range of 20-30 to 300 nm has been found in practice. The SMPS is also able to measure at higher concentrations as it performs a scan over several minutes and therefore is only counting a smaller fraction of the particles at any one time. The SMPS system is however significantly more expensive and even less suited to the hostile mine environment. This nevertheless highlights the importance of specifying the instrument to be used for measurement and performing calibrations if reference back to EC are to be performed.

It should also be noted that the particle counters used measure all particles within a given range. Therefore some of the particles measured may have included components of DPM that are not EC (about 20-30% of the mass of DPM is OC or non-carbon compounds), ultrafine salt particles, or ultrafine crustal dust. However, the close correlations between EC and particle concentration show that the main source of ultrafine particles in the mine was DPM.

#### 4.6 Watu Exhaust Shaft

Figure 14 shows gas and particulate levels at WATU outlet. SMPS spectrometry was not conducted, however particle number concentrations were recorded using the CPC. The average concentration measured was 43107 p/cm<sup>3</sup>. Table-6 also gives 33.1 µg/m<sup>3</sup> of EC. It is somewhat curious that the values found here are comparable with levels high in the mine intake/drive region such as Cosmo 1815. This is possibly due to dilution due to the high flow of air, or also inadequate extraction from deep in the mine. The temporal gas data in Fig. 14 (c,d) shows a strong temporal dependence, likely due to activity levels in the mine.

#### 4.7 Traverse Measurements

Figure 15 show gas and particulate levels during a mine traverse. The samplers were detached from Rig 2 and battery operated from a light vehicle while traveling down to Cosmo East 1510 and back. These results show the near-linear evolution of particulates and gases with increasing depth in the mine. These results raise questions about the ability to effectively ventilate deeper parts of a mine. The results may however be influenced by significant activity in the mine in the deeper parts at the time of measurement.

#### 4.8 Summary of Key Findings - Personal Monitors, Stationary and Mobile Measurements

As expected, the personal and stationary monitoring showed a correlation between ultrafine particulate levels and NO<sub>x</sub>, as both are the dominant emissions from diesel engines. 16% of the personal monitoring (EC) concentrations were above the guideline level of 100 μg/m<sup>3</sup>, as were average levels at 2 of the stationary sites measured. Particle count data showed a generally good correlation with monitored EC levels, whether measured using the personal spectrometers of the SMPS systems. Some outliers with high nanoparticle exposure but lower EC exposure were however present.

In general, the data suggests that conventional EC measurement methods provide a reasonable indication of nanoparticle concentrations. Correlations between the two could be applied given a larger dataset, however these may be mine specific. For example, the use of DPFs and or variations in plant and fuel may change correlations between EC and nanoparticle concentration.

Further insight on the data and implications for mine management will be provided by the health study, which will interpret these data in conjunction with health measures.

#### 4.9 CFD - DPM and SF<sub>6</sub> (tracer) Migration in Confined Regions of the Underground Mine

##### 4.9.1 Shotcreting Activity

As mentioned in the preceding section, for the range of flow rates and concentrations of DPM expected, the dispersion of DPM or SF<sub>6</sub> is predominantly controlled by the mean flow and turbulence levels in the air stream. It is hence important to understand the airflow behavior

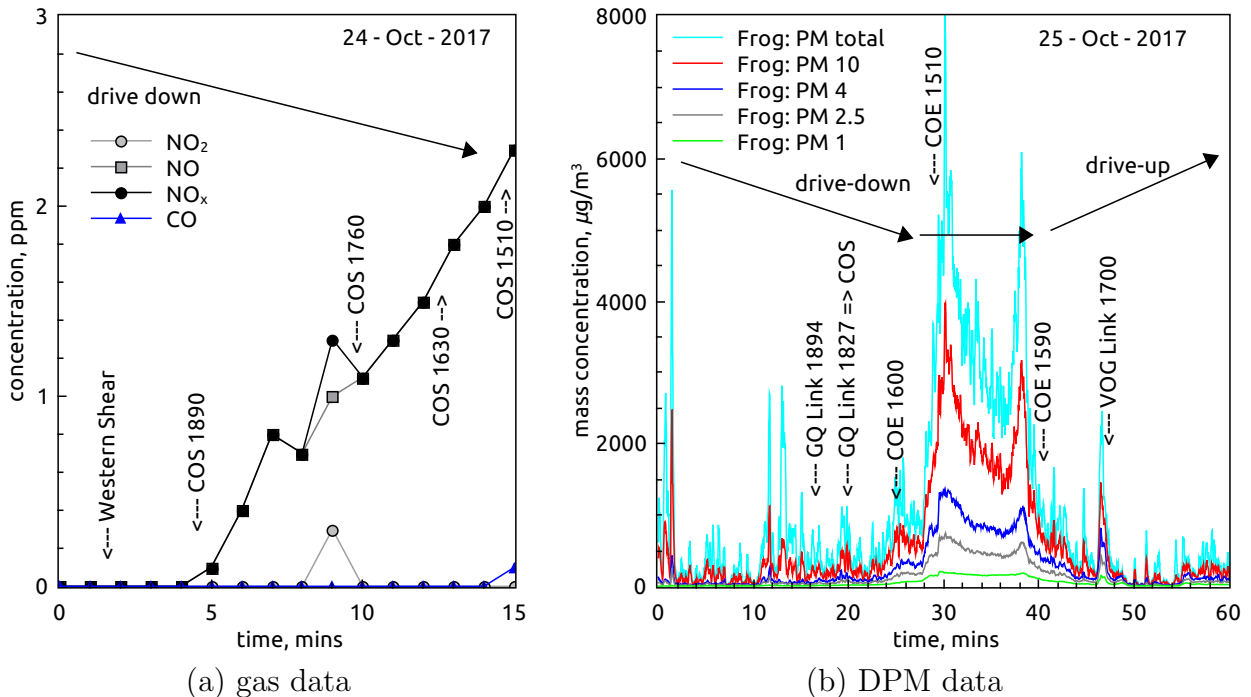


Figure 15: Mine traverse measurements of particulate and gas concentrations at different altitudes underground; (a) gas monitor data, (b) particle concentration

in the development face. The velocity vectors at 3 m height above the floor are given in Fig. 16. As can be seen, a vortex is generated at the front of the Spraymec due to the combined effects of the airflow from the duct and reversed airflow after hitting the heading face. Another small vortex existed at the behind of the Spraymec. In the tunnel, the air velocity near the duct side wall was lower than that near the other side. The pollutant may accumulate in the low-velocity zone and vortex areas.

The DPM distributions at vertical and horizontal cross section are given in Figs. 17(a,b). Concentrations greater than  $0.1 \text{ mg/m}^3$  are represented in red. As can be seen in the figure, the DPM concentrations are uniform in the tunnel except the vicinity of the exhaust pipe. As the tail pipe is located at the front face of the duct in the configurations considered, the particulates are seen to be carried by airflow to the front of the Spraymec from where it is dispersed to the rest of the tunnel. The confinement, and hence the limited air flow into the cuddy due to its geometry, resulted in relatively lower concentrations of DPM in the cuddy.

The recommended limit of DPM concentration for underground mines is  $0.1 \text{ mg/m}^3$  [13]. Figure 18 indicates the DPM distribution with the concentrations large than the limit. The DPM concentrations for the most of the areas in the tunnel were less than the limit. For the shotcreting activity, the miners did not have the hazard to over exposure to DPM under current ventilation conditions.

In the onsite tracer gas experiments (refer Part A: Chemcentre/BBE Study), the  $\text{SF}_6$  was released near the tailpipe. To better compare the  $\text{SF}_6$  and DPM, we assumed that the  $\text{SF}_6$  was released at the tailpipe in the simulation. The  $\text{SF}_6$  concentration distributions at vertical and horizontal cross section are shown in Figs. 19(a,b). As can be seen,  $\text{SF}_6$  illustrated a similar

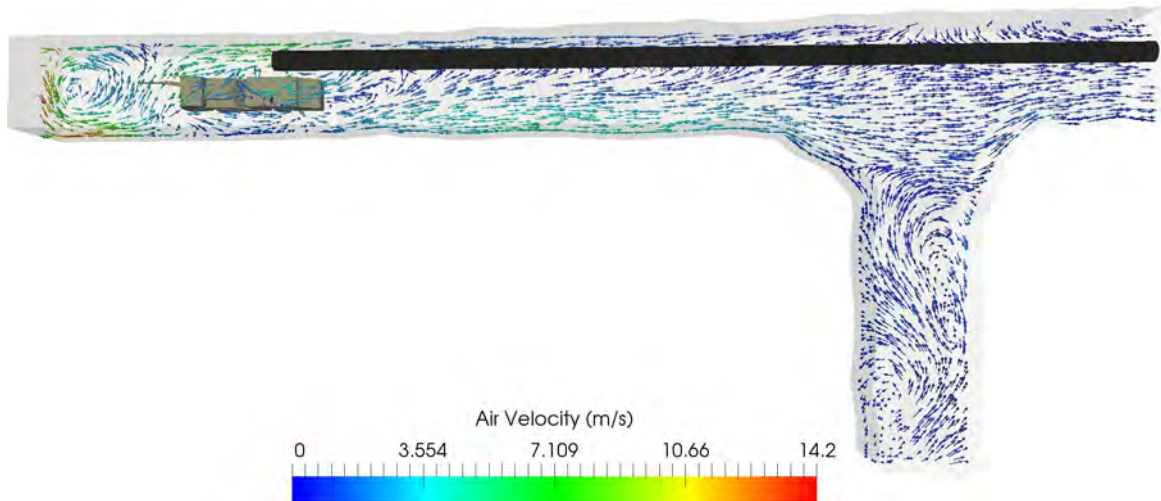


Figure 16: Velocity vectors at a height of 3 m from the ground in the mine region during shotcreting activity

Table 7: Comparison between CFD predictions and measurements during shotcreting

	Measurement	CFD	Error
Location P1	$4000 \pm 300$	4211	5.3 %
Location P2	$2400 \pm 200$	1778	25.9 %

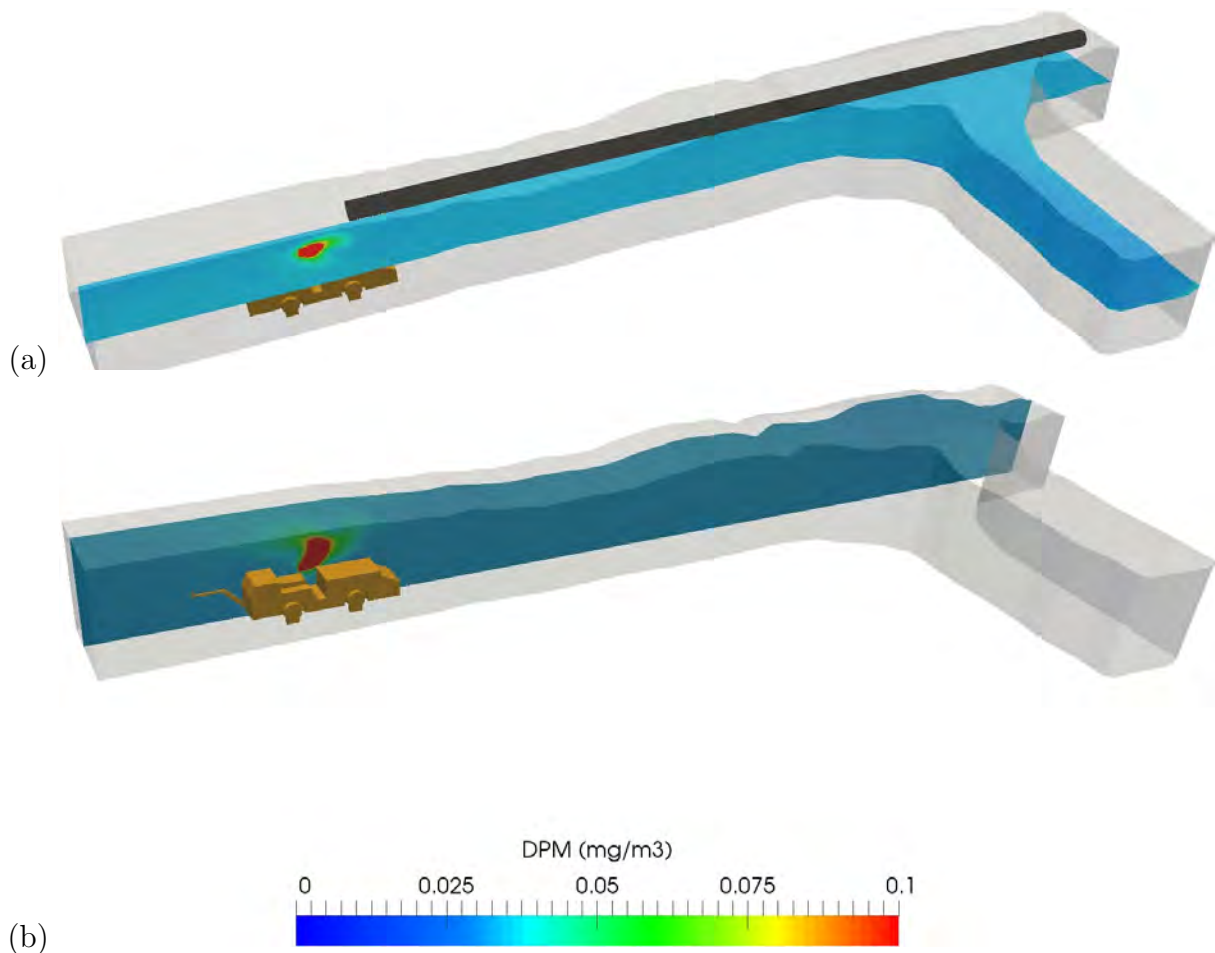


Figure 17: Contours of DPM concentration in the mine region during shotcreting activity

concentration distributions as that of DPM. For this reason, it was reasonable to use SF<sub>6</sub> to represent DPM during the experiment.

Model Validation: To ensure the accuracy of simulation results of air field for further analysis, the results were compared with onsite measured results (refer Part A: Chemcentre/BBE

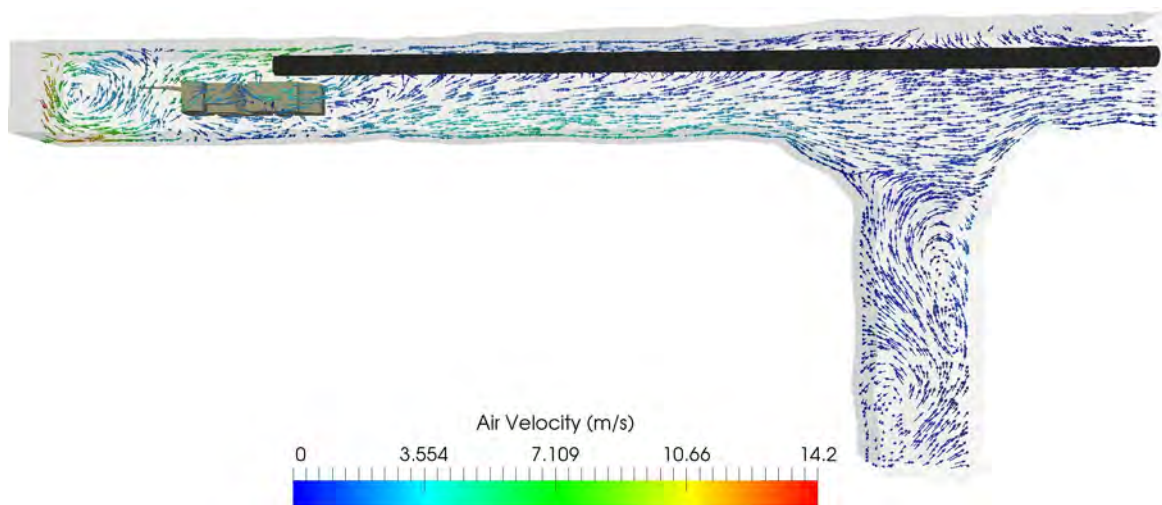


Figure 18: Regions where DPM concentrations are greater than 0.1 mg/m<sup>3</sup> in the mine region during shotcreting activity

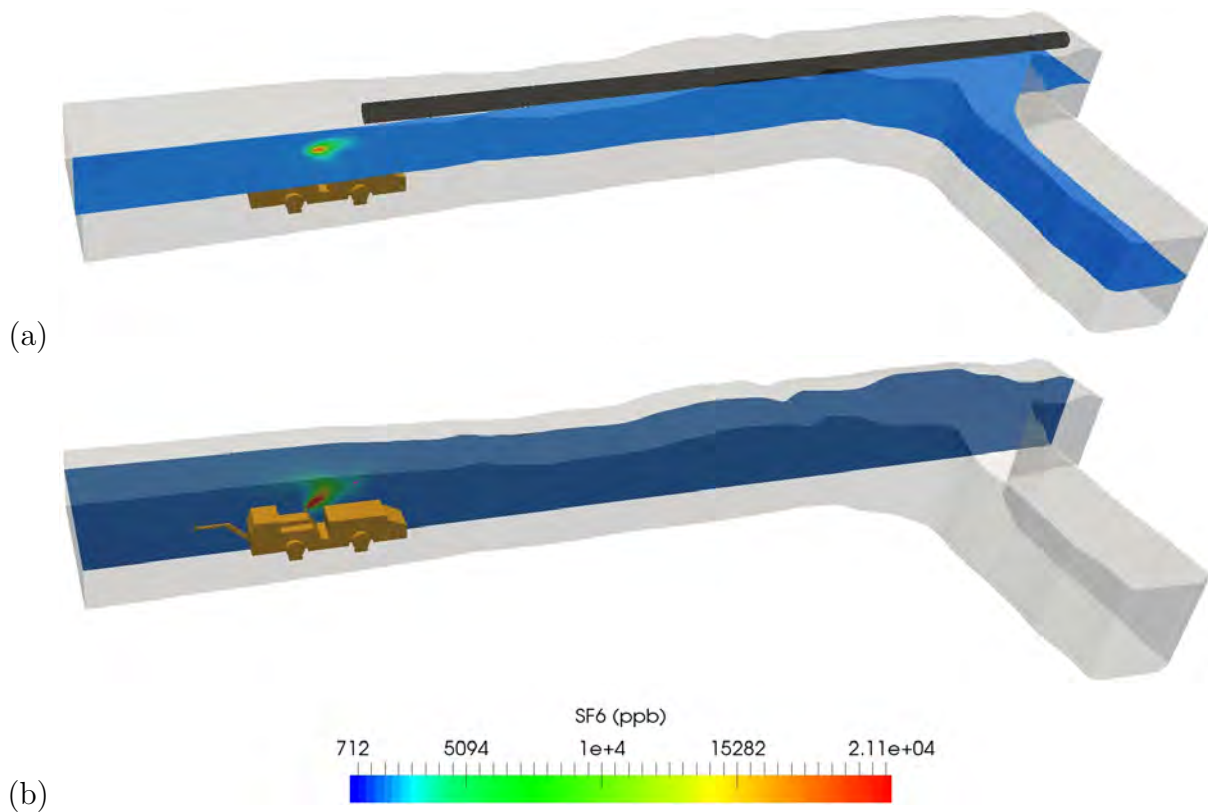


Figure 19: Contours of SF<sub>6</sub> concentration in the mine region during shotcreting activity

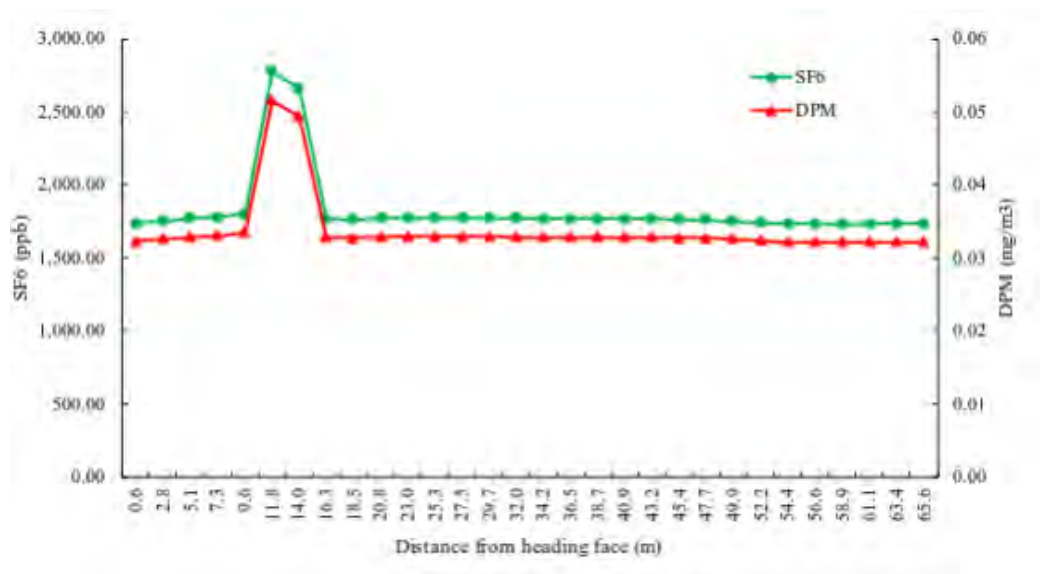


Figure 20: Comparison of SF<sub>6</sub> and DPM concentrations along the length of the heading, during shotcreting activity

Study) for validation. SF<sub>6</sub> concentrations at two monitor points were measured. Point 1 was near the release source, around the vehicle tailpipe. Point 2 was located at about 1.7 m above the floor and 30 m away from the heading. The comparison between CFD results and measured data is given in Table-7. The average error between the measured data and CFD results is less than 10%. Since the complicated measurement environment, this error is acceptable for the simulation.

Equivalent equation: SF<sub>6</sub> is nontoxic, odorless, colorless chemically and thermally stable, and does not exist naturally in the environment. It could be use to evaluate the DPM distribution. For this reason, it is important to obtain the equivalent equation between SF<sub>6</sub> concentration and DPM concentration. The SF<sub>6</sub> and DPM concentration at 30 points in the center of tunnel along the  $x$ -direction are selected to evaluate the equivalent equation. The SF<sub>6</sub> and DPM concentration curves are given in Fig. 20. A linear relationship between SF<sub>6</sub> and DPM concentrations can be observed from the figure. The equivalent equation can be given as:

$$\text{DPM (mg/m}^3\text{)} = \frac{\text{SF}_6 \text{ (ppb)}}{5.3838 \times 10^4} \quad (10)$$

#### 4.9.2 *Bogging Activity*

The airflow velocity vectors at a height of 3 m from the floor during bogging activity are given in Fig. 21. As can be seen, a vortex is generated near the face heading for 3 scenarios. For scenarios 1 and 2, the exhaust tailpipe is located behind of the duct outlet, which results in a relatively lower concentration of DPM ahead of the bogger. However, for scenario 3, appreciable concentrations of DPM are possible as seen in the figure due to the lower air velocities in the cuddy. The velocity vectors in the cuddy are also indicate of the greater residence time for particles and exhaust while the bogger is active in the cuddy.

The DPM concentration distributions for the three scenarios are presented in Figs. 22(a-f). Concentrations greater than 0.1 mg/m<sup>3</sup> are represented in red. It is evident from the figure that for scenario 1, the DPM concentration behind the vehicle is in excess of the average allowable limits. This is indicative miners who work in the vicinity of the bogger in such a configuration, downstream of the tunnel are potentially at a high risk to over-exposure to DPM levels. Hence, protective measures such as protective wear must be worn at to eliminate conti-

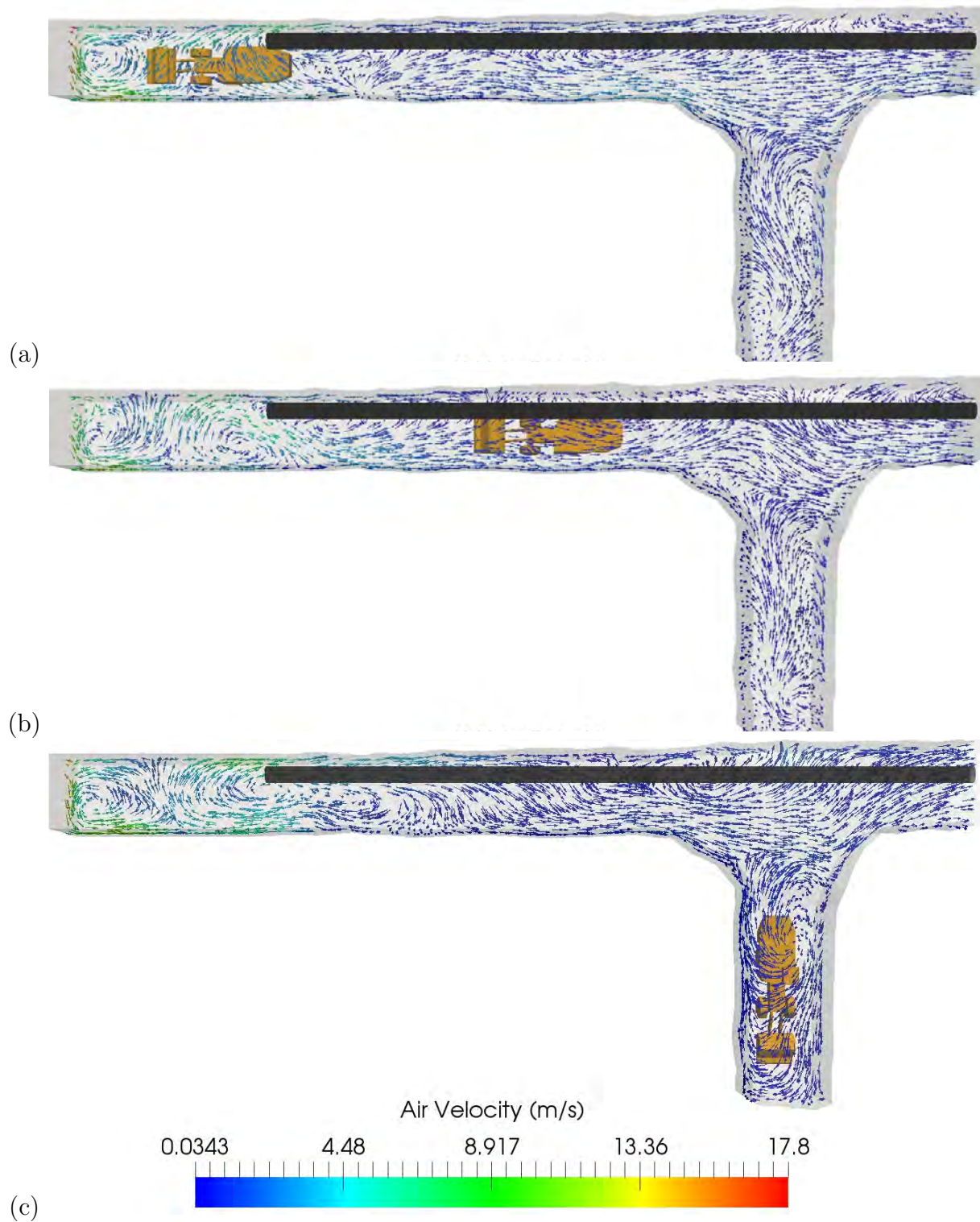


Figure 21: Velocity vectors at a height of 3 m from the ground in the mine region during bogging activity

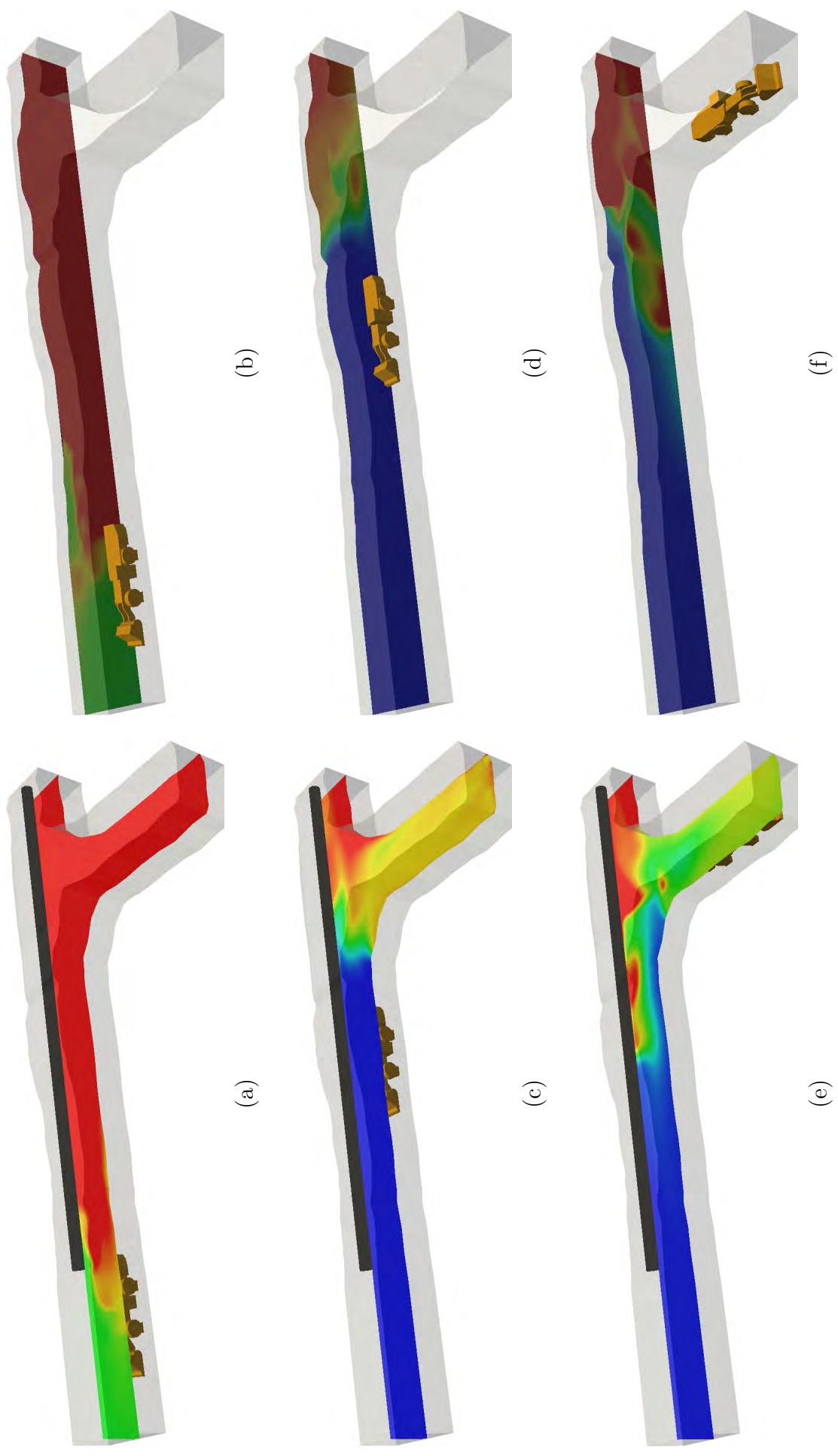


Figure 22: Contours of DPM concentration in the mine region during bogging activity

nued over-exposure. For the areas front of the bogger, DPM concentrations are at safe levels due to the clear air from the duct. It is seen from the figure that the the relative location of the bogger from the cuddy also has a significant influence on the DPM concentrations in the cuddy. Figure 22(c,e) shows that particulate concentrations in cuddy are relatively lower for scenarios 2 and 3 as compared to scenario 1. The bogger for scenario 2 located near the cuddy. Most of the DPM was carried to the downstream by fresh air before it diffused to the cuddy. For scenario 3, DPM accumulation can be seen due to the orientation of the vehicle exhaust with the side walls.

Figure 23 presents the DPM distribution with the concentrations large than the limit ( $0.1 \text{ mg/m}^3$ ). As expected, most of the regions downstream of the bogger show DPM levels exceeding  $0.1 \text{ mg/m}^3$  when bogger worked near the heading face (scenario 1) or mid-way between the cuddy and the heading face (scenario 2). However, for scenario 3, DPM was first injected to the duct-side wall, thus generated a high DPM concentration zone. Then this zone expanded to the downstream due to the airflow direction. It is noticed that a small region of high DPM concentration zone also exists at the upstream, due to the local re-circulation in the region – as seen Fig. 21(c).

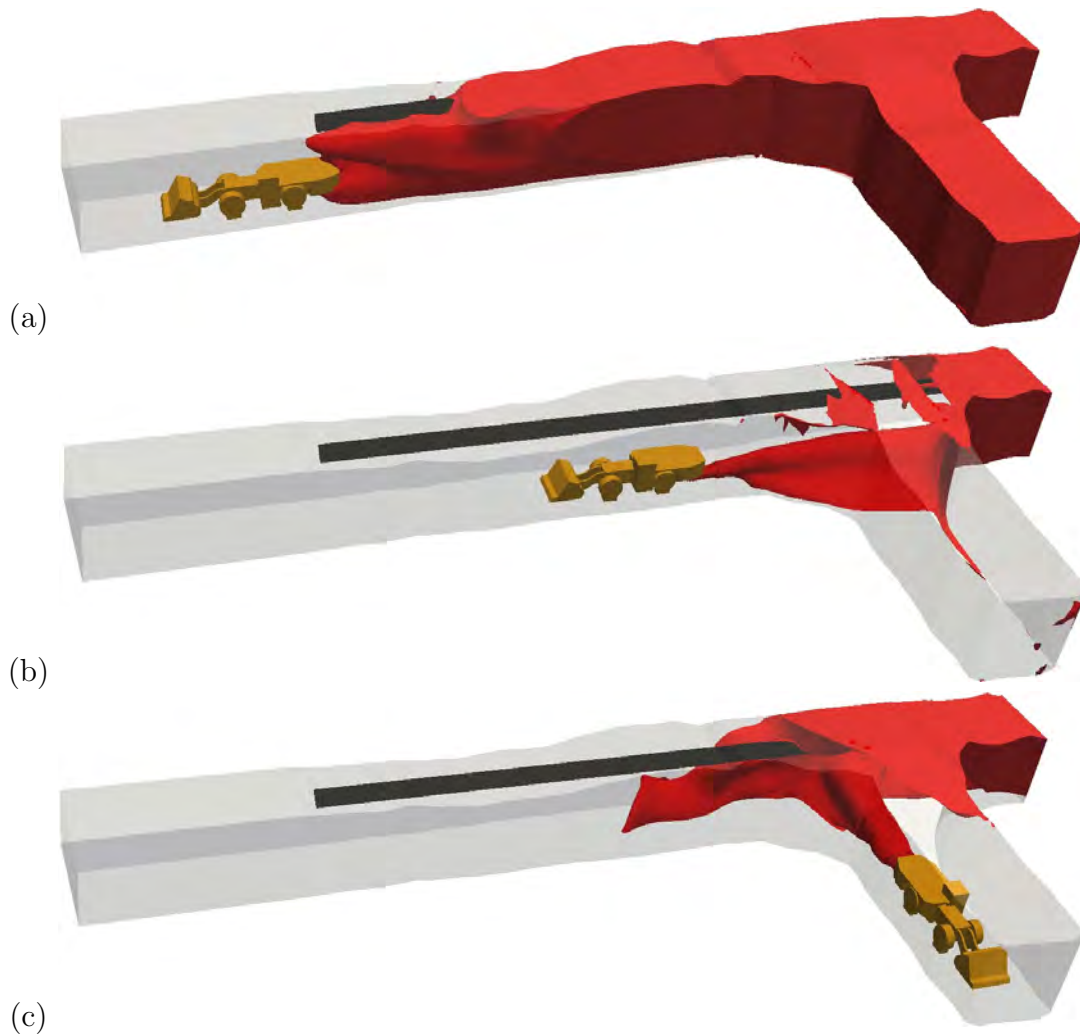


Figure 23: Regions where DPM concentrations are greater than  $0.1 \text{ mg/m}^3$  in the mine region during bogging activity

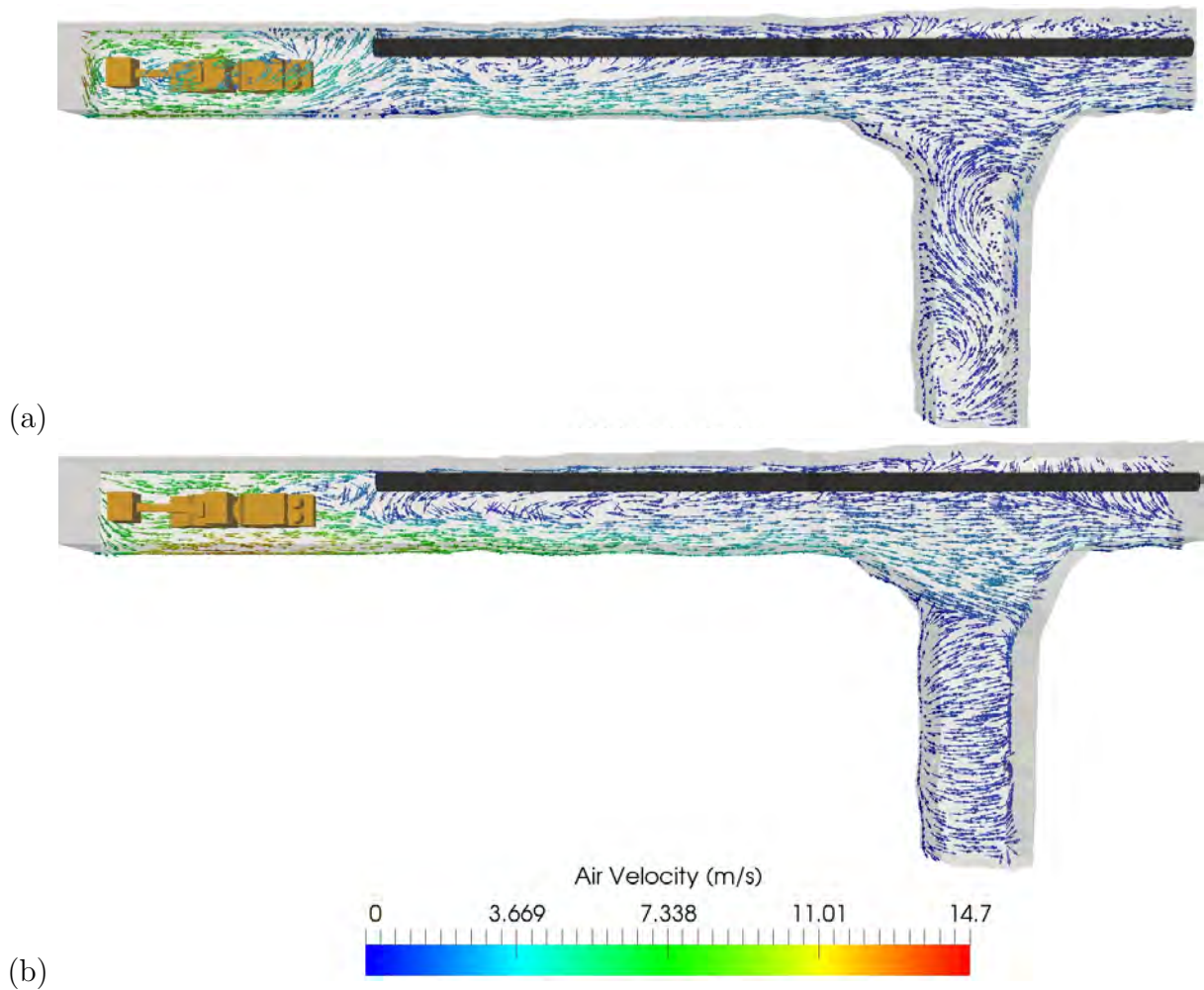


Figure 24: Velocity vectors at a height of (a) 3 m and (b) 5 m, from the ground in the mine region during charging activity

#### 4.9.3 Charging Activity

The airflow velocity vectors at 1.5 m and 3 m height above the floor for charging activity are given in Fig. 24. As shown in Fig. 24(a), a local re-circulation region exists around the Charmec bucket. However, as the exhaust pipe is located at the bottom of the Charmec, the upstream flow in the region was not sufficient to carry any significant fraction of the diesel particulates upstream from the vehicle. This, along with Fig. 24 indicate that DPM concentrations during charging are mostly low as compared to allowable limits, in configurations such as those considered in this study. As seen in the figure, a region of low velocity exists downstream of the Charmec, which can be expected to retain greater DPM concentrations. The flow velocity in the non-duct side wall was large enough for the DPM to diffuse sufficiently with the air at this side firstly and then dispersed to other areas slowly in the tunnel.

The DPM distributions at vertical and horizontal cross section are given in Fig. 25. As expected, the DPM concentration around the Charmec was quite low. Some DPM accumulated at the right behind of the Charmec due to the low-velocity re-circulation region, as shown in Fig. 25 (a). Beyond about 3 m downstream from the Charmec, the DPM a uniform distribution of diesel particulates can be seen in the figure at the steady state. Figure 26 illustrates the

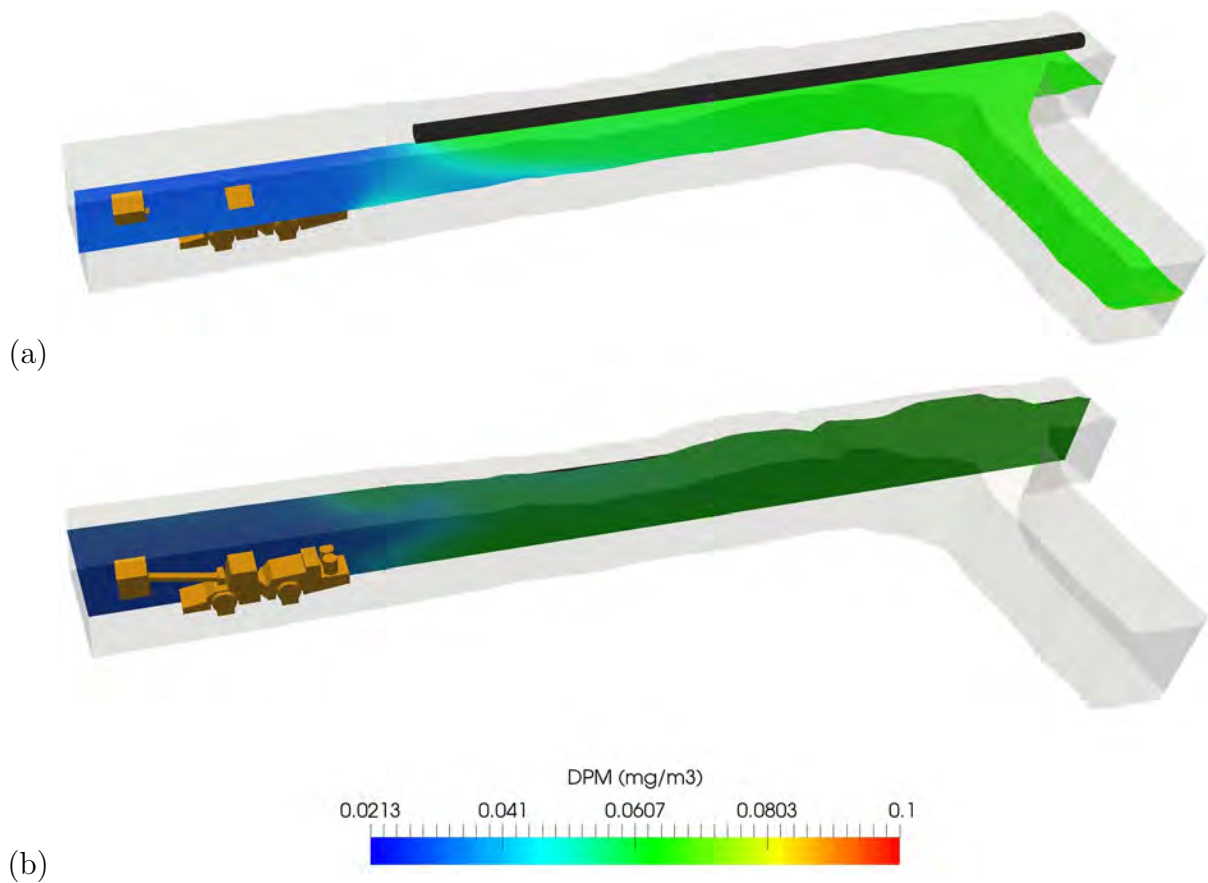


Figure 25: Contours of DPM in the mine region during charging activity

DPM distribution with the concentrations large than the limit. It is noticed that no DPM concentration in the tunnel exceeded the allowable limit except the area close to the tailpipe. In summary, the DPM levels in the vicinity and downstream of the Charmec are relatively low an under safe levels, at least for underground configurations as considered in this study, and given the current ventilation system.

For the charging activity, the SF<sub>6</sub> was released at same position of the DPM (exhaust tailpipe). As shown in Fig. 27, SF<sub>6</sub> gave the similar concentration distribution as DPM.

Equivalent equation: To obtain the equivalent equation between SF<sub>6</sub> and DPM concentration, simulation results at 30 points in the center of tunnel along the downstream direction were selected. The concentration curves for SF<sub>6</sub> and DPM are given in Fig. 28. A linear relationship between SF<sub>6</sub> and DPM concentrations can be observed from the figure. The equivalent



Figure 26: Regions where DPM concentrations are greater than 0.1 mg/m<sup>3</sup> in the mine region during charging activity

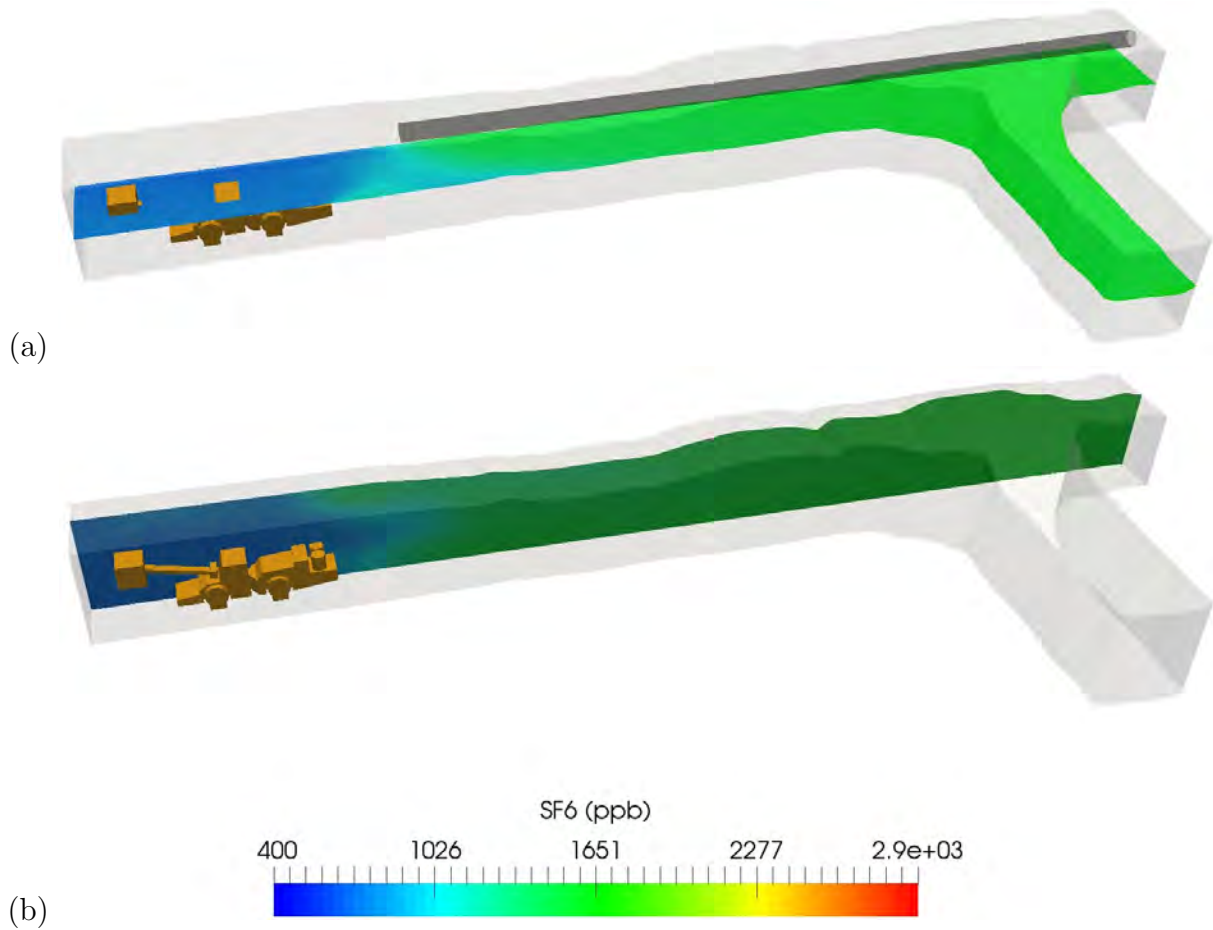


Figure 27: Contours of SF<sub>6</sub> concentration at (a) 3 m from the ground and (b) 3 m from the side walls in the mine region during charging activity

equation can be given as:

$$\text{DPM (mg/m}^3\text{)} = \frac{\text{SF}_6 \text{ (ppb)}}{2.429 \times 10^4} \quad (11)$$

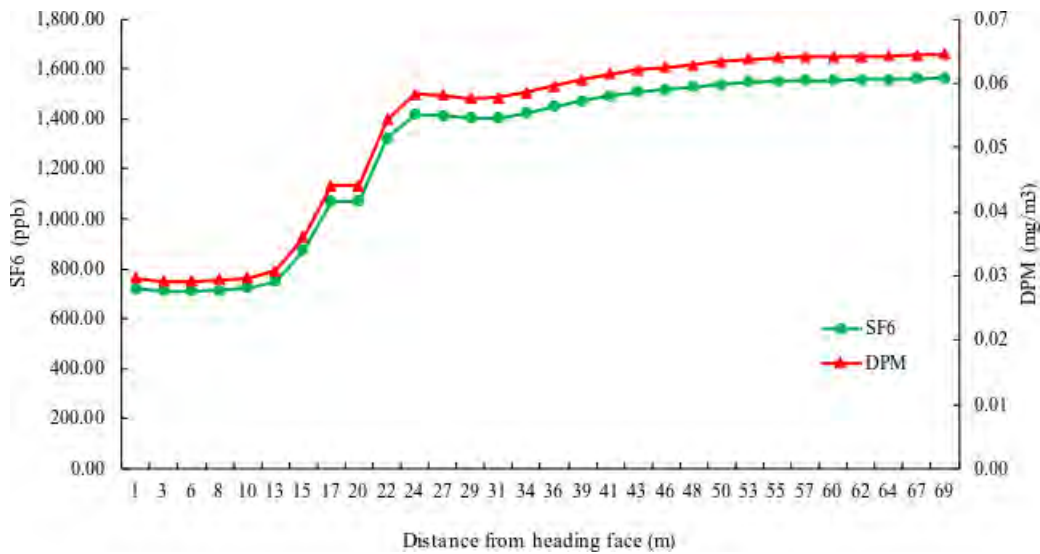


Figure 28: Comparison of SF<sub>6</sub> and DPM concentrations along the length of the heading, during charging activity

#### 4.9.4 Summary of Key Findings - Simulation of DPM and SF<sub>6</sub> Migration in Confined Regions

Steady-state RANS CFD simulations of DPM and SF<sub>6</sub> dispersion in a development face (AST 1900) were conducted for 3 case studies which include shotcreting activity, bogging activity consisting 3 scenarios, and charging activity. The SF<sub>6</sub> simulation results were further compared with the DPM results and the equivalent equations between SF<sub>6</sub> concentration and DPM concentration were obtained. In addition, the high DPM concentration ( $\geq 0.1 \text{ mg/m}^3$ ) zone were determined for each activity. The key findings are summarized below:

- i. Given that mean flow and turbulence are the key factors affecting the dispersion of DPM of SF<sub>6</sub> in the mine under the considered operating conditions, the distribution of the two species are equivalent. This exercise confirms that SF<sub>6</sub> can be used as an indicator for the dispersion of DPM in the mines. An equivalence relationship between the concentrations of SF<sub>6</sub> and DPM were given in Eqs. (10,11).
- ii. For the shotcreting and charging activities, the concentration of DPM in the tunnel is consistently lower than the allowable limit except for the areas close to the exhaust tailpipe. For these two activities, the current ventilation system is sufficient to ensure that the miners are not exposed to DPM above guideline levels. However, for the bogging activity, the DPM concentration in most of the areas behind the bogger exceeded the limit. The miners who working in the downstream regions are likely to be exposed to the high concentrations of DPM. For this activity, additional controls are necessary to avoid over-exposure to DPM.
- iii. The power of diesel vehicles were different for the different activities considered. The Bogger, for example, has a more powerful diesel engine than Spraymec and Charmec. Thus, generated more DPM than other two vehicles. For this reason, different ventilation could be used for different activities to ensure the DPM levels are maintained below the allowable limits at all times. For bogging activity, the DPM concentration could be decreased by increasing the ventilation rates.

The scalar transport equation gave a less computational cost for the SF<sub>6</sub> and DPM dispersion simulation. The accuracy of the results can be improved with more measurements and further validations. However, the results presented by the CFD simulation here are sufficiently validated for reliable indicative indicatively SF<sub>6</sub> and DPM concentration distributions in the development face of the mine.

#### 4.9.5 Comparison of Tracer Gas and CFD Results

This section presents a comparison between the SF<sub>6</sub> measurements in Part A and the comparable simulations in the previous subsection. Simulations were undertaken for the same time as the SF<sub>6</sub> release time. It can be observed that all simulations have reached a steady state during this period. Fig. 29 presents data for the Spraymec/Hydroscaling activity. Only the Spraymec was working, the Agi truck was not operating during this activity. Thus, only the data at M1 (at the Spraymec operator cabin side) are presented here. As can be seen, a generally good agreement can be observed, though this is likely influenced by the vortices as mentioned earlier.

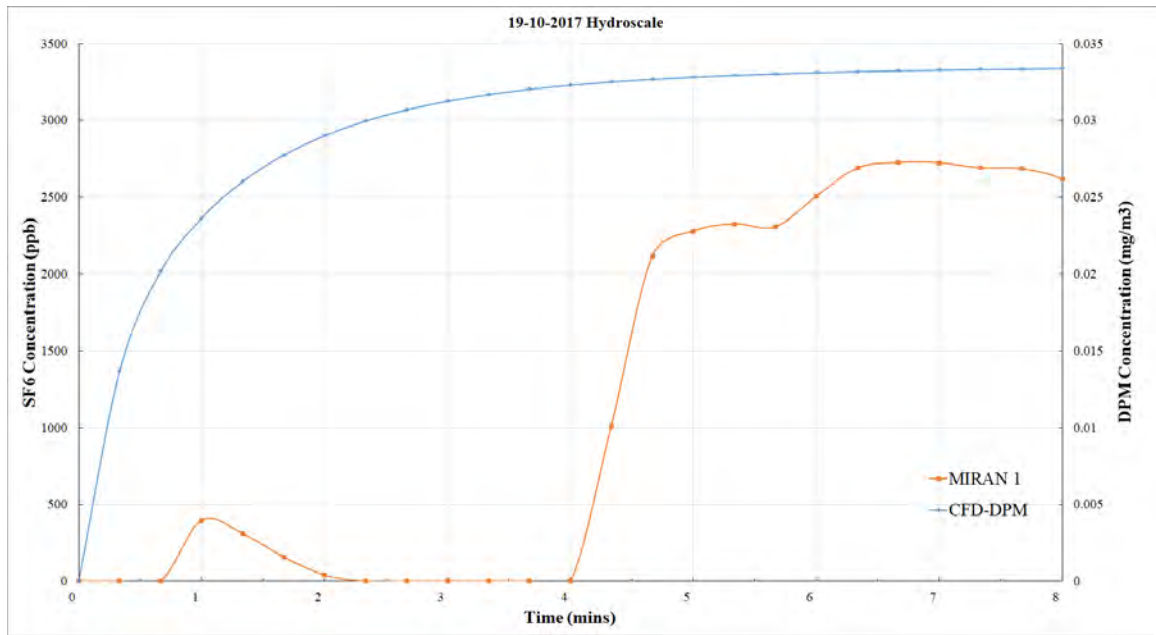


Figure 29: Comparison of tracer gas and CFD results for the Hydroscale (Spraymec) activity

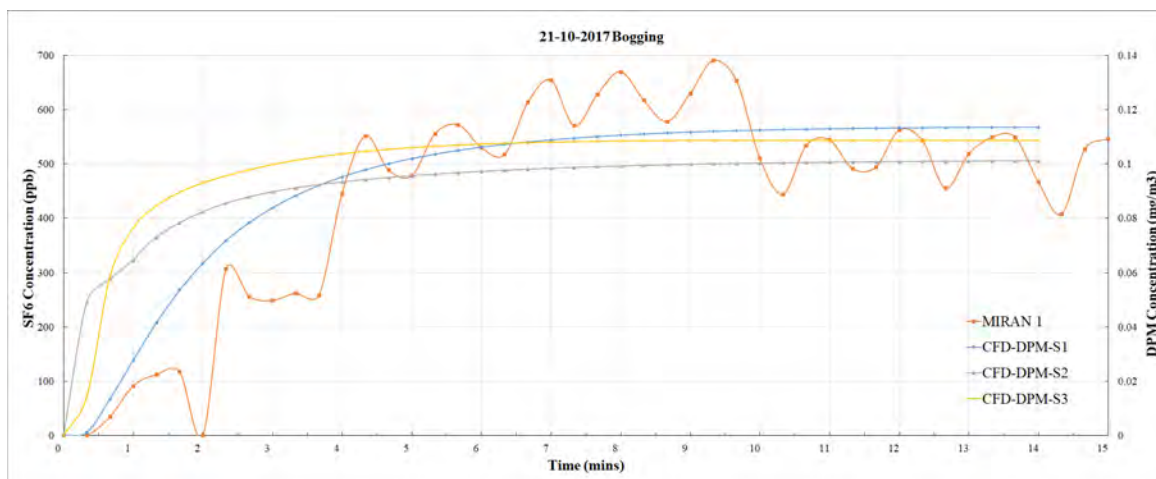


Figure 30: Comparison of tracer gas and CFD results for the Loading (Bogging) activity

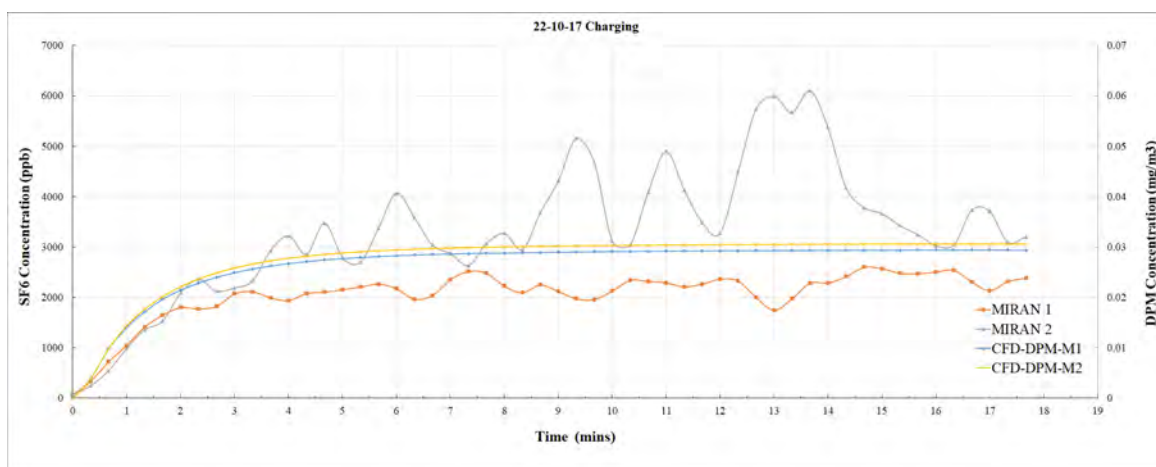


Figure 31: Comparison of tracer gas and CFD results for the Charging activity

Fig. 30 presents the comparison for the Boggging activity. Based on the CFD modelling, the DPM data at M1 (at the downstream of the heading face, near the heading entrance) for 3 scenarios is presented. For scenario1 and scenario 2, the bogger is 5 m and 30 m from the heading face, respectively. For scenario 3, the bogger was located in the cuddy and 5 m from the cuddy heading. A very good agreement between the mean observed value and the simulated values can be seen

Fig. 31 presents data for Charging where M1 is the nearest face to the heading. For the tracer gas measurement, M2 in the open charge-up cabin on driver's seat. However, in the CFD simulation, the cabin is not open for the Charmech, thus a point at the driver side near the operator cabin is selected to represent M2. Once again simulated values agree well with the measured values.

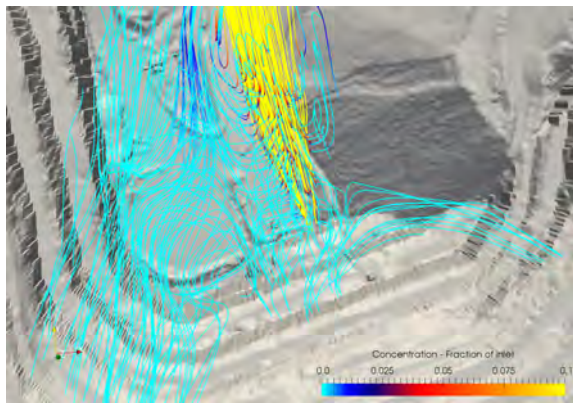
#### 4.10 CFD - DPM Re-entrainment into Ventilation Inlets due to Proximity with Outlets

As mentioned in the preceding section, three simulations are carried out to investigate potential re-entrainment of DPM into the inlet ventilation stream due to the proximity of inlet and outlet (return shaft) and the topography of the open-pit. The three cases correspond to flow rates of (i) 100 m<sup>3</sup>/s and (ii) 50 m<sup>3</sup>/s, using the Western Shear decline as the flow inlet and Watu as the outlet, as it is presently in the Sunrise Dam Gold Mine, and (iii) using the same geographical location, but reversing the flow directions, as there is a barrier for the outlet flow in this configuration – see Figs. 5(a,b) – due to the topography of the open-pit.

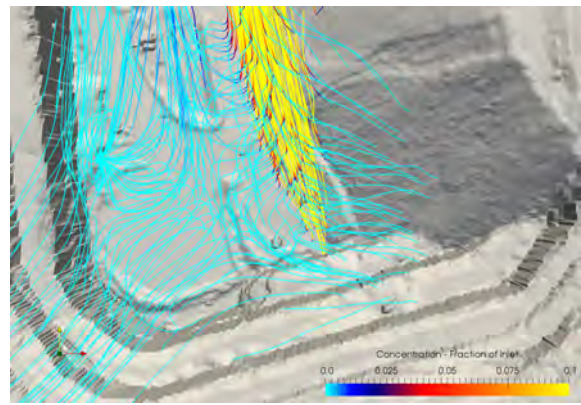
The results from the three simulations are discussed below. In all the following images, the streamlines are colored by the DPM concentration in the range 0 – 10 % of that at the exhaust portal.

Figures 32(a-d) illustrate the streamlines and the envelope of DPM concentrations corresponding to 0.5 % and 4 % of the Watu outlet for a flow rate of 100 m<sup>3</sup>/s, and Figs. 32(e-h) illustrate the corresponding images for 50 m<sup>3</sup>/s. It can be seen that the topography of the present site is such that there is no obstruction to the outlet flow and most of the stream is undeflected by the equivalent suction/ flow into the Western Shear portal. The average DPM concentration at the inlet face of the Western Shear portal was calculated to be negligible ( $\approx 0$ ) for these two cases. The analysis with two different flow rates (one being half the operating flow rate) indicates that the separation between the two ventilation channels are sufficient to avoid any re-entrainment into the clean air stream that is pumped underground.

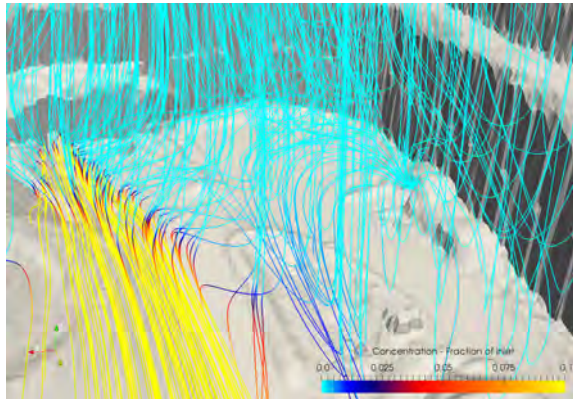
To investigate the influence of an obstruction to the outlet flow – for example, the face of the pit opposite to the Western Shear portal that is about 75 m from the inlet to the portal – a scenario, where the ventilation inlet and outlet are interchanged, is considered. The flow streamlines and envelope of DPM concentrations are illustrated in Fig. 33(a-e). Unlike the existing arrangement at Sunrise Dam Gold Mine, this assumed scenario shows that an obstruction to the outflow even at a distance of 75 m from the suction side of the ventilation channel can have a significant influence on the flow field in the region. It is also seen in Fig. 33(e) that a substantial fraction of the DPM is now re-entrained into the ventilation -



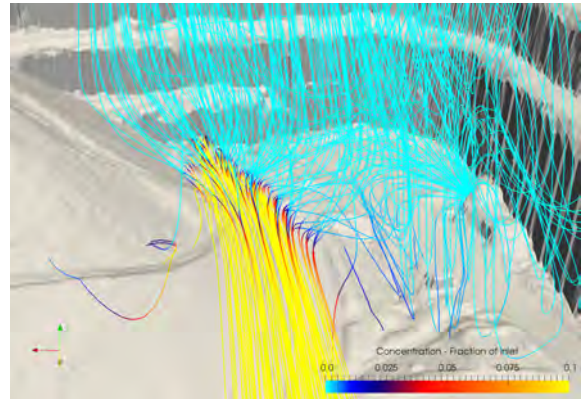
(a) 100 m<sup>3</sup>/s



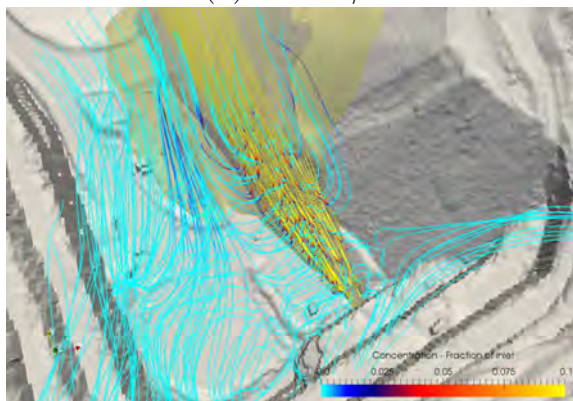
(e) 50 m<sup>3</sup>/s



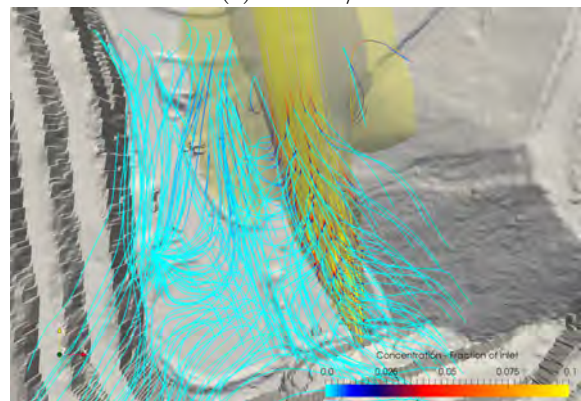
(b) 100 m<sup>3</sup>/s



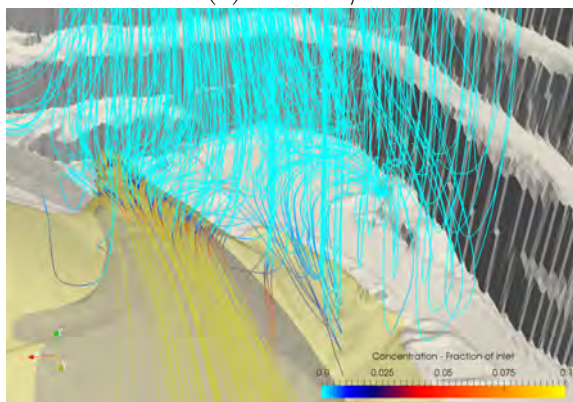
(f) 50 m<sup>3</sup>/s



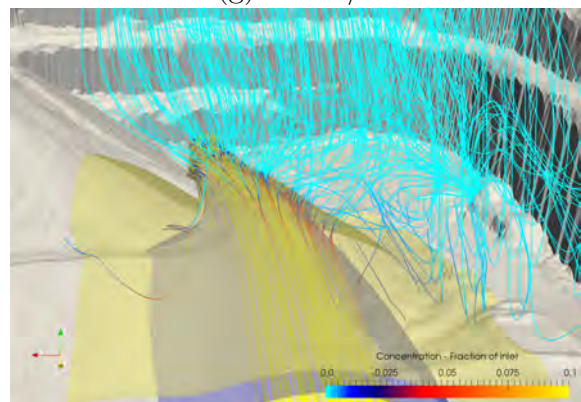
(c) 100 m<sup>3</sup>/s



(g) 50 m<sup>3</sup>/s



(d) 100 m<sup>3</sup>/s



(h) 50 m<sup>3</sup>/s

Figure 32: Comparison of streamlines and iso-surfaces of DPM concentrations corresponding to 0.5 % and 4 % of that at the Watu outlet, between flow rates of 100 and 50 m<sup>3</sup>/s. The WATU outlet can best be seen in (e) located at the base of the yellow streamlines, while the Western Shear portal is located at the concentration of blue streamlines to the left.

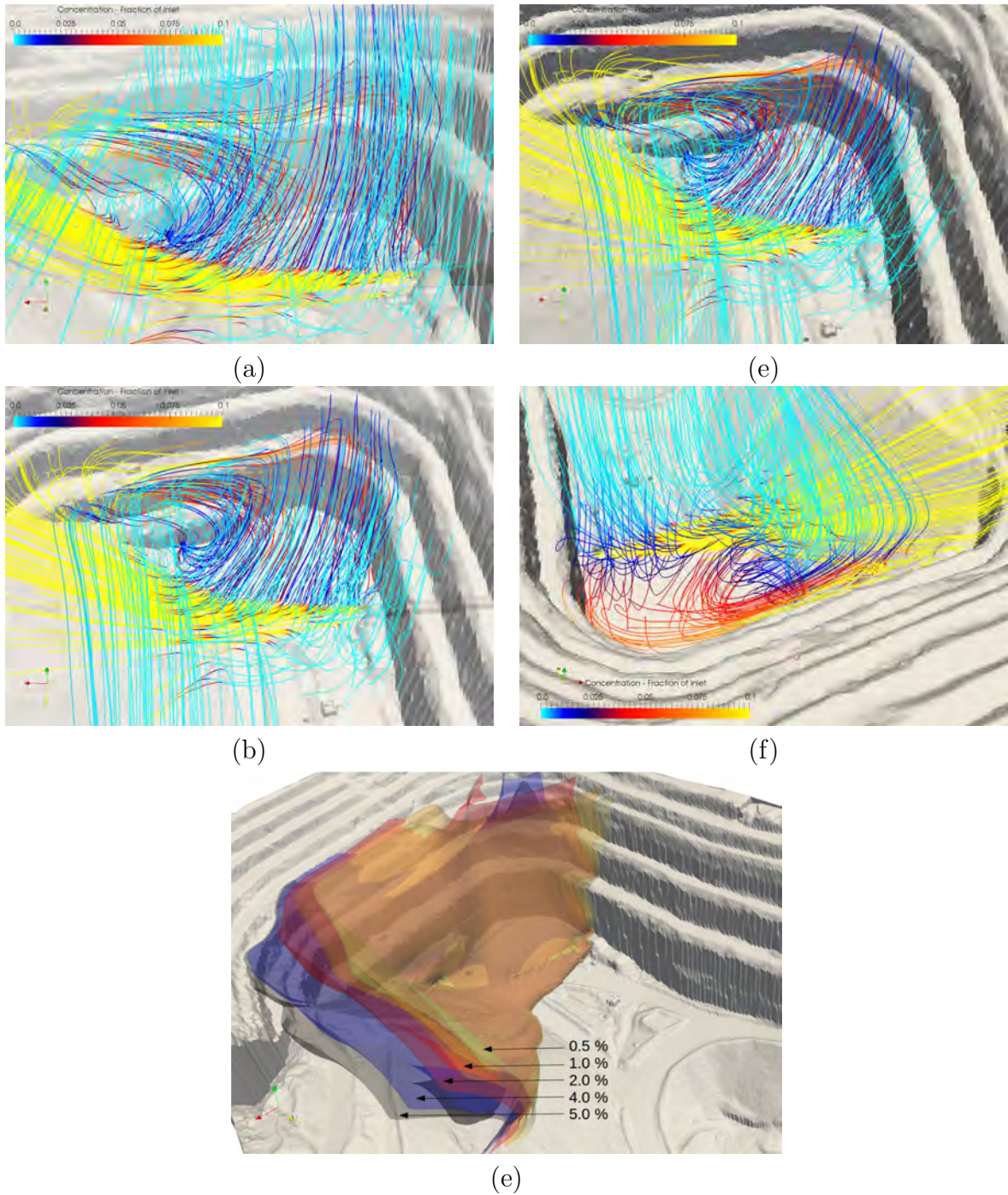


Figure 33: Comparison of streamlines and iso-surfaces of DPM concentrations corresponding to 0.5 % and 4 % of that at the Watu outlet, between flow rates of 100 and 50 m<sup>3</sup>/s

- stream into the Watu shaft. An average of the DPM at the inlet stream was estimated from the present CFD simulations to be about 2.2 % of that released through the (assumed) Western Shear outlet. This would correspond to approximately an additional emission from several additional bidders or LHDs operating over a period of a year.

#### *4.10.1 Summary of Key Findings - Simulation of DPM Re-entrainment into Vent-Stream*

Steady-state RANS CFD simulations of DPM dispersion and in an open-pit region with ventilation inlet and outlets were carried out in the AST1900 region of Sunrise Dam Gold Mine, to investigate the influence of the proximity of the ventilation inlet/ outlet on the re-entrainment of DPM. Three cases, corresponding to two different flow rates and an additional case with the inlet and outlet interchanged, were considered for the study. The key conclusions from the CFD study are presented below:

- i. While it may be challenging to design appropriate ventilation ducts/ channels while expanding an existing mine for underground operations, it is important to ensure that the channels are sufficiently far from each other to avoid any re-entrainment of DPM into the stream. CFD analysis of the existing WATU / Western Shear region of Sunrise Dam Gold Mine shows no significant DPM re-entrainment into the air stream from the WATU outlet into the Western Shear portal.
- ii. From an exercise carried out by reversing the flow directions – representative of a plausible configuration at another site – it was found that about 2.2 % of the DPM from the outlet can potentially be continuously be re-circulated into the ventilation stream. This can lead to significant accumulation of diesel particulates in the underground environment, and can lead to potentially high occupational exposures. This could be avoided by extending the vent outley vertically, or possibly horizontally. It should be noted that since this study was undertaken, new centrifugal extraction fans have been installed at the WATU outlet which extends the exhaust point approximately 10 m vertically, as well as providing increased air flow.

#### 4.11 Chamber Study (Deeper Mines)

Refer Appendix-2.

## **5 Summary**

The findings from this component of the work were as follows:

- (a) Underground workers in the study were found to be exposed to significant levels of DPM, both in terms of EC levels (16% were above guideline levels - before any correction for shift length or work pattern was applied) and particulate number (nanoparticle) concentration. A significant correlation was however found between mean EC and mean (nano)particle exposure for each worker, however deviations from the agreement were most notable on the

nanoparticle side (high nanoparticle exposure with comparatively low EC exposure). EC exposure would however appear to be a reasonable indicator of nanoparticle exposure, and vice versa.

- (b) Stationary monitoring revealed significant levels of all particle sizes in the mine, as well as gases (NO<sub>2</sub> and CO) at significant levels. Particulate and gas levels were generally found to increase with depth in the mine, as well as activity level. Significant transient variation in particulate number, size and mass was found due to local activity level.

Most notably, modal sizes of DPM / nanoparticles in the mine were found to be significantly lower than in previous studies (further into the nano range). Diesel engines consistently produce a peak particle size at or near 80 nm, however this study generally found significantly smaller particles. Given the nature of the mine, some interference from salt nuclei can be expected, however it is most likely the decreased size was due to the widespread fitment of diesel particulate filters (DPFs) to most of the heavy plant.

- (c) CFD analyses of key activities in the mine and a vent portal highlighted key areas where ventilation could be improved. Correlations between DPM and tracer gas (refer Part A: Chemcentre/BBE Study) were also developed, to allow the calibration of tracer gas measurements.
- (d) The deeper mine study found no significant changes in DPM due to pressures up to 1.4 atmospheres and ammonia concentrations up to 100 ppm. However significant changes were found if ozone or UV light were introduced. Therefore care should be taken to ensure sources of UV and/or ozone are not present in the mine, particularly if diesel engines with selective catalytic reduction are in use.

This work has found that the widespread use of diesel particulate filters in the mine tended to result in a slightly reduced modal particle diameters in the mine – hence reducing particle sizes to which miners are exposed.

Nevertheless, it was found that nanoparticle exposures and EC exposures possessed a reasonable correlation. Further analysis of the data in conjunction with appropriate biological/health data should be conducted to determine the most appropriate monitoring strategy for the future. i.e. whether traditional EC monitoring methods are sufficient or whether realtime nanoparticle spectrometry is required.

## 5.1 Limitations

It was not within the scope of this work to undertake source characterisation, indeed this has been conducted in detail and published extensively for a range of new and in-service diesel equipment. Only the influence of pressure in the mine could be expected to produce variations in such results (due to pressure) however the chamber study suggests that such changes would be minor. It should be noted however that particle count-based emissions of vehicles retrofitted with DPFs have likely not been performed by independent testing agencies.

In many cases, due to the complexity of the mine tunnels and ventilation circuit, workers would be exposed diesel equipment from a range of sources. It was not possible to conduct ageing or deposition studies in the mine without significantly impacting production. Nevertheless, the chamber study results would suggest that ageing processes that typically occur at surface conditions are suppressed in the mine environment due to the lack of UV and OH radicals. Deposition and agglomeration of particles are well understood and can be simulated using CFD.

## 5.2 Recommendations

The preliminary recommendations from this work are as follows.

- i. It would be advisable that standards or guidelines be developed for (nano) DPM (personal) monitoring in underground mines, similar to the measurement standards for nanoparticle testing from vehicle exhausts which exist under the EURO emissions standards. i.e. requiring both (nano) particle counts and mass-based measurements.
- ii. If EC analysis method is to remain the main measure for exposure to diesel exhaust, a more extensive study to establish the relationship between nanoparticle number concentration and EC concentration should be conducted. Noting that such a method will only be relevant to average concentrations, and will not capture peak exposures or other temporal variation. The relationships presented here should be evaluated in other mines using a range of mobile plant and emissions controls.
- iii. It has been shown in this study that the CFD predictions are in good agreement with the field measurements made using SF<sub>6</sub>. CFD methods are likely much more accurate than one dimensional methods currently used for mine ventilation design. This can be a potential alternative for effective design of underground ventilation systems.
- iv. Furthermore, CFD can be employed to optimize the ventilation flow rates in desired regions depending on the intended activities for a period of time. This can aid in greater control over the DPM and exhaust gas composition in the underground environment, and hence the occupational exposure to underground miners.
- v. It is often challenging to design appropriate ventilation ducts/ channels while expanding an existing mine for underground operations while ensuring that the channels are sufficiently far from each other to avoid any re-entrainment of DPM into the stream. CFD analysis of the existing AST1900 region of Sunrise Dam Gold Mine shows no significant DPM re-entrainment into the air stream. However, a simple change such as interchanging the inlet and outlet vents results in significant re-entrainment, due to the topography of the mine. Once again, CFD can be effectively employed to design and optimize ventilation channels.
- vi. As mines become deeper and SCR becomes more widespread, it is important to ensure no sources of ozone or UV light are present in the mine, to ensure formation of SOA does not occur.

## References

- [1] National Institute of Occupational Safety and Health (NIOSH), Diesel Particulate Matter (as Elemental Carbon) (2003).
- [2] M. Fierz, C. Houle, P. Steigmeier, H. Burtscher, Design, calibration and field performance of a miniature diffusion size classifier, *Aerosol Science and Technology* 45 (1) (2011) 1–10.
- [3] C. Asbach, H. Kaminski, D. von BARANY, T. A. J. Kuhlbusch, C. Monz, N. Dziurawitz, J. Pelezer, K. Vossen, K. Berlin, S. D. U. Gotz, H.-J. Kiesling, R. Schierl, D. Dahmann, Comparability of portable nanoparticle exposure monitors, *The Annals of Occupational Hygiene* 56 (5) (2012) 606–621.
- [4] S. Bau, B. Zimmermann, R. Payet, O. Witschger, A laboratory study of the performance of the handheld diffusion size classifier (discmini) for various aerosols in the 15–400 nm range, *Environmental Science: Processes and Impacts* 17 (2015) 261–269.
- [5] Fondazione Salvatore Maugeri - IRCCS, Radiello - Volatile organic compounds (VOCs) – thermally desorbed (2006).
- [6] Fondazione Salvatore Maugeri - IRCCS, Radiello - Nitrogen and sulfur dioxides (NO<sub>2</sub> and SO<sub>2</sub>) (2006).
- [7] D. Maximilien, C. Caroline, N. Pierre-Eric, N.-G. Eve, L. Guillaume, C. Hugo, H. Stephane, A. Simon, Diesel engine exhaust exposures in two underground mines, *International Journal of Mining Science and Technology* 27 (4) (2017) 641–645.
- [8] E. D. Thimmons, F. N. Kissell, Bureau of Mines Report of Investigations – Tracer gas as an aid in mine ventilation analysis, United States Department of Interior (1974).
- [9] Mine Safety and Health Administration (MSHA), <https://www.msha.gov/support-resources/equipment-approval-certification> (2018).
- [10] Donaldson Filtration Solutions, Exhaust Product Guide for Medium- and Heavy-duty Vehicles and Equipment (2015).
- [11] J. H. Graaf, T. Parrott, Guidelines for the design and construction of underground portals in open pits – a case study of the gateway mine, *Ground Support 2013, Proceedings of the Seventh International Symposium on Ground Support in Mining and Underground Construction* (2013) 421–436.
- [12] B. J. Mullins, R. Mead-Hunter, S. Abishek, A. J. C. King, Diesel Particulate Filter – Dynamometer Test Results, Contract research report for Mammoth equipment and exhausts (Copy available from author), Mammoth Equipment and Exhausts (2018).
- [13] Australian Institute of Occupational Hygienists, AIOH, Diesel Particulate Matter and Occupational Health Issues Position Paper, AIOH Exposure Standards Committee (2017).

**Appendix-1: Personal Monitoring Data**

Table A1: Personal sampling results for metals

ID	Al (µg/m <sup>3</sup> )	Ba (µg/m <sup>3</sup> )	Cd (µg/m <sup>3</sup> )	Ca (µg/m <sup>3</sup> )	Ce (µg/m <sup>3</sup> )	Cr (µg/m <sup>3</sup> )	Cu (µg/m <sup>3</sup> )	Fe (µg/m <sup>3</sup> )	Pb (µg/m <sup>3</sup> )	Li (µg/m <sup>3</sup> )	Mg (µg/m <sup>3</sup> )	Mn (µg/m <sup>3</sup> )	Ni (µg/m <sup>3</sup> )	K (µg/m <sup>3</sup> )	Zn (µg/m <sup>3</sup> )
A1						0.00021	0.00048	0.04821				0.01171	0.00034		0.00138
A2	0.00138			0.00482		0.00530		0.00675		0.00014	0.00138	0.00324			0.00138
A3				0.00069											
A4	0.00413			0.00826	0.00001		0.00007	0.00758			0.00413	0.00019			
A5				0.00069											
A6	0.00138		0.00023				0.00041	0.00227	0.00055		0.00138	0.00005			
A7	0.00069			0.00138				0.00310			0.00069	0.00010			0.00138
A8															
A9								0.00055							
A10	0.00138			0.00344			0.00386	0.00448				0.00009			
A11								0.00041							
A12				0.00138				0.00069			0.00069				
A13								0.00062							
A14															
A15				0.00138				0.00041							
A16				0.00138				0.00041							
A17				0.00138				0.00034							
A18							0.00007	0.00055							
A19	0.00069					0.00007		0.00138							0.00138
A20				0.00138				0.00041							
U1	0.00069					0.00014		0.00482			0.00275	0.00131		0.00344	
U2	0.01033	0.00007		0.03581	0.00002	0.00014		0.01171			0.00758	0.00027		0.00413	0.00482
U3	0.00413			0.00551	0.00001	0.00014	0.00014	0.00964			0.00344	0.00083		0.00344	
U4	0.00275			0.00551	0.00001	0.00021		0.00517			0.00344	0.00012		0.00344	
U5	0.00138			0.00413		0.00007		0.00282				0.00007		0.00413	
U6	0.00138					0.00014	0.00014	0.00289				0.00008		0.00344	
U7	0.00069			0.00138		0.00014		0.00186			0.00138	0.00003		0.00344	
U8	0.00069			0.00275		0.00014	0.00007	0.00289			0.00138	0.00006		0.00344	
U9	0.00138			0.00344		0.00014	0.00007	0.00448				0.00011		0.00413	
U10	0.00413			0.01446		0.00007	0.00014	0.00668			0.00413	0.00012		0.00344	0.00758
U11				0.00138		0.00007		0.00172			0.00138	0.00004		0.00344	

ID	Al ( $\mu\text{g}/\text{m}^3$ )	Ba ( $\mu\text{g}/\text{m}^3$ )	Cd ( $\mu\text{g}/\text{m}^3$ )	Ca ( $\mu\text{g}/\text{m}^3$ )	Ce ( $\mu\text{g}/\text{m}^3$ )	Cr ( $\mu\text{g}/\text{m}^3$ )	Cu ( $\mu\text{g}/\text{m}^3$ )	Fe ( $\mu\text{g}/\text{m}^3$ )	Pb ( $\mu\text{g}/\text{m}^3$ )	Li ( $\mu\text{g}/\text{m}^3$ )	Mg ( $\mu\text{g}/\text{m}^3$ )	Mn ( $\mu\text{g}/\text{m}^3$ )	Ni ( $\mu\text{g}/\text{m}^3$ )	K ( $\mu\text{g}/\text{m}^3$ )	Zn ( $\mu\text{g}/\text{m}^3$ )
U12	0.00138			0.00482		0.00014		0.00220			0.00275	0.00005		0.00275	
U14	0.00138			0.00275		0.00007	0.00028					0.00005		0.00413	
U15	0.00138			0.00275		0.00014		0.00241				0.00006		0.00413	
U16	0.00138			0.00275		0.00014		0.00282				0.00007		0.00413	
U17	0.00138			0.00344		0.00007		0.00758				0.00008		0.00344	
U18				0.00482		0.00007		0.00365			0.00344	0.00008		0.00344	
U19				0.00275	0.00001	0.00014	0.00007	0.01102			0.00275	0.00010		0.00344	
U20				0.00482		0.00014	0.00007	0.00365			0.00275	0.00008		0.00344	0.00138
U21	0.00138	0.00014		0.00689		0.00007		0.00241				0.00006		0.00344	
U22				0.00138		0.00007		0.00069			0.00069			0.00344	
U23				0.00138	0.00001	0.00014		0.00145			0.00069			0.00413	
U24	0.00138					0.00007		0.00165			0.00138	0.00003		0.00344	
U26	0.00069					0.00014		0.00227				0.00005		0.00344	
U27	0.01377	0.00007		0.09642	0.00002	0.00007		0.00393			0.00826	0.00025		0.00344	0.01102
U28	0.00069					0.00007		0.00220			0.00138	0.00004		0.00344	
U29	0.00275			0.01171		0.00007		0.00282			0.00275	0.00004		0.00344	0.00551
U30	0.00069					0.00007		0.00399				0.00004		0.00344	
U31	0.01584			0.04821	0.00002	0.00014		0.01446			0.01377	0.00024		0.00344	0.02824
U32	0.00482			0.01171	0.00001	0.00014	0.00007	0.00661			0.00551	0.00014		0.00344	0.00482
U33				0.00138		0.00007		0.00076			0.00138			0.00413	
U34	0.00138			0.01102		0.00007	0.00007	0.00399						0.00344	
U35	0.00138			0.00413		0.00007						0.00005		0.0413	
U36	0.00138			0.00344		0.00021						0.00005		0.00344	
U37	0.00138			0.00689		0.00007		0.00152			0.00138			0.00344	
U38				0.00275		0.00007	0.00034	0.00041						0.00344	
U39	0.00275			0.00620		0.00007		0.00255				0.00006		0.00344	
U40	0.00551			0.00275		0.00014		0.00640			0.00138	0.00004		0.00344	
U41	0.00069			0.00413		0.00007		0.00262			0.00069			0.00344	
U42	0.00138			0.00551		0.00014		0.00344				0.00006		0.00344	
U43	0.00275			0.01171		0.00007		0.00386			0.00275	0.00009		0.00344	
U44	0.00138	0.00007		0.00344		0.00007		0.00158			0.00138	0.00003		0.00344	
U45				0.00620		0.00014	0.00048	0.00427			0.00482	0.00008		0.00413	0.00344
U46	0.00138			0.00413		0.00014		0.00241				0.00004		0.00344	0.00138
U47	0.00344			0.02066	0.00001	0.00007		0.00255			0.00275	0.00009		0.00344	0.00138
U48				0.00275		0.00007	0.00014	0.00592			0.00069			0.00344	

ID	Al ( $\mu\text{g}/\text{m}^3$ )	Ba ( $\mu\text{g}/\text{m}^3$ )	Cd ( $\mu\text{g}/\text{m}^3$ )	Ca ( $\mu\text{g}/\text{m}^3$ )	Ce ( $\mu\text{g}/\text{m}^3$ )	Cr ( $\mu\text{g}/\text{m}^3$ )	Cu ( $\mu\text{g}/\text{m}^3$ )	Fe ( $\mu\text{g}/\text{m}^3$ )	Pb ( $\mu\text{g}/\text{m}^3$ )	Li ( $\mu\text{g}/\text{m}^3$ )	Mg ( $\mu\text{g}/\text{m}^3$ )	Mn ( $\mu\text{g}/\text{m}^3$ )	Ni ( $\mu\text{g}/\text{m}^3$ )	K ( $\mu\text{g}/\text{m}^3$ )	Zn ( $\mu\text{g}/\text{m}^3$ )
U49	0.00138			0.00413		0.00007	0.00028	0.00317				0.00006		0.00344	
U50	0.00138			0.00413		0.00014	0.00007	0.00406				0.00008		0.00344	
U51	0.00138			0.00551		0.00007		0.00475				0.00006		0.00344	
U52				0.00482		0.00007		0.00296				0.00006		0.00413	
U53	0.00069	0.00007		0.00275		0.00007	0.00021	0.00386			0.00138			0.00413	
U55	0.00344			0.00758	0.00001	0.00014		0.00895			0.00482	0.00014		0.00138	0.00275
U56	0.00138			0.00413		0.00007		0.00255				0.00006		0.00138	
U57	0.00620			0.02479	0.00001	0.00007	0.00007	0.00758			0.00551	0.00019		0.00138	
U58	0.00138			0.00275				0.00200			0.00138	0.00003		0.00138	
U59								0.00200			0.00069			0.00138	
U60	0.00069			0.00275				0.00179			0.00138	0.00004		0.00138	
U61	0.00138			0.00620				0.00213				0.00005			
U62	0.00069			0.00275			0.00014	0.00096			0.00138				
U63				0.00344				0.00826				0.00007		0.00138	
U64				0.00344			0.00014	0.00248			0.00138			0.00138	
U65				0.00482		0.00007	0.00014	0.00523			0.00275	0.00010		0.00138	
U66				0.00551				0.01033				0.00008		0.00138	
U67	0.00826			0.03099	0.00001		0.00014	0.00475			0.00482	0.00016		0.00138	
U68	0.00138			0.00482		0.00014		0.00455				0.00006		0.00344	0.00138
U69	0.00275			0.00689		0.00014		0.00523			0.00344	0.00015		0.00138	
U70								0.00331			0.00138	0.00005		0.00138	
U71				0.00758			0.00014	0.00337				0.00006		0.00138	
U72				0.00275				0.00110			0.00069				
U73	0.00138			0.00344							0.00138	0.00004			
U74	0.00138			0.00482			0.00034	0.00289			0.00344	0.00009		0.00138	0.00275
U75							0.00021	0.00895			0.00069	0.00008		0.00138	
U76							0.00021	0.00489			0.00138	0.00052		0.00138	
U78	0.00069			0.00275				0.00124			0.00138	0.00003		0.00138	
U79	0.00069			0.00275				0.00152			0.00138	0.00004			
U80	0.00138			0.00344				0.00317				0.00006		0.00138	

Blank values denote samples which were below the detection level and therefore could not be reliably converted to an average exposure concentration. Metals which did not yield any results have been omitted—these were Molybdenum, Vanadium, Sodium, Cobalt and Beryllium.

**Appendix-2: Personal monitoring data for NO<sub>2</sub> and SO<sub>2</sub>**

**Table A2.1 Personal sampling results (µg/m<sup>3</sup>) for NO<sub>2</sub> and SO<sub>2</sub>**

ID	NO <sub>2</sub> (µg/m <sup>3</sup> )	SO <sub>2</sub> (µg/m <sup>3</sup> )		ID	NO <sub>2</sub> (µg/m <sup>3</sup> )	SO <sub>2</sub> (µg/m <sup>3</sup> )		ID	NO <sub>2</sub> (µg/m <sup>3</sup> )	SO <sub>2</sub> (µg/m <sup>3</sup> )
A1	17.48			U16	679.88			U49	330.23	
A2	21.37			U17	388.50			U50	330.23	
A3	17.48			U18	194.25			U51	932.40	
A4	13.60			U19	524.48			U52	1204.35	
A5	13.60			U20	252.53			U53	932.40	
A6	36.91			U21	213.68			U54	252.53	
A7	17.48			U23	213.68			U56	718.73	101.86
A8	23.31			U24	330.23			U57	757.58	
A9	17.48			U25	83.53			U58	233.10	
A11	21.37			U26	31.08			U59	213.68	
A12	50.51			U27	1184.93			U60	194.25	
A13	27.20			U28	93.24			U61	427.35	
A14	25.25			U29	446.78			U62	213.68	280.11
A15	27.20			U30	213.68			U63	815.85	
A16	17.48			U31	893.55			U64	132.09	
A17	19.43			U32	310.80			U65	699.30	356.51
A18	15.54			U33	660.45			U66	718.73	
A19	54.39			U34	87.41			U67	48.56	
A20	54.39			U35	777.00			U68	252.53	980.39
U1	192.31			U36	388.50			U69	1087.80	
U2	1359.75			U37	165.11			U70	213.68	1209.57
U3	184.54	738.48		U38	157.34			U71	388.50	
U4	427.35			U39	446.78			U72	407.93	101.86
U5	213.68			U40	330.23			U73	271.95	292.84
U7	349.65			U41	126.26			U74	835.28	
U8	97.13	483.83		U42	602.18			U75	213.68	
U9	271.95			U43	174.83			U76	48.56	
U10	132.09			U44	621.60			U77	679.88	229.18
U12	738.15			U45	543.90			U78	485.63	101.86
U13	699.30			U46	485.63			U79	56.33	
U14	271.95			U47	835.28	63.66		U80	271.95	76.39
U15	388.50			U48	446.78					

*Blank values denote samples which were below the detection level and therefore could not be reliably converted to an average exposure concentration.*

**Table A2.2 Personal sampling results (ppm) for NO<sub>2</sub> and SO<sub>2</sub>**

ID	NO <sub>2</sub> (ppm)	SO <sub>2</sub> (ppm)		ID	NO <sub>2</sub> (ppm)	SO <sub>2</sub> (ppm)		ID	NO <sub>2</sub> (ppm)	SO <sub>2</sub> (ppm)
A1	0.01			U16	0.36			U49	0.18	
A2	0.01			U17	0.21			U50	0.18	
A3	0.01			U18	0.10			U51	0.50	
A4	0.01			U19	0.28			U52	0.64	
A5	0.01			U20	0.13			U53	0.50	
A6	0.02			U21	0.11			U54	0.13	
A7	0.01			U23	0.11			U56	0.38	0.04
A8	0.01			U24	0.18			U57	0.40	
A9	0.01			U25	0.04			U58	0.12	
A11	0.01			U26	0.02			U59	0.11	
A12	0.03			U27	0.63			U60	0.10	
A13	0.01			U28	0.05			U61	0.23	
A14	0.01			U29	0.24			U62	0.11	0.11
A15	0.01			U30	0.11			U63	0.43	
A16	0.01			U31	0.47			U64	0.07	
A17	0.01			U32	0.17			U65	0.37	0.14
A18	0.01			U33	0.35			U66	0.38	
A19	0.03			U34	0.05			U67	0.03	
A20	0.03			U35	0.41			U68	0.13	0.37
U1	0.10			U36	0.21			U69	0.58	
U2	0.72			U37	0.09			U70	0.11	0.46
U3	0.10	0.28		U38	0.08			U71	0.21	
U4	0.23			U39	0.24			U72	0.22	0.04
U5	0.11			U40	0.18			U73	0.14	0.11
U7	0.19			U41	0.07			U74	0.44	
U8	0.05	0.18		U42	0.32			U75	0.11	
U9	0.14			U43	0.09			U76	0.03	
U10	0.07			U44	0.33			U77	0.36	0.09
U12	0.39			U45	0.29			U78	0.26	0.04
U13	0.37			U46	0.26			U79	0.03	
U14	0.14			U47	0.44	0.02		U80	0.14	0.03
U15	0.21			U48	0.24					

*Blank values denote samples which were below the detection level and therefore could not be reliably converted to an average exposure concentration.*

Table A3: Personal sampling results for VOCs (alkanes and chlorinated alkanes and alkenes)

ID	Hexane ( $\mu\text{g}/\text{m}^3$ )	Heptane ( $\mu\text{g}/\text{m}^3$ )	Octane ( $\mu\text{g}/\text{m}^3$ )	Nonane ( $\mu\text{g}/\text{m}^3$ )	Decane ( $\mu\text{g}/\text{m}^3$ )	Undecane ( $\mu\text{g}/\text{m}^3$ )	Cyclohexane ( $\mu\text{g}/\text{m}^3$ )	1,1,1-Trichloroethane ( $\mu\text{g}/\text{m}^3$ )	Trichloroethylene ( $\mu\text{g}/\text{m}^3$ )	Tetrachloroethylene ( $\mu\text{g}/\text{m}^3$ )
A1		4.911	2.138				2.910			
A3	29.709	8.384	11.316	4.545	1.631	3.535	8.783			
A4	1.783	4.551	7.544	3.896	1.087		5.215			
A5						2.020	1.866			
A6						4.545	1.592			
A7		2.036	0.943		1.563	3.914	27.448			1.074
A8	0.891	3.713	1.257				1.647			
A9										
A10	1.367	5.989	4.652	1.876			2.141			
A11	4.694	2.036					2.635			
A12	1.010	0.958		1.371	1.223	2.652	1.208			
A13	7.724	5.689					2.086			
A14						2.273				
A15	1.070					2.020				
A16	1.129			1.299	2.106	3.914				
A17	1.070	2.276					3.843			
A18	1.367	3.354					7.137			
A19	1.129	2.276			1.087	2.020	5.490			
A20	0.891	1.138		1.154			1.372			
U2	1.367	1.677	1.320	1.154	1.291	3.409	2.361			
U3	29.709	29.944	31.435	1.876	1.902	4.293	27.448	1.136		
U4	3.387	8.983	2.515	2.814	2.038	3.409	5.270			
U5	1.604	3.414	1.446	1.371	1.291		5.435			
U6	2.317	7.186					4.062			
U9	16.637	10.780	2.641	2.453	1.970	8.460	5.435			
U10	24.361	29.944	31.435	33.911	16.986	12.626	27.448			
U11	15.449	16.768	15.717	12.266	6.794	8.712	27.448			
U12	2.852	2.994	2.138	1.948	1.359		7.686			
U13		1.078			1.563	3.914	1.482			
U14	16.043	13.175	11.316	10.101	6.047	8.965	27.448			
U15	10.101	9.582	7.544	5.483	2.922	2.778	26.350			
U16	4.397	3.893	2.641	2.165	1.427	4.419	5.490			
U17	22.579	7.785	6.916	5.195	3.465	6.944	17.018			
U18	19.014	4.072	6.916	6.926	7.474	13.889	3.623			
U19	1.783	2.336	1.635	3.391	2.106	2.904	2.306			
U20	3.446	4.012	2.955	3.247	2.242	2.273	6.588			
U21	2.852	1.916					5.490			
U22	2.258	2.216	3.206	5.483	2.718	2.020	3.184			
U23	3.268	1.737	1.446	1.371			3.513			
U24	5.942	5.570	6.035	4.978	2.242	3.030	11.528			
U25							1.757			
U26	0.951	0.898			1.155	3.914				
U27	2.139	3.114					2.196			
U28	13.072	2.395					1.592			
U29							1.427			
U30	1.783	9.582				2.399	1.757			
U31	1.901	2.635	2.326	2.525	2.038	3.283	5.435			
U32	3.684	3.473			1.427	3.662	4.556		1.062	2.326
U33	5.288	5.809	5.281	5.772	4.688	2.778	17.018			
U34	1.961	1.916	3.081	4.401	2.718	7.955	3.294			

ID	Hexane (µg/m <sup>3</sup> )	Heptane (µg/m <sup>3</sup> )	Octane (µg/m <sup>3</sup> )	Nonane (µg/m <sup>3</sup> )	Decane (µg/m <sup>3</sup> )	Undecane (µg/m <sup>3</sup> )	Cyclohexane (µg/m <sup>3</sup> )	1,1,1-Trichloroethane (µg/m <sup>3</sup> )	Trichloroethylene (µg/m <sup>3</sup> )	Tetrachloroethylene (µg/m <sup>3</sup> )
U35	3.743	7.186	6.916	8.658	4.688	4.419	8.783			
U36	1.367	1.198					3.513			1.969
U37	0.891	0.958	1.257	4.978	10.192	9.217				
U38	0.951	1.318				3.535	2.031			
U39	0.891			2.597	2.446	4.545	1.043			
U40	1.545						1.482			
U41	3.446	1.078					1.537			
U42	29.709	28.147	20.747	13.709	3.873		27.448			
U43	2.733	1.916	1.006				6.039			
U44	1.783	1.976	2.452	2.381	1.631	4.167	2.800			0.954
U45	10.695	4.012	3.835	4.257	4.145	3.030	8.783			
U46	3.387	3.234	3.081	3.463	1.699	2.399	7.686			
U47	11.289	14.972	14.460	11.544	6.659	5.177	27.448			
U49	2.971	7.785	12.574	12.987	10.871	11.111	3.898			
U50	7.130	4.611	3.206	1.876	1.087		15.920			
U51	16.043	18.565	16.346	11.544	4.077	4.167	27.448			
U52	3.090	2.395	2.515	3.824	8.833	20.202	4.062			
U53	2.674	2.395	2.389	2.597	1.563	2.904	6.588			
U54	4.694	4.192	2.263	2.020	2.786	7.449	10.979			1.312
U55	1.307	0.958	1.132	1.082	1.223	2.020	2.086			
U56	8.318	1.318			1.495	2.904	5.380			
U57	21.985	18.565	1.069			2.904	6.039			
U58							1.208			
U59	1.842	1.018	1.132	1.082	1.359	2.020	2.910			
U60	1.129	1.078				2.652	3.458			
U71	2.377	1.377	1.069	1.227			4.227			
U72	7.724	9.582	3.584	2.092	1.223	2.778	19.763			
U74							1.537			
U75	2.139	1.198	1.195	1.299	2.106	4.167	1.592			
U76	29.709	1.617					2.086			
U77	1.545	5.150	1.949	1.732	1.970	8.081	6.588			
U78	1.367	3.354					1.921			
U80	1.723	1.497					1.427			

Blank values denote samples which were below the detection level and therefore could not be reliably converted to an average exposure concentration.

Table A4: Personal sampling result for VOCs (aromatic hydrocarbons)

ID	Benzene ( $\mu\text{g}/\text{m}^3$ )	Toluene ( $\mu\text{g}/\text{m}^3$ )	Ethylbenzene ( $\mu\text{g}/\text{m}^3$ )	o-Xylene ( $\mu\text{g}/\text{m}^3$ )	m- & p-Xylene ( $\mu\text{g}/\text{m}^3$ )	Styrene ( $\mu\text{g}/\text{m}^3$ )	1,2,4-Trimethylbenzene ( $\mu\text{g}/\text{m}^3$ )	1,4-Dichlorobenzene ( $\mu\text{g}/\text{m}^3$ )
A1	0.872	24.242	1.120	1.109	3.645			
A3	1.635	25.253	29.478	30.796	28.480	8.386	3.252	1.102
A4	1.744	14.646	3.537	1.971	5.696			
A5	1.690	7.071	2.240	2.094	5.240		1.176	2.273
A6	3.052	6.566	1.238	1.047	2.449			1.653
A7	1.635	18.182	4.657	2.094	6.266	1.565	1.591	1.240
A8	4.851	15.152	1.533	0.653	3.133			
A9		2.879	3.301	1.909	4.386			1.102
A10	1.145	21.212	1.592	0.985	3.304			
A11	1.962	9.596	1.710	0.653	2.449			
A12	2.616	10.101	2.476	1.909	5.183	3.970	1.868	1.791
A13	3.488	5.556	9.433	3.695	11.392			
A14	1.472	4.848	1.474	1.170	3.304	0.895		1.515
A15	1.690	6.566	2.712	0.653	2.278	1.342	1.730	1.653
A16	1.962	9.091	2.181	1.786	3.930	2.460	2.975	3.099
A17	2.671	12.626	4.363	2.402	6.835	2.180		
A18	1.308	10.606	2.004	0.653	2.335	0.593		
A19	2.616	9.091	2.004	1.109	3.418	1.565	1.245	1.928
A20	1.472	7.071	1.592	1.047	2.620	1.845	1.384	1.309
U2	27.251	25.253	5.483	3.511	9.114	11.182	1.799	
U3	2.943	18.687	3.066	2.464	6.266	10.064	2.629	2.066
U4	25.071	25.253	4.952	4.065	9.114	21.805	4.151	1.240
U5	25.071	25.253	4.245	3.203	9.114	26.837	2.214	1.377
U6	25.071	25.253	15.328	11.702	28.480	27.955	2.006	
U9	10.900	25.253	4.834	3.757	10.253	26.278	2.006	
U10	26.161	25.253	29.478	30.796	28.480	27.955	27.674	
U11	16.896	25.253	28.888	26.484	28.480	27.955	13.145	
U12	13.625	25.253	5.896	5.235	14.810	23.482	2.975	
U13	5.995	16.162	1.651	1.417	3.361	27.955	2.006	1.102
U14	21.256	25.253	17.687	15.398	28.480	27.955	10.378	
U15	13.080	25.253	10.022	9.239	23.354	27.955	4.497	
U16	25.071	25.253	5.837	4.989	11.392	24.041	3.667	
U17	14.716	25.253	10.612	9.855	26.202	27.955	3.044	
U18	10.355	25.253	10.612	8.623	19.936	27.955	7.610	
U19	7.085	23.737	3.301	3.942	9.114	27.955	4.566	
U20	27.251	25.253	12.970	9.855	27.341	27.955	4.635	
U21	11.445	25.253	3.301	2.648	6.835	24.041	1.591	
U22	4.851	14.646	5.660	6.775	14.810	10.064	5.051	
U23	14.170	23.737	5.365	4.619	10.253	27.955	2.491	
U24	26.706	25.253	29.478	24.021	28.480	27.955	4.705	
U25	1.526	25.253	1.946	2.464	5.411	2.516		
U26	2.344	10.101	2.181	1.971	5.525	8.386	1.937	
U27	9.265	25.253	5.896	2.648	8.544	15.096		
U28	3.270	14.141	4.422	4.681	10.823	3.914	3.598	1.240
U29	5.995	18.182	2.417	3.080	6.266	11.741	1.799	
U30	5.123	25.253	1.356	0.985	2.734	8.386		
U31	26.161	25.253	6.485	6.775	15.379	22.364	3.528	
U32	18.531	25.253	2.476	1.971	5.183	15.096	0.734	
U33	21.801	25.253	7.075	7.391	17.658	27.955	7.610	
U34	5.450	19.192	4.834	5.420	12.531	8.946	4.359	
U35	9.265	25.253	14.149	12.934	28.480	8.386	5.673	
U36	6.540	15.152	1.474	1.355	3.304	7.827		

ID	Benzene (µg/m <sup>3</sup> )	Toluene (µg/m <sup>3</sup> )	Ethylbenzene (µg/m <sup>3</sup> )	o-Xylene (µg/m <sup>3</sup> )	m- & p-Xylene (µg/m <sup>3</sup> )	Styrene (µg/m <sup>3</sup> )	1,2,4-Trimethylbenzene (µg/m <sup>3</sup> )	1,4-Dichlorobenzene (µg/m <sup>3</sup> )
U37	3.815	6.061	2.299	3.572	7.405	4.752	8.994	2.204
U38	6.540	25.253	2.535	2.402	6.835	16.773	2.145	
U39	3.597	15.657	7.075	3.819	8.544	7.268	3.528	
U40	5.123	25.253	2.063	1.909	5.183	15.096	1.453	
U41	2.889	25.253	14.739	10.471	28.480	25.718		
U42	27.251	25.253	18.276	16.014	28.480	11.741	8.994	
U43	11.990	22.727	2.653	2.094	5.582	18.450		
U44	15.261	25.253	12.381	4.804	11.962	27.955	3.113	
U45	16.351	25.253	6.485	5.666	14.810	27.955	3.944	
U46	11.445	25.253	17.687	13.550	28.480	27.955	4.151	
U47	13.080	25.253	15.918	14.782	28.480	27.955	11.070	
U49	9.810	25.253	29.478	30.796	28.480	27.955	5.051	
U50	7.085	25.253	4.540	3.634	9.683	15.655	2.629	
U51	19.076	25.253	15.918	15.398	28.480	27.955	9.686	
U52	24.526	25.253	5.837	4.866	12.531	27.955	4.289	
U53	26.161	20.707	5.306	7.391	10.823	27.955	5.535	
U54	9.810	18.687	4.834	3.572	10.253	13.977	3.183	
U55	13.625	25.253	4.127	3.326	8.544	15.096	2.352	
U56	10.355	25.253	3.419	3.080	7.974	20.687	3.390	
U57	15.806	25.253	8.843	3.388	9.114	8.386		
U58	3.488	16.162	1.120		2.335	8.946		
U59	9.265	25.253	2.535	2.402	6.266	16.773	3.736	
U60	3.543	14.646	1.592	1.109	3.304	15.655		
U71	8.720	9.091		1.109	2.278	6.150		
U72	16.351	22.727	3.184	2.833	7.405	13.418	1.453	
U74	3.706	4.192						
U75	8.175	12.626	2.771	2.279	5.183	20.127	3.183	
U76	4.306	7.071	1.592	1.601	5.297			
U77	2.725	12.626	1.356	1.478	3.645	7.827	1.107	
U78	7.085	15.152	1.474	0.985	3.076	10.064		
U79								
U80	3.543	10.101						

*Blank values denote samples which were below the detection level and therefore could not be reliably converted to an average exposure concentration.*

Table A5: Personal sampling results for VOCs (ethers, sulphides and terpenes)

ID	Ethyl tert-butylether ( $\mu\text{g}/\text{m}^3$ )	Dimethyl disulphide ( $\mu\text{g}/\text{m}^3$ )	$\alpha$ – Pinene ( $\mu\text{g}/\text{m}^3$ )	Limonene ( $\mu\text{g}/\text{m}^3$ )
A1				1.776
A3				
A4				
A5				
A6				
A7				2.249
A8				
A9		2.429		11.719
A10				
A11				13.021
A12				
A13				
A14				4.261
A15				
A16		1.598		2.841
A17		1.790		2.723
A18		2.046		6.629
A19				8.759
A20				2.249
U2				3.906
U3	1.061		3.551	
U4				
U5				5.800
U6				4.735
U9				
U10	1.414			
U11				
U12				6.392
U13		1.023		2.367
U14		1.151		
U15				2.367
U16				6.155
U17				
U18				
U19				7.339
U20				4.380
U21				
U22				8.523
U23				
U24		0.959		
U25				2.841
U26				2.012
U27				
U28				2.131
U29				
U30		1.215		
U31				
U32				
U33				
U34				
U35				
U36				8.878
U37				

<b>ID</b>	<b>Ethyl tert-butylether (µg/m<sup>3</sup>)</b>	<b>Dimethyl disulphide (µg/m<sup>3</sup>)</b>	<b>a – Pinene (µg/m<sup>3</sup>)</b>	<b>Limonene (µg/m<sup>3</sup>)</b>
U38				
U39				8.641
U40				
U41	0.859			10.298
U42				
U43				
U44				
U45				
U46				4.498
U47				2.131
U49		1.215		
U50				
U51				6.155
U52				
U53				
U54				6.037
U55				
U56				2.012
U57				
U58				
U59				
U60				
U71				
U72				
U74				
U75				
U76				
U77				4.143
U78				
U80				

*Blank values denote samples which were below the detection level and therefore could not be reliably converted to an average exposure concentration.*

Table A6. PAH results for stationary monitoring sites.

PAH	Cosmo 1815 ( $\mu\text{g}/\text{m}^3$ )	Astro 1965 ( $\mu\text{g}/\text{m}^3$ )	Cos. East 1510 ( $\mu\text{g}/\text{m}^3$ )	Cos. East 1510 ( $\mu\text{g}/\text{m}^3$ )	Vogue 1600 ( $\mu\text{g}/\text{m}^3$ )	WATU ( $\mu\text{g}/\text{m}^3$ )
<b>Acenaphthene</b>						
<b>Acenaphthylene</b>						
<b>Anthracene</b>						
<b>Benzo(a)pyrene</b>						
<b>Benz(a)anthracene</b>						
<b>Benzo(b)fluoranthene</b>						
<b>Benzo(g,h,i)perylene</b>						
<b>Benzo(k)fluoranthene</b>						
<b>Chrysene</b>						
<b>Dibenzo(a,h)anthracene</b>						
<b>Fluoranthene</b>						
<b>Fluorene</b>						
<b>Indeno(1,2,3-cd)pyrene</b>						
<b>Naphthalene</b>	17		2.5	4.4		
<b>Phenanthrene</b>						
<b>Pyrene</b>						

*Blank values denote samples which were below the detection level and therefore could not be reliably converted to an average exposure concentration.*

**Appendix 2:**  
**Deeper Mines Study: Influence of elevated pressure and**  
**ammonia concentration on diesel exhaust particulate**  
**matter**

**12/2018**

**Authors**

**Reece Brown (QUT)**

**Joel Alroe (QUT)**

**Ben Mullins (Curtin)**

**Zoran Ristovski (QUT)**

## Contents

<b>1. Introduction</b> .....	62
<b>2. Methodology</b> .....	64
<b>2.1. Instrumentation</b> .....	64
<b>2.1.1. Diesel Engine</b> .....	64
<b>2.1.2. Rapid Aging Determination (RAD) Chamber</b> .....	66
<b>2.1.3. DMS500 Fast Particle Analyser</b> .....	68
<b>2.1.4. Aerosol Mass Spectrometer (AMS)</b> .....	69
<b>2.1.5. CA-10 Carbon Dioxide Analyzer</b> .....	71
<b>2.2. Experimental Setup</b> .....	72
<b>2.2.1. Pressurized Engine Exhaust Sample</b> .....	72
<b>2.2.2. Pressurized Diesel Emissions</b> .....	73
<b>2.2.3. Pressurized Diesel with Ammonia</b> .....	74
<b>3. Results</b> .....	77
<b>3.1. Diesel Engine Emissions Under Pressure</b> .....	77
<b>3.2. Particle size and number concentration</b> .....	78
<b>3.3. Particle mass and composition</b> .....	80
<b>3.4. Atmospheric Aging Simulation</b> .....	83
<b>4. Discussion</b> .....	84
<b>4.1. Diesel Emissions at different pressures</b> .....	84
<b>4.2. Influence of pressure and ammonia on diesel exhaust</b> .....	85
<b>4.3. Photochemical Reaction of Diesel Exhaust</b> .....	87
<b>4.4. Photochemical Reaction of Diesel Exhaust with Ammonia</b> .....	88
<b>5. Summary</b> .....	90
<b>6. References</b> .....	91

## 1. Introduction

It is well known that diesel exhaust emissions can lead to the generation of “new” or secondary nanoparticles, termed secondary aerosols (SOAs) (Gentner et al. 2017). It has further been documented that diesel engines equipped with selective catalytic reduction (SCR) for NO<sub>x</sub> control, may emit significant quantities of free ammonia (Mendoza-Villafuerte et al. 2017), especially at transient conditions (Suarez-Bertoa et al. 2017) which in turn can also lead to SOA formation (Amanatidis et al. 2014). However, such research has generally been conducted above ground (less than 1 atmosphere pressure) and as such is less relevant to mining operations.

Metalliferous mines around the world currently reach depths of up to 4 km below the surface, however these generally do not use diesel equipment. Australia’s deepest mines using diesel equipment are currently up to 2 km deep, however mines down to 3 km and deeper are believed to be currently planned. It is therefore vital to study the implications of diesel exhaust transport and secondary (ageing) effects at pressures and environments corresponding to these depths.

This report investigates the potential influence elevated pressure and ammonia (NH<sub>3</sub>) concentrations may have on the physiochemical characteristics of diesel exhaust particulate matter. In atmospheric conditions ammonia plays an important role in the generation of secondary organic aerosols (SOA). This is of particular concern for regulatory bodies as SOA formation can lead to greatly increased particulate matter (PM) mass concentrations and significant changes in chemical composition. The process through which SOA is typically formed, termed atmospheric aging, is a photochemical process in which volatile organic compounds (VOCs) react with other pollutants under the influence of light to form less volatile organic species. Depending on atmospheric conditions, these organics either condense into new ultrafine particles (< 100 nm), or condense onto PM already present in the air. This increases the total PM mass and organic mass concentrations, which are tied to many pulmonary and cardiovascular disorders. In underground mine environments there is no sunlight to drive these chemical processes, making normal SOA formation unlikely. However, the combination of increased pressure and high levels of reactive ammonia gas mixed with concentrated diesel exhaust could potentially lead to similar outcomes.

In order to investigate this a series of experiments were conducted at the Biofuel Engine Research Facility (BERF) located at the Queensland University of Technology (QUT). Exhaust was continuously generated using a heavy duty diesel engine and maintained under pressure levels comparable to those found in deep underground mines. The pressurized exhaust was mixed with different concentrations of ammonia gas and allowed to interact over several minutes inside a prototype oxidation flow reactor (OFR) developed at QUT. After this time period the size, concentration and chemical composition of

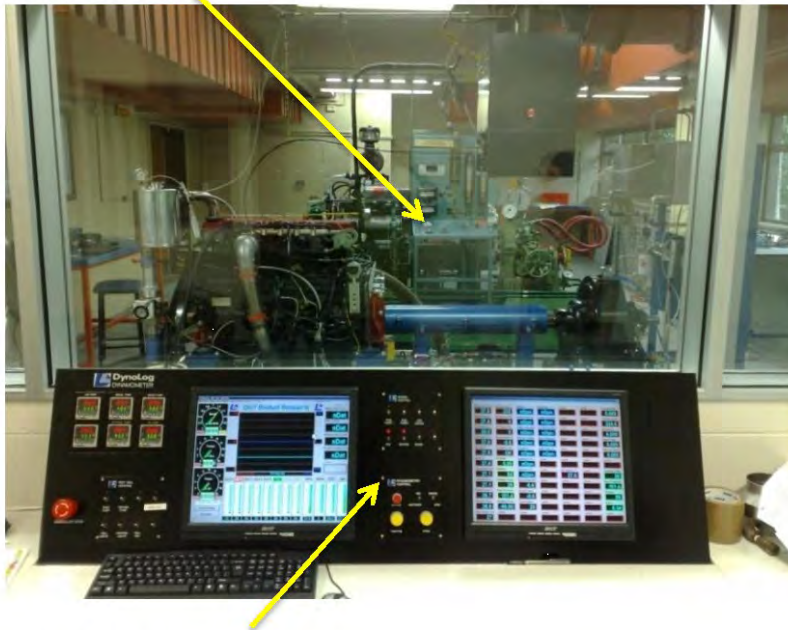
the diesel exhaust particulate matter (PM) was measured. These measurements were contrasted with exhaust which had been artificially aged through photochemical processes to simulate the chemical interactions in normal atmospheric conditions both with and without the addition of ammonia.

## 2. Methodology

### 2.1. Instrumentation

#### 2.1.1. Diesel Engine

### Engine (s)



### CONTROL ROOM

Figure 1 Engine and control room in BERF

The engine used to generate aerosol in this project was a Cummins ISBe220 31. This is a 5.9 litre, turbo charger after cooled, 6 cylinder common rail diesel engine developed for use in medium sized trucks. This engine is essentially a smaller version of a typical underground mine mobile plant engine such as the Cummins QSK19. The engine was coupled to a water break dynamometer and both were controlled in tandem using an electronic control unit. Further specifications can be found in Table 1. The fuel used in the engine during this project was standard automotive diesel.

Feature	Specifications
Cylinders	6 (in-line)
Capacity	5.9 L
Bore x stroke (mm)	102 x 120
Maximum power	162 kW at 2000 rpm

<b>Maximum torque</b>	820 N-m at 1500 rpm
<b>Compressions ratio</b>	17.3:1
<b>Aspiration</b>	Turbocharged
<b>Bore</b>	102 mm
<b>Stroke length</b>	120 mm
<b>Fuel injection</b>	High pressure common rail (2000 bar)
<b>Dynamometer type</b>	Electronically controlled water brake dynamometer
<b>Emission standard</b>	Euro III
<b>Year of manufacture</b>	2000

*Table 1 Specifications of the Cummins diesel engine used to generate exhaust in this project.*

### 2.1.2. Rapid Aging Determination (RAD) Chamber

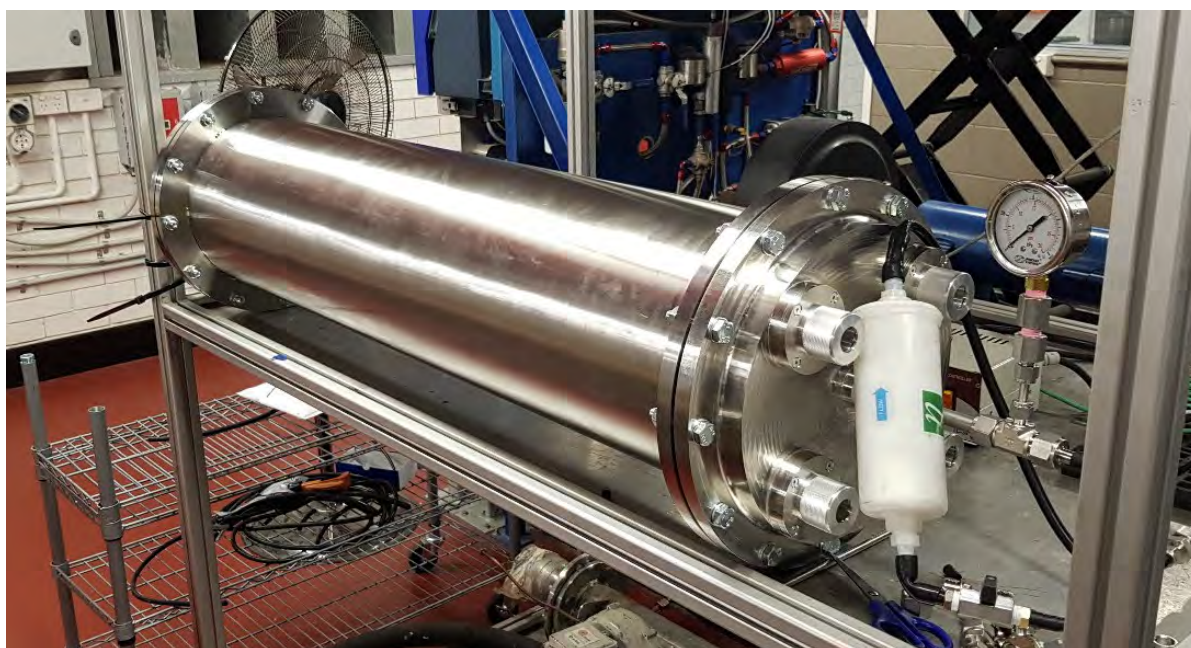


*Figure 2 Image of the RAD chamber taken during construction of the experimental setup.*

The Rapid Aging Determination (RAD) Chamber is a novel oxidation flow reactor (OFR) designed at the Queensland University of Technology to investigate the formation of SOA through photochemical interactions (George et al., 2007; Kang et al., 2007; Keller and Burtscher, 2012; Lambe et al., 2011; Simonen et al., 2017). The instrument (shown in Figure 2) is constructed primarily of 304 Stainless Steel and consists of an inlet, outlet and a large central chamber. The central chamber contains four UVC lamps which generate high concentrations of OH radicals through a chemical reaction involving ozone, water vapour and UVC radiation. A sample flow is continuously drawn through the central chamber where it reacts with the OH radicals to form SOA. The degree of the reaction can be regulated using three variables: The number of UVC lamps powered; the relative humidity of the sample; and the residence time in the main chamber, which can be altered by changing the aerosol sample flowrate.

The RAD chamber contains two exit flows, the sample exit flowrate and the excess flowrate. The sum of these two flowrates equals the aerosol sample inlet flowrate. The purpose of this dual flow system is to optimize the residence time of particles inside the chamber in order to narrow the time distribution to provide a higher degree of repeatability than earlier OFRs. The sample exit flowrate contains the aerosol sample which was analysed in this study. Currently the RAD prototype and its design, characterization and operating procedure have not been finalized.

In this study the RAD was principally used to provide a pressurized environment and to allow sufficient time for any reactions between ammonium and diesel exhaust to take place. However, some

experiments were also performed with the lamps active in order to contrast results with those expected in normal atmospheric conditions.

### 2.1.3. DMS500 Fast Particle Analyser



*Figure 3 Image of the DMS500 Fast Particle Analyser<sup>1</sup>*

The physical characteristics of PM were measured using a DMS500 fast particle analyser (Cambustion Ltd., UK). The sample aerosol is given a unipolar charge distribution and separated based on size using electrical mobility. The separated aerosol is counted into 26 discrete size bins by depositing the particles onto electrodes where they are detected by electrometers. This instrument was selected over a Scanning Mobility Particle Sizer (SMPS) as it is capable of continuously monitoring its entire size range, resulting in sampling time resolutions of as low as 10Hz.

For this study the instrument response was fit with a bimodal lognormal size distribution to track the nucleation and accumulation mode particle size distributions typical of diesel exhaust. These distributions are described by their particle number concentration (PNC) and count median diameter (CMD). The second stage heated dilution was not used and instead the sampling line from the RAD was connected directly to the DMS500 inlet to minimize the time between depressurization of the sample and measurement. Data was logged at a rate of 10Hz.

---

<sup>1</sup> Cambustion Limited, DMS500 Fast Particle Analyzer, 10/11/2018, <https://www.cambustion.com/products/dms500>

#### 2.1.4. Aerosol Mass Spectrometer (AMS)



*Figure 4 Image of the Aerosol Mass Spectrometer used in this project undergoing laboratory testing.*

Measurement of the aerosol composition was made using a compact time of flight Aerosol Mass Spectrometer (AMS) (Aerodyne Research Inc., United States of America (USA)). The AMS samples aerosol with diameters  $< 1 \mu\text{m}$  and provides mass concentrations of non-refractory compounds which vaporise at  $600 \text{ }^\circ\text{C}$ . This includes inorganic species containing nitrate ( $\text{NO}_3$ ), sulfate ( $\text{SO}_4$ ), chloride (Cl), and ammonium ( $\text{NH}_4$ ) and several organic species collectively referred to as organics (Org).

All AMS measurements were performed at a time resolution of 30 s, to capture the rapid aerosol formation and composition changes. At this sampling rate, the mean detection limits were 0.07, 0.01, 0.009, 0.04 and  $0.006 \mu\text{g}/\text{m}^3$  for organics,  $\text{NO}_3$ ,  $\text{SO}_4$ ,  $\text{NH}_4$  and Cl respectively. To protect the instrument sensitivity against the high mass loadings observed in the chamber, sampling was restricted to a five minute interval after stable equilibrium conditions were achieved for each set of chamber parameters.

AMS measurement accuracy is influenced by fluctuations in the inlet flow rate, particle losses at the inlet, molecular ionisation efficiency and the background signal from stray gas-phase ions. The inlet flow rate was calibrated with a primary standard flow meter (Gilian Gilibrator-2). Laboratory-generated 400 nm ammonium nitrate aerosol was used as a calibration standard to determine the

ionisation efficiency. Background measurements were performed through a high efficiency particulate air filter after each change in chamber pressure and  $\text{NH}_3$  gas concentration. After calibration, the mass concentration uncertainties for each species are estimated as  $\pm 37\%$  for organics,  $\pm 35\%$  for  $\text{SO}_4$  and  $\text{Cl}$ , and  $\pm 33\%$  for  $\text{NO}_3$  and  $\text{NH}_4$ .

### 2.1.5. CA-10 Carbon Dioxide Analyzer



Figure 5 Image of CA-10 Carbon Dioxide Analyzer<sup>2</sup>

The CA-10 Carbon Dioxide Analyzer (Sable Systems International, United States of America (USA)) is an instrument used to measure the carbon dioxide (CO<sub>2</sub>) concentrations in an aerosol sample. In this investigation the CA-10 was used to measure the dilution ratio of the ejector dilutor at different pressures. The CO<sub>2</sub> concentration exiting the engine was monitored by the engine setup, and the Ca-10 was connected after the RAD to monitor the CO<sub>2</sub> concentration post dilution. Using these two values the dilution ratio was found through Equation 1.

Equation 1

$$D.R. = \frac{CO_{2eng}}{CO_{2RAD}}$$

Where:  $CO_{2eng}$  is the CO<sub>2</sub> concentration exiting the engine; and  $CO_{2RAD}$  is the CO<sub>2</sub> concentration exiting the RAD.

---

<sup>2</sup> Sable Systems International, CA-10 Carbon Dioxide Analyzer, 10/11/2018, <https://www.sablesys.com/products/classic-line/ca-10-carbon-dioxide-analyzer/>

## 2.2. Experimental Setup

### 2.2.1. Pressurized Engine Exhaust Sample

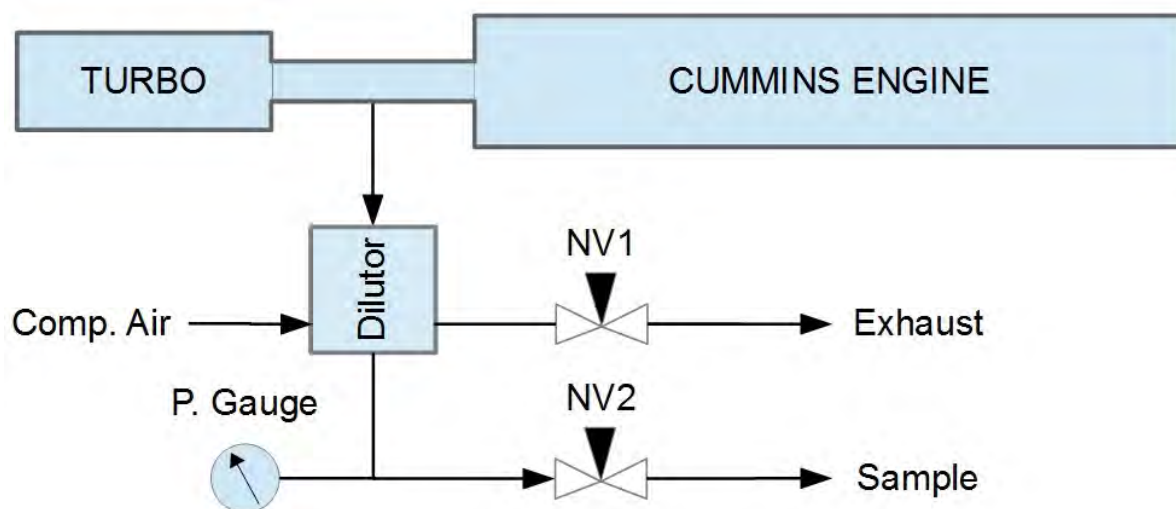


Figure 6 Flow diagram to illustrate the pressure regulation concept used in the experiments detailed in further sections. Exhaust sample is tapped from the manifold prior to the turbocharger to ensure pressurized sample. Sample then passes through the ejector dilution system where it is diluted with compressed air. Two needle valves denoted NV1 and NV2 are used to regulate sample pressure exiting the dilutor, with pressure measured by an analogue gauge. After depressurization of the sample after NV2 the sample aerosol can be carried to instruments for analysis.

In order for this investigation to be successful it was necessary to maintain the diesel exhaust under mining-relevant pressures from the time of combustion until directly before measurement. To achieve this, the sampling point was connected prior to the turbocharger and the engine was operated at its max speed of 2000 rpm with a load of 50 %. This setup generated a high pressure sample well above the maximum tested pressure in all experiments, which could then be regulated down to the required test pressure using an ejector diluter (DI-1000, Dekati Ltd., Finland) system and two needle valves as shown in the setup in Figure 6. One needle valve was connected to the exhaust of the ejector diluter (NV1), whilst the other was connected on the sample outlet (NV2). By balancing the opening of these two valves the pressure of the sample after the ejector diluter can be regulated from atmospheric up to the maximum pressure of the exhaust prior to the turbocharger. After the aerosol passes through NV2 it is depressurized to atmospheric pressure in order to be sampled by instrumentation.

### 2.2.2. Pressurized Diesel Emissions

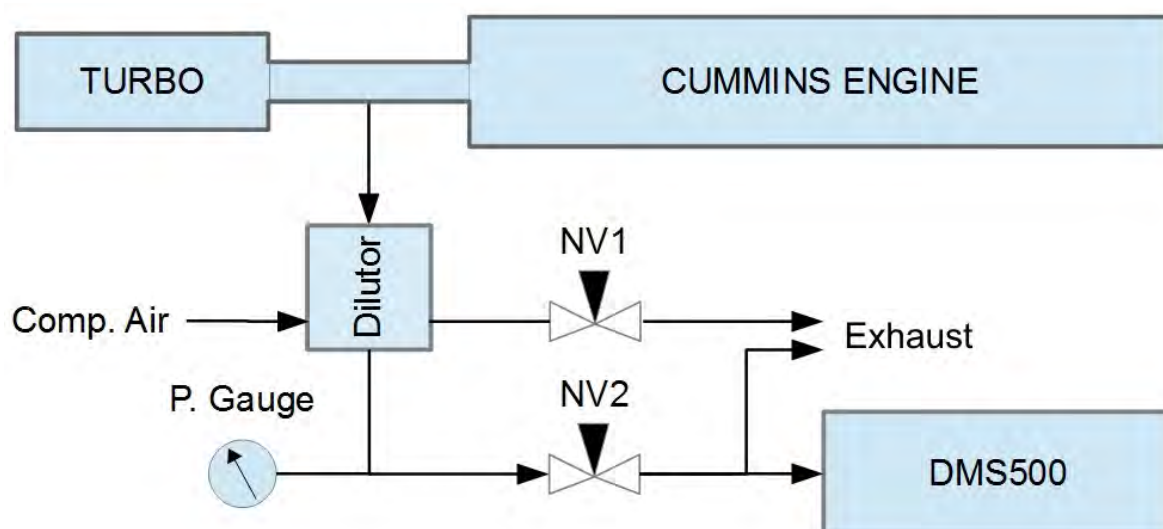


Figure 7 Flow diagram to validate the pressure regulation setup for pressurized diesel emissions testing. Exhaust sample is tapped from the manifold prior to the turbocharger to ensure pressurized sample. Sample then passes through the ejector dilution system where it is diluted with compressed air. Two needle valves denoted NV1 and NV2 are used to regulate sample pressure exiting the dilutor, with pressured measured by an analogue gauge. After depressurization of the sample after NV2 the PNC and CMD of the resultant sample aerosol is measured with the DMS500. Excess sample flow is dumped to exhaust.

In the final test setup the pressure regulated sample exiting the Dekati was mixed with ammonia and input into the RAD chamber. However, it was important to confirm that this pressure regulation method did not adversely influence the exhaust output. Therefore, in order to test the viability of this setup an experiment was constructed as shown in Figure 7. The engine was operated at a continuous engine speed of 2000 rpm at 50 % load to maximize initial sample pressure. The aerosol sample flowrate out of the ejector dilutor was set to 13 std L.min<sup>-1</sup> using a mass flowmeter (4143, TSI Inc., USA) and the two needle valves. This is higher than the flowrate required by the DMS500, however it was selected as this is the sample flowrate used in latter experiments and thus allowed for better comparability. 5 minute samples were collected by the DMS500 for pressures ranging from 1.0 atm to 1.5 atm, in 0.1 atm increments. The additional sample was dumped to a large waste exhaust manifold along with the exhaust flow of the ejector dilutor.

### 2.2.3. Pressurized Diesel with Ammonia

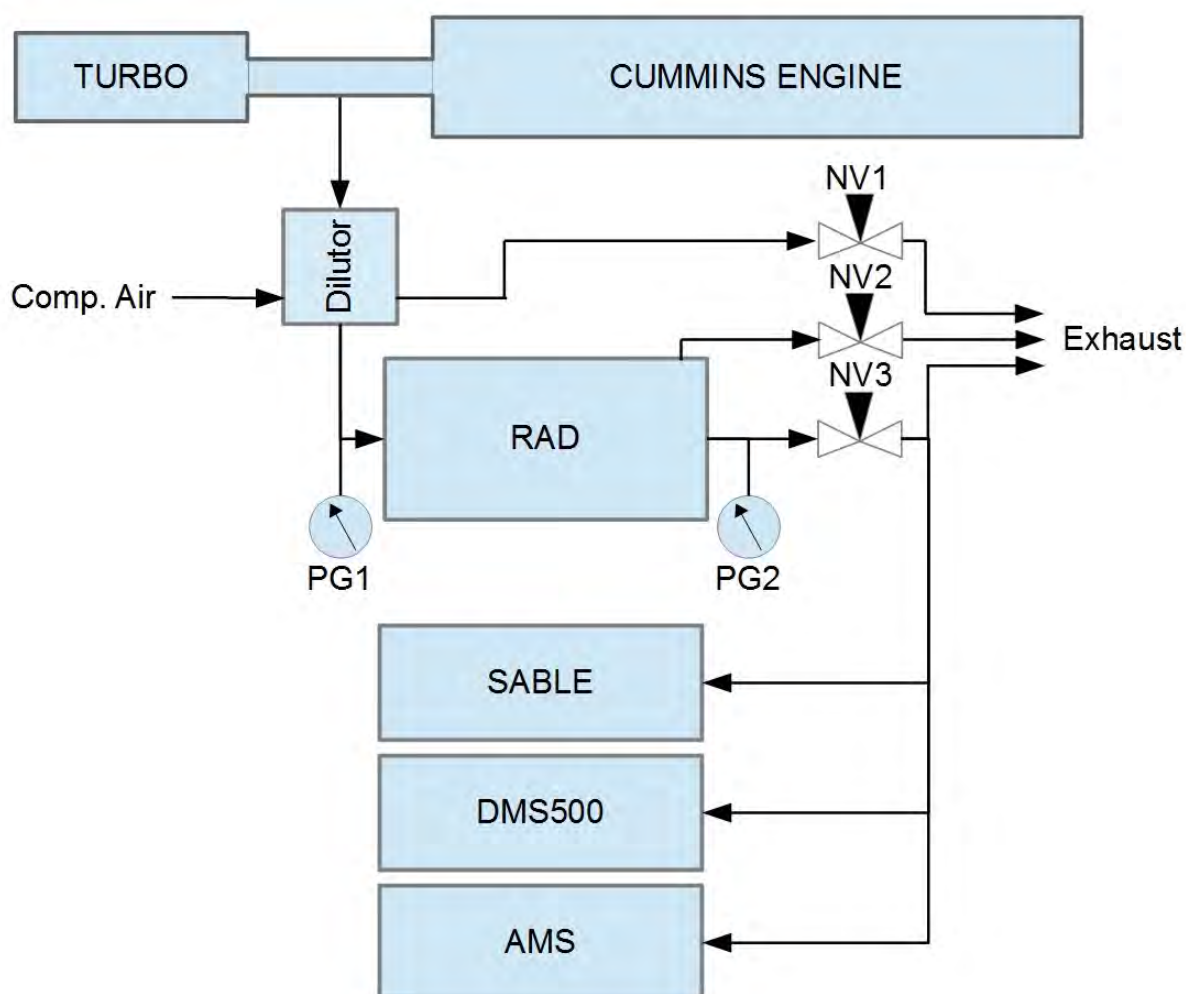


Figure 8 Flow diagram of the setup used to test the interaction of ammonia and diesel exhaust under different pressures. Exhaust sample is tapped from the manifold prior to the turbocharger to ensure pressurized sample. Sample then passes through the ejector dilution system where it is diluted with compressed air. Three needle valves denoted NV1, NV2 and NV3 are used to regulate sample pressure exiting the dilutor and aerosol flowrates. NV1 constrains the flow on the dilutor exhaust to increase the pressure and flow through the RAD. NV2 constrains the aerosol flow exiting out the RAD excess line, and NV3 constrains the flow exiting out the RAD sample line. PG1 and PG2 are pressure gauges used to measure the pressure before and after the RAD chamber to ensure correct pressure is set, and to confirm there is no significant pressure drop across the chamber. After sample depressurization after passing through NV3 the sample aerosol is measure by the Sable, DMS500 and AMS. A slight excess in sample flowrate is intentionally generated to ensure no backflow in the system. This excess sample, along the RAD exhaust flow and ejector dilutor exhaust flow are dumped to the exhaust manifold.

The setup was built as shown in Figure 8. During all sampling the engine was operated at a continuous engine speed of 2000 rpm at 50 % load. The sampling line was tapped into the engine exhaust prior to the turbocharger to pressurize the sample. The sample was then passed through an ejector diluter (DI-1000, Dekati Ltd., Finland) to dilute the sample concentration and to provide a method of pressure regulation downstream. The diluted sample was mixed with a flow of high purity ammonia gas (> 99.99 % Anhydrous Ammonia Gas, BOC Limited) regulated with a mass flow controller (MFC 2132, Axetris

AG, Switzerland) and input into the RAD chamber. On exiting the RAD the flow was split between the AMS, DMS500 and the CA-10, with an exhaust line used to remove excess flow.

Pressure and flow regulation of the sample was achieved using three needle valves denoted NV1, NV2 and NV3 in Figure 8. This is the same concept as described in Sect. 2.2.1, with an additional needle valve to regulate the RAD excess flowrate. Sample pressure inside the RAD was measured using pressure gauges attached to the inlet (Swagelok Ltd., USA) and outlet (Process Systems Pty. Ltd., Australia) of the RAD. This dual gauge setup was used to ensure there was no substantial pressure drop across the RAD chamber. The sample and excess flowrates were set to 11 and 2 std L.min<sup>-1</sup> respectively using a mass flowmeter (4143, TSI Inc., USA) in all samples.

The RAD chamber was pressurized to 1.2 and 1.4 atm, with samples taken with pure diesel exhaust, diesel exhaust with 10 ppm ammonia, and diesel exhaust with 100 ppm ammonia. 3 minute averages were taken for each sampling pressure and ammonia concentration. After changing a pressure or ammonia concentration the setup was left to 15 minutes to ensure equilibrium conditions had been achieved before taking another sample. All wetted materials downstream of mixing with ammonia were compatible with ammonia gas to ensure no undue corrosion or sample contamination occurred. The engine test facility was well ventilated and sample exhaust was heavily diluted with ambient air to reduce ammonia concentrations to trace levels after sampling.

#### **2.2.4. Pressurized Diesel with Secondary Organic Aerosol (SOA) Formation**

The purpose of this investigation is to generate secondary organic aerosol (SOA) from diesel exhaust through photochemical reactions typical of those generated under normal atmospheric conditions. This allows comparison between atmospheric processes and any change in the physiochemical properties that the combination of elevated pressure and ammonia may have on diesel exhaust. The sampling setup for this investigation is identical to that described in Figure 8, and the sampling methodology the same as discussed in Sect. 2.2.3. Pressures of 1.0, 1.2 and 1.4 atm were tested with no ammonia added at flowrates of 11 and 2 std L.min<sup>-1</sup> through the RAD sample and excess lines, respectively. After setting a pressure the sample was allowed to reach equilibrium conditions in the chamber over 15 minutes. Then the RAD lamps were activated for ~ 5 minutes and the aerosol was measured over this period. It was not possible for the AMS to measure for more than this period due to the very high mass concentrations generated inside the RAD. An additional experiment was performed in which 100 ppm of ammonia was added to the diesel exhaust and aged using the RAD lamps. This generated high concentrations of ammonium nitrate as discussed in Sect. 4.4 and thus was not repeated at other pressures. The lack of a full characterization of the RAD as a photochemical aging chamber and the short lamp activation time leads the data from the experiment described in this section to be qualitative.

### 3. Results

#### 3.1. Diesel Engine Emissions Under Pressure (no addition of ammonia)

The particle size distributions measured by the DMS500 of diesel exhaust exiting the engine at pressures of 1.0, 1.2 and 1.4 atm are shown in Figure 9.

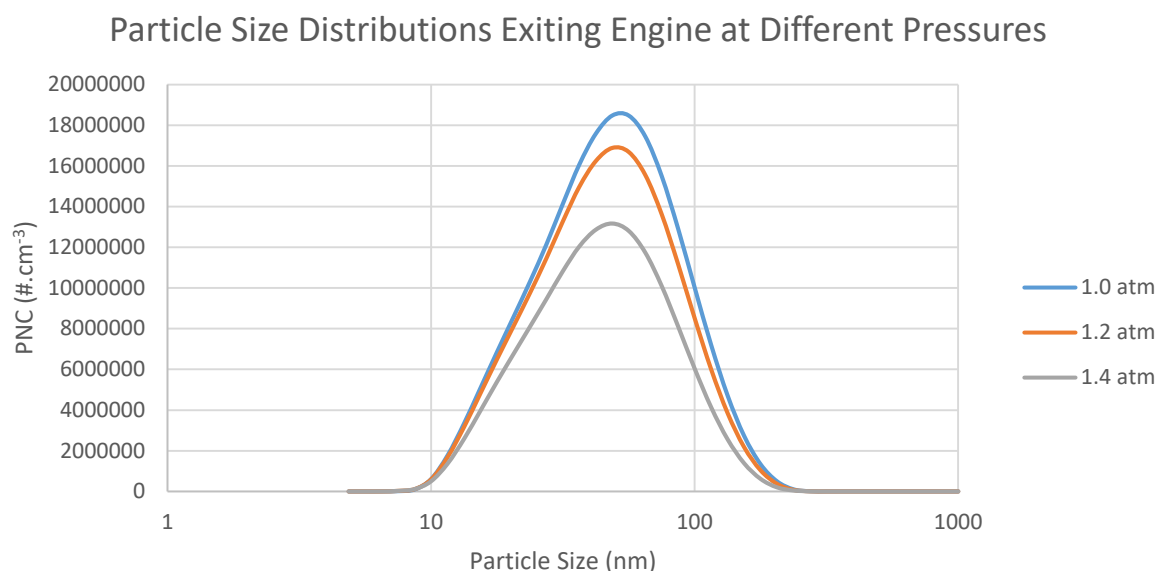


Figure 9 Particle size distributions measured by the DMS500 for the particle concentrations exiting the engine at pressures of 1.0, 1.2, and 1.4 atm. There is a clear decrease in concentration as the pressure is increased.

Particle number concentration (PNC) is given in number of particles per cubic centimetre ( $\#.cm^{-3}$ ). Particle size is described using the count median diameter (CMD) of the fitted distribution in nanometres (nm). PNC values were corrected for dilution as detailed in Sect. 2.1.5.

The fitted accumulation mode PNC and CMD of the distributions shown in Figure 9 is provided in Table 2.

Pressure (atm)	PNC ( $\#.cm^{-3}$ )	CMD (nm)
1.0	$(1.07 \pm 0.05) \times 10^7$	$51 \pm 2$
1.2	$(9.8 \pm 0.5) \times 10^6$	$50 \pm 2$
1.4	$(7.7 \pm 0.4) \times 10^6$	$48 \pm 2$

Table 2 PNC and CMD of the particle size distributions for each of the three pressures shown in Figure 9.

### 3.2. Particle Size and Number Concentration with the Addition of Ammonia

No nucleation mode particles were detected with the DMS500 in any of the described tests without the RAD lamps active. Therefore, all data presented in this section is from the fitted accumulation mode lognormal distribution.

<b>Ammonia concentration (ppm)</b>	<b>PNC (#.cm<sup>-3</sup>)</b>	<b>CMD (nm)</b>
<b>0</b>	$(2.45 \pm 0.08) \times 10^6$	$91 \pm 2$
<b>10</b>	$(2.34 \pm 0.06) \times 10^6$	$93 \pm 2$
<b>100</b>	$(2.32 \pm 0.06) \times 10^6$	$93 \pm 1$

Table 3 PNC and CMD of raw diesel exhaust, diesel exhaust with 10ppm ammonia, and diesel exhaust with 100 ppm ammonia at 1.2 atm of pressure. All samples are within error of each other.

<b>Ammonia concentration (ppm)</b>	<b>PNC (#.cm<sup>-3</sup>)</b>	<b>CMD (nm)</b>
<b>0</b>	$(2.23 \pm 0.09) \times 10^6$	$86 \pm 2$
<b>10</b>	$(2.28 \pm 0.07) \times 10^6$	$85 \pm 1$
<b>100</b>	$(2.38 \pm 0.07) \times 10^6$	$84 \pm 1$

Table 4 PNC and CMD of diesel exhaust, diesel exhaust with 10ppm ammonia, and diesel exhaust with 100 ppm ammonia at 1.4 atm of pressure. All samples are within error of each other.

The PNC and CMD data for each pressure set all fell within error of each other, showing no significant variation with ammonia concentration. To better illustrate this, the data for the sample mixed with ammonia was expressed as the relative percentage of pure diesel exhaust at the same pressure.

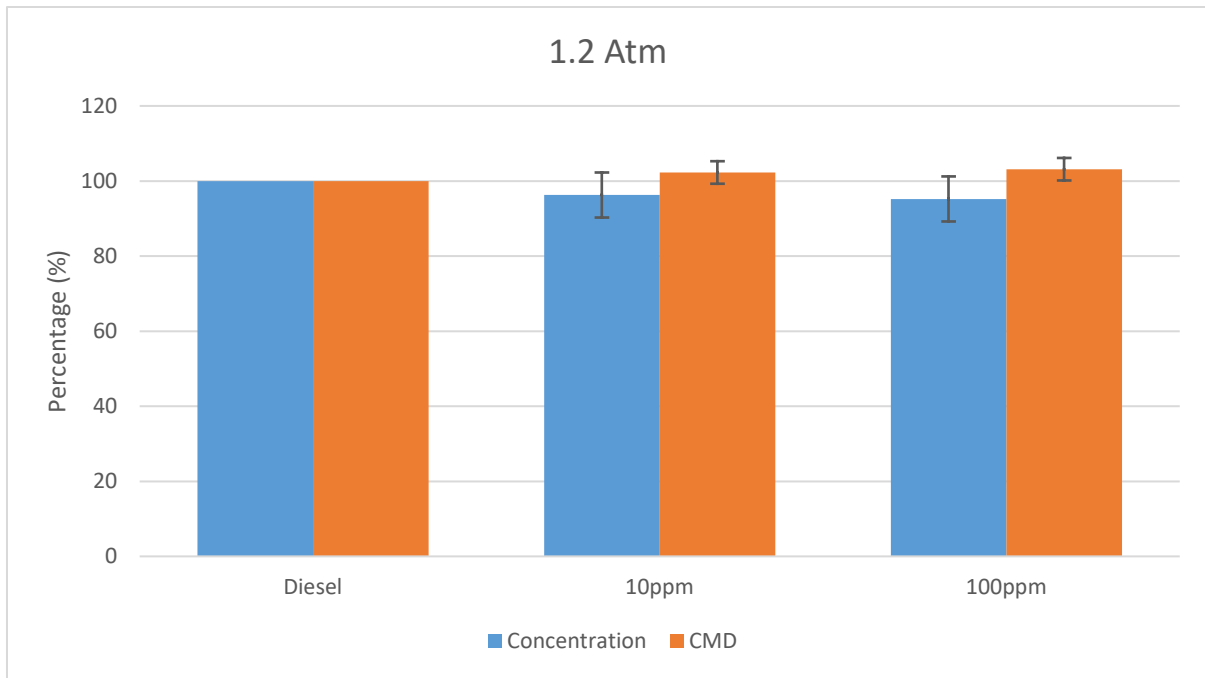


Figure 10 Graph for data at 1.2 atm showing the PNC (Concentration) and CMD measured for the accumulation mode at 10 ppm and 100 ppm ammonia concentrations expressed as the percentage of the PNC and CMD of raw diesel exhaust. Error bars all contain 100 % showing no significant change in parameters when ammonia is added.

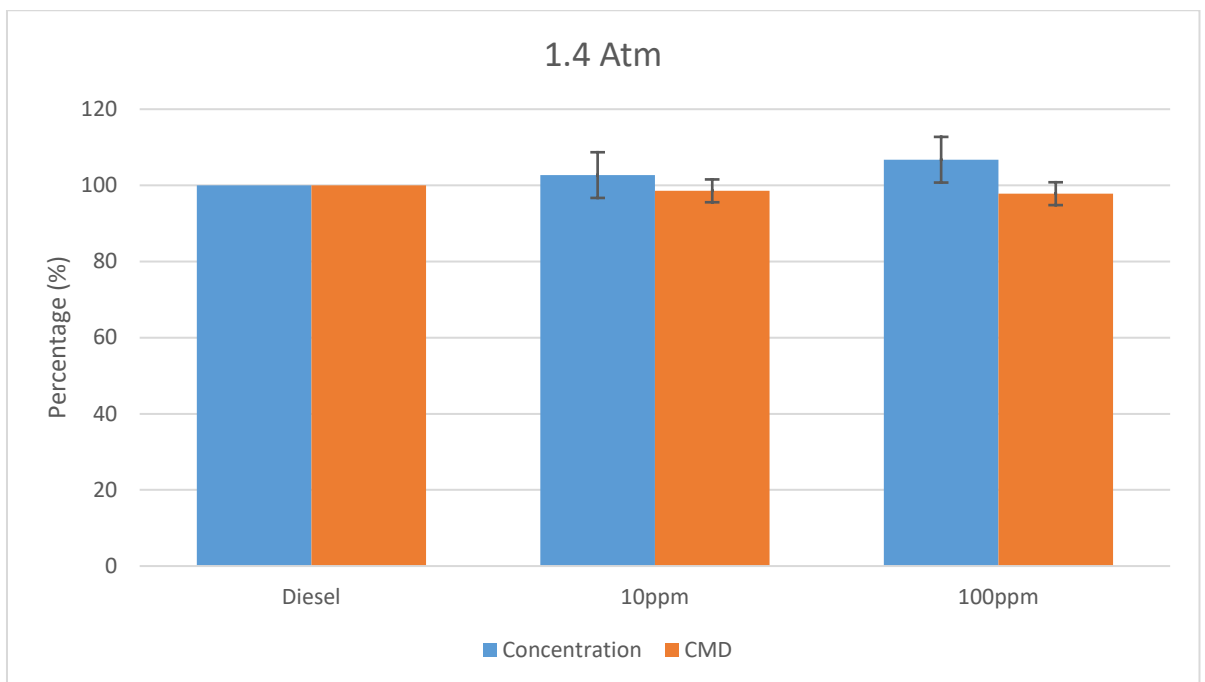


Figure 11 Graph for data at 1.4 atm showing the PNC (Concentration) and CMD measured for the accumulation mode at 10 ppm and 100 ppm ammonia concentrations expressed as the percentage of the PNC and CMD of raw diesel exhaust. Error bars all contain 100 % showing no significant change in parameters when ammonia is added.

### 3.3. Particle Mass and Composition

The particle composition and mass data collected from the AMS was processed and is presented in Tables 3 and 4 for 1.2 atm and 1.4 atm respectively. Due to the high concentrations of aerosol mass the AMS was only connected to each sample for  $\sim 5$  minutes. This, combined with a suspected pressure build up in the line after changing connections; resulted in higher uncertainties than would otherwise be normal for the instrument. Sulphates and chlorides have been excluded from this analysis as they were not present in any significant concentrations. At 1.2 atm, the ammonium concentrations, in the particle phase, were consistently below the detection limit and therefore cannot be treated as quantitative, however they have been included for comparison with measurements at 1.4 atm.

	<b>Ammonium</b> ( $\mu\text{g}\cdot\text{m}^{-3}$ )	<b>Nitrate</b> ( $\mu\text{g}\cdot\text{m}^{-3}$ )	<b>Organics</b> ( $\mu\text{g}\cdot\text{m}^{-3}$ )	<b>Total</b> ( $\mu\text{g}\cdot\text{m}^{-3}$ )
<b>Diesel</b>	$0.02 \pm 0.02$	$1.23 \pm 0.03$	$92 \pm 4$	$93 \pm 4$
<b>10 ppm</b>	$0.03 \pm 0.02$	$1.35 \pm 0.04$	$110 \pm 10$	$110 \pm 10$
<b>100 ppm</b>	$0.03 \pm 0.02$	$1.31 \pm 0.04$	$100 \pm 9$	$102 \pm 9$

Table 5 Chloride, ammonium, nitrate, organics and total mass concentrations as measured by the AMS at 1.2 atm.

	<b>Ammonium</b> ( $\mu\text{g}\cdot\text{m}^{-3}$ )	<b>Nitrate</b> ( $\mu\text{g}\cdot\text{m}^{-3}$ )	<b>Organics</b> ( $\mu\text{g}\cdot\text{m}^{-3}$ )	<b>Total</b> ( $\mu\text{g}\cdot\text{m}^{-3}$ )
<b>Diesel</b>	$7.0 \pm 0.5$	$24 \pm 9$	$50 \pm 20$	$80 \pm 30$
<b>10 ppm</b>	$5.8 \pm 0.2$	$20 \pm 7$	$50 \pm 20$	$80 \pm 30$
<b>100 ppm</b>	$3.8 \pm 0.1$	$13 \pm 5$	$60 \pm 30$	$70 \pm 30$

Table 6 Chloride, ammonium, nitrate, organics and total mass concentrations as measured by the AMS at 1.4 atm. Ammonia and nitrate concentrations indicate ammonium nitrate contamination from an earlier experiment.

To better illustrate any influence from the addition of ammonia, mass concentration of each chemical species was expressed as the percentage of the mass concentration of the same species observed in pure diesel exhaust at the same pressure.

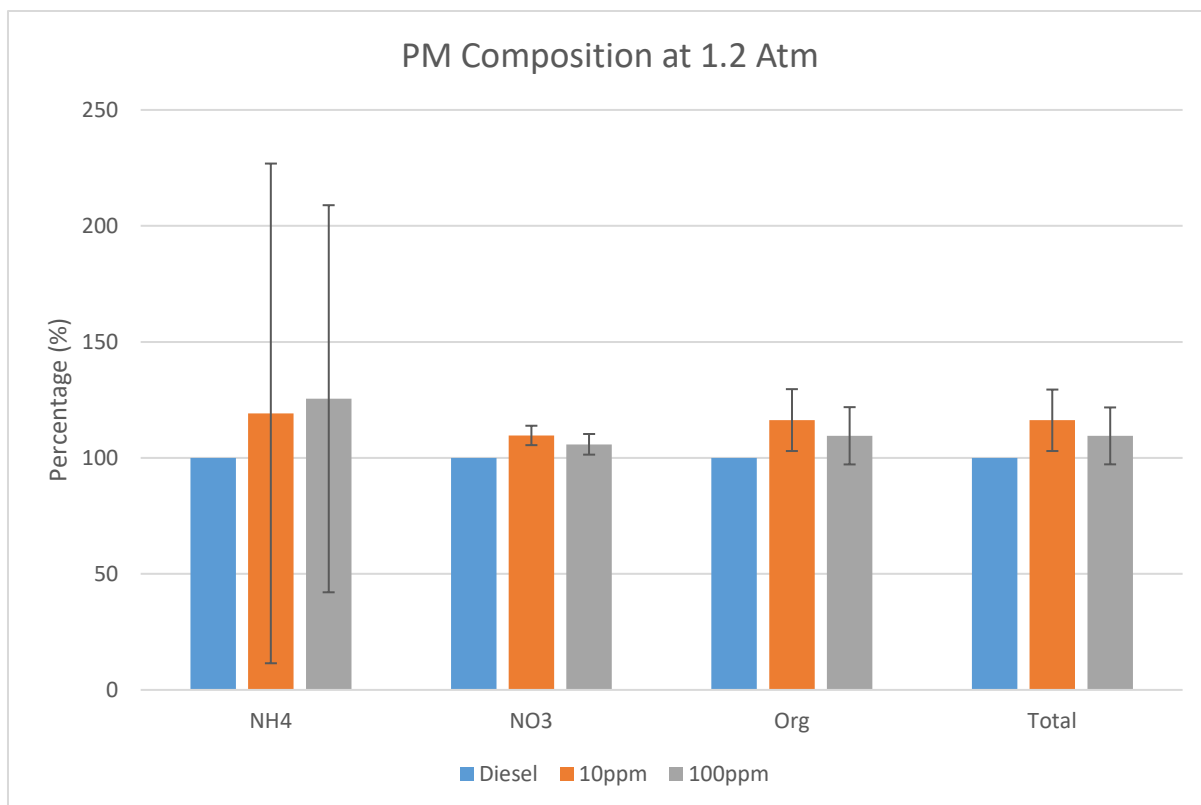


Figure 12 Ammonium, nitrates, organics, and total mass concentrations expressed as the percentage of the mass concentration of each chemical species measured in raw diesel exhaust at 1.2 atm. Ammonium concentrations have large error bars as the concentrations are close to the limit of detection of the AMS for all measurements shown. Some deviations from 100 % are measured, however there is no clear relationship with ammonia concentration.

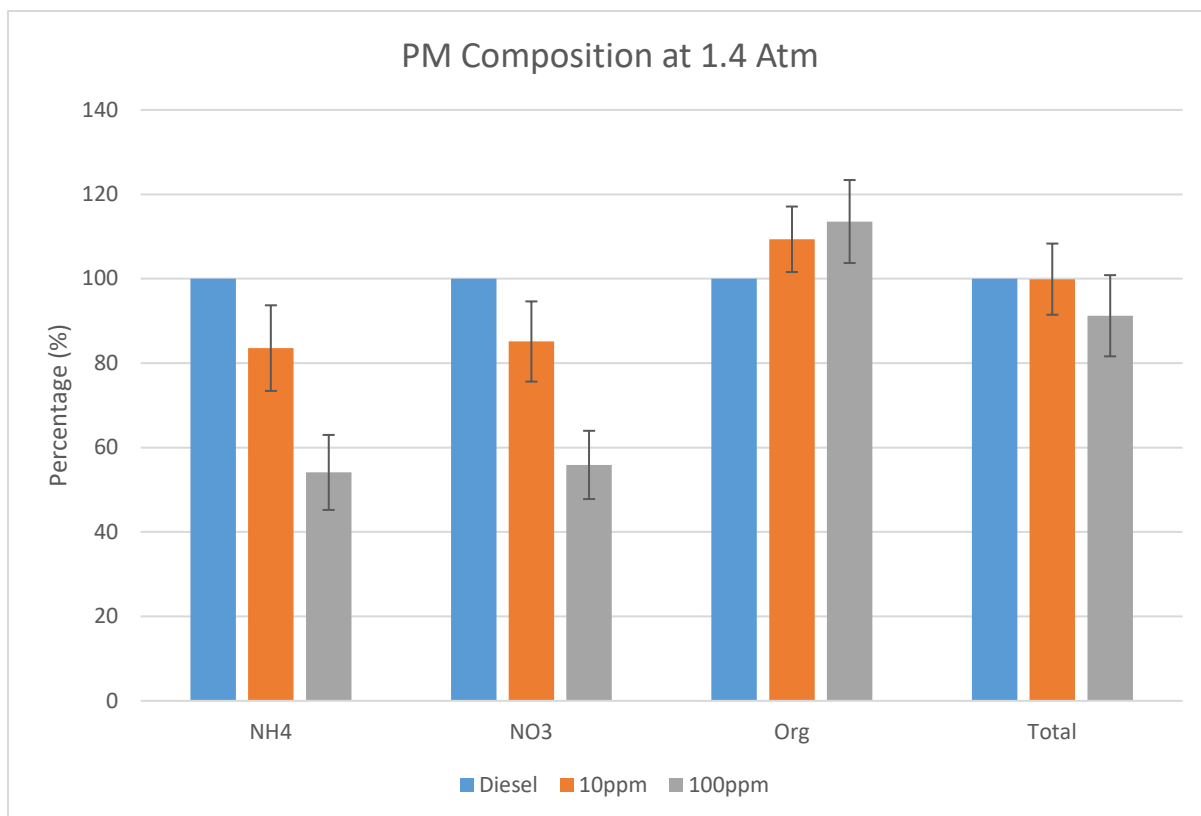


Figure 13 Ammonium, nitrates, organics, and total mass concentrations expressed as the percentage of the mass concentration of each chemical species measured in raw diesel exhaust at 1.4 atm. Ammonium and nitrate concentrations decayed over time due to potential contamination of the RAD chamber by ammonium nitrate. Organic concentrations appeared to increase with increasing ammonia.

### 3.4. Atmospheric Aging Simulation

The lamps inside the RAD were turned on in order to simulate the chemical processes which generate secondary organic aerosols in outdoor ambient conditions. This was repeated for three pressures, with 100 ppm ammonia added for one sample to observe any potential changes in the resulting aerosol.

Ammonia (ppm)	Pressure (atm)	Nucleation Mode		Accumulation Mode	
		CMD (nm)	PNC (#.cm <sup>-3</sup> )	CMD (nm)	PNC (#.cm <sup>-3</sup> )
-	1.0	28 ± 2	(4 ± 2) × 10 <sup>5</sup>	138 ± 1	(3.0 ± 0.1) × 10 <sup>6</sup>
-	1.2	27 ± 2	(3 ± 1) × 10 <sup>5</sup>	143 ± 2	(1.5 ± 0.1) × 10 <sup>6</sup>
-	1.4	11 ± 2	(3 ± 1) × 10 <sup>5</sup>	108 ± 2	(1.7 ± 0.1) × 10 <sup>6</sup>
100	1.4	-	-	76 ± 1	(1.75 ± 0.05) × 10 <sup>6</sup>

Table 7 Peak CMD and PNC of the nucleation and accumulation mode measured with different pressures and ammonia concentrations were exposed to OH radicals inside the RAD chamber.

The large mass concentrations generated were dangerously high for the AMS so the instrument was only briefly exposed to the resultant aerosol. The values in Table 8 represent the difference between the mean concentration observed before turning the lamps on and the maximum concentration observed during the brief AMS sampling period while the lamps were activated. Due to the short sampling time and strongly varying concentrations, the composition could not be precisely characterized. These AMS results are primarily useful for qualitative comparison and as such have been provided without error margins.

Ammonia (ppm)	Pressure (atm)	ΔCl (μg.m <sup>-3</sup> )	ΔNH <sub>4</sub> (μg.m <sup>-3</sup> )	ΔNO <sub>3</sub> (μg.m <sup>-3</sup> )	ΔOrg (μg.m <sup>-3</sup> )	ΔSO <sub>4</sub> (μg.m <sup>-3</sup> )
-	1.0	4.1	4.1	50	470	18
100	1.4	4.6	160	470	81	1.6

Table 8 AMS data collected when the RAD aging lamps were activated. Values are given as the difference between the maximum mass concentrations measured by the AMS before disconnecting, and the mass concentrations measured before the lights were activated. No error margins are provided as the data is considered qualitative. Significant differences in the chemical species are generated when ammonia is added to the diesel exhaust.

## 4. Discussion

### 4.1. Diesel Emissions at Different Pressures

The investigation into the influence of pressure and ammonia on diesel exhaust requires the sample to remain pressurized from combustion until directly before measurement by the instruments. In order to achieve this the sample is drawn from the engine prior to the turbocharger and regulated down to the required pressure by the setup detailed in Sect. 2.2.1. The influence of this setup on the particle size distributions of the sample generated was investigated using the DMS500. The particle size distributions are shown graphically in Figure 9, and the fitted accumulation mode CMD and PNC values are provided in Table 2. Whilst the CMD remains within error for the three measured pressures, there is a clear decrease in the PNC as the pressure is increased. This is due to the increased losses that occur as the pressure increases.

The final sample flow after sample depressurization was set to a mass flowrate of 13 std L.min<sup>-1</sup> in all experiments. However, the volumetric flowrate in the pressurized portion of the sampling setup will decrease as the pressure is increased. This leads to higher residence times in the sampling setup prior to measurement, creating higher particle losses in the system as the pressure increases. An additional factor which will also cause a similar effect is the use of a needle valve to constrain the sample flow in order to pressurize this. In order to increase the pressure of the sample the needle valve must be closed further, which constrains the aerosol flow through the valve. This flow constraint and increasingly rapid expansion as the pressure is increased will also generate higher sample losses as the pressure is increased. The combination of these two effects explains the significant reduction in PNC observed as pressure is increased.

The losses due to increased residence time will be increased substantially when the RAD chamber is added to the sampling setup due to its large internal volume. The consequence of this is that it will not be possible to directly compare the results collected at 1.2 and 1.4 atm as the residence time, losses and particle interactions will be significantly different. Instead, the focus will be on the influence the addition of ammonia has on the physiochemical properties of the diesel exhaust at each pressure separately, and whether the magnitude of the influence changes with pressure.

#### 4.2. Influence of Increased Pressure and Ammonia on Diesel Exhaust

In atmospheric conditions the presence of ammonia can lead to: increased PNC and CMD; the presence of nucleation mode particles; and changes in PM chemical composition. Therefore, this investigation focused on these parameters in order to observe if elevated ammonium levels and increases in ambient pressure, characteristic of mining environments, could have a similar influence on diesel PM emissions.

Physical characteristics of PM were measured using the DMS500, which measured the PNC and CMD of any nucleation and accumulation mode particles exiting the RAD chamber. In all experiments performed with any combinations of pressure and ammonia there was no nucleation mode observed. This indicates that ammonia does not react with any other gases present to generate secondary products in sufficient quantity to homogeneously nucleate new particles. For this reason only accumulation mode data is provided in Sect. 3.1.

The data displayed in Figure 10 and Figure 11 shows the CMD and PNC of the accumulation mode at each ammonia concentration expressed as percentages relative to measurements of pure diesel exhaust for 1.2 and 1.4 atm, respectively. In all experiments, the CMD and PNC did not significantly change, with the values for pure diesel PM lying within the error bars. Hence, there are not sufficient secondary species generated through pressure and elevated ammonia to condense onto accumulation mode particles to change their size. Further evidence for a lack of secondary products can be found in the AMS results. In atmospheric conditions the primary PM product expected to form from ammonia is ammonium. However, in the 1.2 atm AMS measurements the ammonium concentrations remained low at around the limit of detection of instrument, showing no evidence of secondary formation. There is significant ammonium detected at 1.4 atm, however this is due to a contamination of the RAD chamber which is discussed in the next section.

Within the error margins there is a small trend of decreasing PNC and increasing CMD with increasing ammonia concentration at 1.2 atm; and an opposing trend is observed at 1.4 atm. These variances are likely due to small fluctuations in the chamber pressure, which will influence the physical interactions between particles and their losses inside the RAD chamber; leading to changes in the physical properties of the sample. Whilst every effort was made to ensure stable pressure and flowrate prior to sampling, needle valves are prone to shift overtime leading to small changes in pressure which are not detectable with the analogue gauges used. Active pressure regulation with elevated ammonia concentrations would require dedicated corrosion resistant equipment which were not available for this study.

The AMS data at 1.2 atm shown in Figure 12 indicates that in the test in which ammonia was added to diesel exhaust, the composition varied outside of the error margins of raw diesel exhaust. These error margins were calculated as the standard deviation of the averaged sample used to calculate each data point. However, this does not take into account the variations in size and concentration brought on by small pressure fluctuations in the chamber discussed in the previous paragraph. These variations coupled with: the short averaging times used to collect samples; the lack of an overarching trend with increased ammonia; and no measurable increase in ammonium, which is the primary expected product in the particle phase of reactions with ammonia; indicates that there is no significant change in particle chemical composition measured with the AMS with the addition of ammonia at 1.2 atm. This conclusion agrees with the physical characteristics measured with the DMS500 that shows no change in the particle size. The clear change in composition observed at 1.4 atm is due to a contamination issue which is discussed in the following section.

In normal atmospheric conditions the chemical processes which drive the formation of secondary aerosol species are typically photochemical. Therefore, in underground situations without sources of light, ozone and OH radicals there is no reaction pathways available to form secondary products; even with elevated pressure and ammonia concentrations. The results collected in this study confirm that there is no significant variation in the physiochemical properties of PM with elevated ammonia concentration and pressure.

### **4.3. Photochemical Reaction of Diesel Exhaust**

In this study the RAD was primarily used as a pressurized chamber to provide a time delay sufficient to ensure any reaction between ammonia and diesel exhaust had taken place prior to measurement. However, the RAD also contains UVC lamps which generate OH radicals to artificially produce secondary organic aerosols typical in ambient conditions. The pure diesel exhaust was exposed to OH radicals at each tested pressure in order to contrast ambient secondary organic generation with any secondary species created at elevated ammonia and pressure levels.

As the RAD is still in the prototype stage the results listed for these experiments in Table 7 should be considered qualitative. However, a significant growth in the accumulation mode is observed in all three tests with raw diesel exhaust, with the highest change observed at 1.2 atm. Furthermore, nucleation mode particles were also detected at all three pressures, increasing total concentrations substantially. There may be some influence of pressure on the resulting size and concentration of both modes, however an in depth characterization of the RAD under pressure would be necessary which is beyond the scope of this study. What can be concluded is that these physical characteristics of PM are significantly changed from raw diesel exhaust at ambient atmospheric pressure. This was not the case for the dark experiments with elevated ammonia and pressure exposures, emphasizing that the combination of ammonia and pressure does not have a significant influence on diesel PM.

#### 4.4. Photochemical Reaction of Diesel Exhaust with Ammonia

When 100 ppm of ammonia was added to diesel exhaust prior to exposure to the RAD UV lamps the results were significantly different than those described in Sect. 4.3. There was no increase in total concentration, no measureable nucleation mode, and a small decrease in accumulation mode particle size when compared with the results at the same pressure in Table 5. This indicates when ammonia is present in high concentrations there is a different reaction pathway present, leading to different physical/chemical PM characteristics.

The significant growth in particle size and concentration in raw diesel exhaust exposed to OH radicals leads to significant increases in mass concentration. This posed a problem for the AMS as it can be damaged by excessively high mass concentrations. Therefore, accurate compositional data was not possible as the AMS could only be safely connected for a few minutes while the lamps were active. The results of the two most successful measurements are provided in Table 8, corresponding to atmospheric pressure with no added ammonia and 1.4 atm with 100 ppm added ammonia. The data is presented as the change in mass concentration of each species from when the lamps were turned on. The total concentrations are not comparable between the two tests as the AMS was not attached long enough for the chamber to reach equilibrium conditions. However, what is very significant is the chemical species produced. When raw diesel exhaust was exposed the primary product was organics, with some nitrates and smaller concentrations of the other species generated as well. In contrast, when ammonia was present the primary products were ammonium and nitrate, present in a mass ratio which strongly indicates significant levels of ammonium nitrate formation.

The reaction pathway for the formation of ammonium nitrate inside the RAD chamber is through a known gas-phase chemical reaction between ozone and ammonia (Khuntia et al., 2012). This reaction appears to dominate over the alternate reaction pathway which results in the formation of organics through photochemical interactions discussed in Sect. 4.3. Due to the gas phase nature of the reaction, it is likely that under the increased pressures observed in mines the rate of ammonium nitrate formation will be higher than under normal ambient conditions.

What is not immediately clear is the physical form the ammonium nitrate takes in the particle phase. The DMS500 data shows no significant increase in total PNC concentrations, nor any nucleation mode which would indicate the formation of new ammonium nitrate particles. In addition, the CMD of the accumulation mode decreases by approximately 10 nm from raw diesel exhaust at the same pressure. The combination of a lack of increase in PNC and a reduction in CMD indicates a reduction in mass. This is counter to the observed production of a significant mass of ammonium nitrate observed by the AMS, indicating a second chemical process reducing particle mass inside the chamber.

The reduction in CMD measured by the DMS500 couples with the increase in total mass measured with the AMS indicates that the size reduction must be due to a significant mass fraction of the PM which is not detectable with the AMS. The AMS is not sensitive to refractory compounds, which includes the elemental carbon cores found in diesel exhaust particles. However, these carbon cores make up a substantial mass fraction of the particle and hence strongly influence the size of the particle measured by the DMS500. Therefore, a reduction in the size of these carbon cores could explain the seemingly contradicting data of the DMS500 and AMS.

Currently the RAD chamber uses high powered hard UVC lamps, which will generate ozone concentrations in excess of 200 ppm inside the chamber. It has been observed that in high ozone environments such as this, ozone will react with the carbon core of diesel exhaust to form carbon dioxide (CO<sub>2</sub>) gas (Babaie et al., 2015). This effect can cause a significant reduction in particle size which would not be detectable with the AMS, but is measureable with the DMS500. This reaction was not substantial enough to be observed in the absence of ammonia as the CMD increased at all three tested pressures (Table 7). This indicates that the presence of ammonia significantly changes the reaction pathways when diesel exhaust undergoes photochemical interactions, leading to: high concentrations of ammonium nitrate; lowered concentrations of organics; and higher rate of reactions between ozone and the carbon cores of diesel PM.

The formation of ammonium nitrate was of such high a magnitude that the AMS data from further 1.4 atm experiments performed three days later were still contaminated. This is evident from the data presented in Table 6 and Figure 13, which show decaying levels of ammonium and nitrate over time in a mass ratio consistent with ammonium nitrate. The ammonium nitrate particles contaminating the AMS would be large in CMD and low in PNC due to particle coagulation and deposition over this long time period. Fortunately, this combination of parameters means that the PNC and CMD are outside of the range considered by the DMS when it fits the accumulation mode distributions used in the analysis presented in Table 6 and Figure 13. Therefore, the data provided from the DMS500 can be used to draw conclusions regarding the physical properties of PM interacting with ammonia at 1.4 atm despite the contaminated AMS data.

If there are potential sources of ozone present, elevated ammonia concentrations should be avoided. In a mining environment potential sources of ozone include: welding; the use of explosives; and ventilation air drawn from the surface.

## 5. Summary

The influence of elevated ammonia and mine-relevant pressures on the physical and chemical characteristics of diesel exhaust PM were investigated. No significant changes to physiochemical characteristics were observed at pressures of up to 1.4 atm and ammonia concentrations of 100 ppm. This represents the upper end of pressures found in underground mines and ammonia concentrations well above those which are safe for human exposure (however such levels have been found in transient tailpipe emissions from SCR-equipped diesel engines). This indicates that the changes to an aerosol observed when ammonia is present in the atmosphere in normal ambient conditions is dependent upon additional factors ((UV) light, ozone), and does not drive significant reactions with PM itself. Therefore, the authors are confident in stating that the combination of elevated pressure and ammonia have no significant influence on the physiochemical properties of diesel PM. However, the findings of this report do indicate that in elevated ammonia concentrations care must be taken to avoid all sources of UV light and ozone; as these can lead to the rapid formation of ammonium nitrate. It is known that electric motors (especially brushed motors) can be sources of ozone. Therefore it would be advisable to ensure electric equipment used in mines does not emit ozone, or conversely to monitor ozone levels in mines where SCR-equipped diesels are in use.

## 6. References

- Amanatidis, S., Ntziachristos, L., Giechaskiel, B., Bergmann, A., Samaras, Z. Impact of selective catalytic reduction on exhaust particle formation over excess ammonia events, *Environmental Science and Technology*, 48 (19), pp. 11527-11534, 2014.
- Babaie, M., Davari, P., Talebizadeh, P., Zare, F., Rahimzadeh, H., Ristovski, Z. and Brown, R.: Performance evaluation of non-thermal plasma on particulate matter, ozone and CO<sub>2</sub> correlation for diesel exhaust emission reduction, *Chem. Eng. J.*, 276(C), 240–248, doi:10.1016/j.cej.2015.04.086, 2015.
- Gentner, D.R., Jathar, S.H., Gordon, T.D., Bahreini, R., Day, D.A., El Haddad, I., Hayes, P.L., Pieber, S.M., Platt, S.M., De Gouw, J., Goldstein, A.H., Harley, R.A., Jimenez, J.L., Prévôt, A.S.H., Robinson, A.L. Review of Urban Secondary Organic Aerosol Formation from Gasoline and Diesel Motor Vehicle Emissions. *Environmental Science and Technology*, 51 (3), pp. 1074-1093, 2017.
- George, I. J., Vlasenko, A., Slowik, J. G., Broekhuizen, K. and Abbatt, J. P. D.: Heterogeneous oxidation of saturated organic aerosols by hydroxyl radicals: uptake kinetics, condensed-phase products, and particle size change, *Atmos. Chem. Phys. Atmos. Chem. Phys.*, 7, 4187–4201 [online] Available from: [www.atmos-chem-phys.net/7/4187/2007/](http://www.atmos-chem-phys.net/7/4187/2007/) (Accessed 13 March 2018), 2007.
- Kang, E., Root, M. J., Toohey, D. W. and Brune, W. H.: Introducing the concept of Potential Aerosol Mass (PAM), *Atmos. Chem. Phys. Atmos. Chem. Phys.*, 7, 5727–5744 [online] Available from: [www.atmos-chem-phys.net/7/5727/2007/](http://www.atmos-chem-phys.net/7/5727/2007/) (Accessed 13 March 2018), 2007.
- Keller, A. and Burtscher, H.: A continuous photo-oxidation flow reactor for a defined measurement of the SOA formation potential of wood burning emissions, *J. Aerosol Sci.*, 49, 9–20, doi:10.1016/j.jaerosci.2012.02.007, 2012.
- Khuntia, S., Majumder, S. K. and Ghosh, P.: Removal of Ammonia from Water by Ozone Microbubbles, , doi:10.1021/ie302212p, 2012.
- Lambe, A. T., Ahern, A. T., Williams, L. R., Slowik, J. G., Wong, J. P. S., Abbatt, J. P. D., Brune, W. H., Ng, N. L., Wright, J. P., Croasdale, D. R., Worsnop, D. R., Davidovits, P. and Onasch, T. B.: Characterization of aerosol photooxidation flow reactors: Heterogeneous oxidation, secondary organic aerosol formation and cloud condensation nuclei activity measurements, *Atmos. Meas. Tech.*, 4(3), 445–461, doi:10.5194/amt-4-445-2011, 2011.
- Mendoza-Villafuerte, P., Suarez-Bertoa, R., Giechaskiel, B., Riccobono, F., Bulgheroni, C., Astorga, C., Perujo, A. NO<sub>x</sub>, NH<sub>3</sub>, N<sub>2</sub>O and PN real driving emissions from a Euro VI heavy-duty vehicle. Impact of

regulatory on-road test conditions on emissions. *Science of the Total Environment*, 609, pp. 546-555, 2017.

Simonen, P., Saukko, E., Karjalainen, P., Timonen, H., Bloss, M., Aakko-Saksa, P., Rönkkö, T., Keskinen, J. and Dal Maso, M.: A new oxidation flow reactor for measuring secondary aerosol formation of rapidly changing emission sources, *Atmos. Meas. Tech.*, 10(4), 1519–1537, doi:10.5194/amt-10-1519-2017, 2017.

Suarez-Bertoa, R., Mendoza-Villafuerte, P., Riccobono, F., Vojtisek, M., Pechout, M., Perujo, A., Astorga, C., On-road measurement of NH<sub>3</sub> emissions from gasoline and diesel passenger cars during real world driving conditions, *Atmospheric Environment*, 166(), 488-497, <https://doi.org/10.1016/j.atmosenv.2017.07.056>, 2017